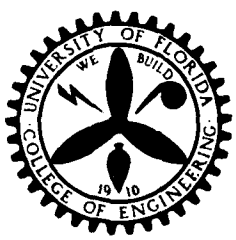

ENGINEERING AND INDUSTRIAL EXPERIMENT STATION

College of Engineering

University of Florida

Gainesville

CONSTRUCTION OF POURBAIX DIAGRAMS FOR ALLOY SYSTEMS WITH SPECIAL APPLICATION TO THE BINARY Fe-Cr SYSTEM

This research was supported by the Advanced Research Project Agency under Contract Number N00014-68-A-0173-0003.

A Report to the Advanced Research Project Agency

June 10, 1970

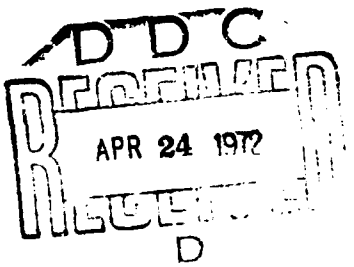

Submitted by:

Ellis D. Verink, Jr., Principal Investigator
Department of Metallurgical & Materials Engineering
University of Florida -- Gainesville, Florida 32601

(To be submitted in part for publication.)

ABSTRACT

Using potentiokinetic techniques with the electrochemical hysteresis method, experimental Pourbaix Diagrams were constructed for a series of six binary Fe-Cr alloys ranging in chromium content from 0.5% to 24.9%. Thirty-six solution variables were employed which included pHs from 4.5 to 11 inclusive and chloride contents from nil to saturated at room temperature. In addition to establishing domains of non-corrosion, general corrosion and passivation, the loci of zero current potentials, pitting potentials and protection potentials were determined as a function of pH, chloride ion concentration and chromium content. Corrosion velocities were determined for each region of the experimental diagrams.

INTRODUCTION

With the publication of the "Atlas of Electrochemical Equilibria in Aqueous Solutions"[1] by M. Pourbaix which extended his earlier work[13], the literature on pure metals in aqueous solutions is well developed. By contrast, very little work has been done on alloy systems. A number of investigators have made electrochemical measurements on iron alloys, ferrous materials containing chromium and nickel, titanium alloys and certain binary copper alloys in aqueous solutions (for example, References 2 through 12 inclusive). These studies have provided valuable guidance to those concerned with chemical inhibition of corrosion reactions and formation of passive films on surgical implant materials, the establishment of conditions necessary for cathodic protection, setting of control limits for anodic protection and so on.

Pourbaix Diagrams provide a basis for the expression of a huge quantity of thermodynamic data in a relatively simple graphic form. While these diagrams are of great qualitative usefulness, they have important limitations. For example, (1) the equilibrium diagrams provide no kinetic information, (2) only pure metals have been studied in depth and (3) various assumptions are made regarding solution composition which are not directly applicable to real engineering situations.

Very few engineering structures are made of pure metals. Much of the corrosion data on the performance of metals in electrolytes is highly specific and quantitative. Materials are used "because they work" without a thorough understanding of the mechanisms involved or of the controlling parameters. The research reported

herein represents an attempt to construct Pourbaix Diagrams for alloys of engineering interest. As part of this investigation, electrochemical techniques were developed which now make it possible to construct experimental Pourbaix Diagrams for alloys. The "Electrochemical Hysteresis" method used in these studies, extends the usefulness of potentiokinetic techniques by providing information on the so-called "Protection Potential," a material property believed to possess considerably more practical significance than the "Pitting Potential" frequently referred to in the literature. While the burden of the research effort has been with binary iron-chromium alloys, many of the details of experimental technique and data handling were evolved using the metallurgically simplier copper-nickel alloy system. Details regarding the copper-nickel alloy investigations are included in a Masters degree thesis entitled "Use of Experimentally Determined Pourbaix Diagrams to Elucidate the Role of Iron in the Passive Behavior of Copper-Rich Alloys Containing Nickel" by P. A. Parrish, University of Florida, June 1970. Therefore, this information will not be included herein.

OBJECTIVE

The objective of this research is to support that area of materials technology related to advancing the science and performance of high strength alloys in corrosive environments. In particular, the research described herein has application to saline environments such as experienced by materials immersed in sea water or boldly exposed to the marine atmosphere. Under such conditions, it is customary to select special alloys to resist general attack. Unfortunately, however, such alloys may still be subject to localized forms of attack, such as pitting, crevice corrosion or stress corrosion cracking which may result in sudden, unexpected failure. Detailed knowledge of the limiting conditions for immunity to these forms of attack is vital to the specification of minimum measures necessary for the avoidance of premature failure.

In the accomplishment of the research objective, it will be necessary to: (1) devise an electrochemical methodology which will provide the experimental evidence which will enable engineers to predict the performance of alloys under stated conditions, (2) show that the evidence so obtained can be explained on a thermodynamic basis, and (3) present the evidence in a form which will make it immediately available to engineers for use. While much work remains to be done, information contained herein gives concrete evidence of considerable progress in the accomplishment of these objectives.

EXPERIMENTAL METHOD

Dr. Marcel Pourbaix has suggested a method for the construction of an experimental potential-pH diagram from potentiokinetic polarization curves[1,21]. Figure 1a shows five such potentiokinetic polarization curves for Armco iron in chloride-free solutions of several pHs. Figure 16 is the corresponding experimental Pourbaix Diagram deduced from this series of curves. Figure 2a shows potentiokinetic polarization curves for Armco iron in 10^{-2} molar chloride solutions adjusted to a range of pH values. At the potential r, the passivating film becomes locally non-protective and pits are formed on the surface. This potential is referred to as the Rupture or Pitting Potential. The potential p, at which the current density reaches zero on the return scan is called the Protection Potential. At this point, the potential difference between pitted areas and unpitted areas on the specimen surface is approximately zero. Figure 2b is the experimental Pourbaix Diagram constructed from these electrochemical hysteresis curves. Notice that at pHs below about six no passivation occurs. A protection potential locus (as a function of pH) divides the passive region into an upper area where pre-existing pits continue to be active and a lower area where previously-formed pits no longer grow, but in fact, heal over.

The electrochemical corrosion cell used in this research shown in Figures 3a, 3b and 3c was adapted from designs by Myers[14] and France[15]. The portions of the specimen holder exposed to the electrolyte are fabricated from polycarbonate and Teflon* to avoid

* Trade name of E. I. DuPont de Nemours and Company, Incorporated.

contamination. The specimen is designed so that only one square centimeter of the sample material is exposed to the solution. A Teflon gasket seals the specimen in place. Electrical continuity is maintained through the back of the specimen via internal copper parts.

The electrolyte is vacuum de-aerated prior to its introduction into the cell. During tests, the cell is constantly purged with hydrogen gas. Saturated calomel is used as the reference electrode. The experimental apparatus, Figure 4, consists of a scanning potentiostat, a logarithmic converter, X-Y recorder, resistance selector box, differential amplifier and low pass RC filter. A detailed equipment list is provided in Table IX. The resistance selector box is a modification of that described by W. D. France, Jr. and R. W. Liety[16] and extends the recording range of the logarithmic recorder to nine cycles, thus facilitating automatic operation.

A current from the potentiostat to the auxiliary platinum electrode is measured as a potential across the precision resistor selected to provide the required logarithmic converter input voltage. Output from the logarithmic converter (current density) is plotted on the X axis and the working electrode (specimen) potential versus saturated calomel is plotted simultaneously on the Y axis. Potential is scanned from active to noble potential and then a reverse scan (noble to active) is made over the same potential range.

The electrochemical hysteresis method has been applied to a series of six binary iron-chromium alloys ranging in chromium con-

tent from 0.5 to 24.9 weight percent. Table I lists the compositions of the individual alloys. Thirty-six electrolyte compositions were employed in this program. These were saline solutions varying in pH from 4.5 to 11 with chloride content from nil to saturation at room temperature. Table II delineates the environmental variables under test. Under each condition of test, experiments were repeated to assure reproducibility. Where applicable, ASTM Recommended Practices and Conventions were utilized[17,18].

Specimens were mechanically polished through 4/0 emery paper and ultrasonically cleaned in laboratory detergent prior to exposure. The detailed configuration of potentiokinetic curves can be influenced by the rate of scan. As a result of studies at various scan rates ranging up to 130 millivolts per minute, it was decided that the optimum scan rate would be between 40 and 50 millivolts per minute. As a consequence, all scans were at 46.7 millivolts per minute. All tests were conducted at room temperature and pressure.

Corrosion velocities were determined from polarization data using the method of Pourbaix[19,1]. Since the indicated corrosion current density is strongly influenced by scan rate, the corrosion velocities determined herein must be calibrated by other methods before quantitative corrosion rates may be obtained. However, since all experiments were conducted at the same scan rate, it is possible to compare the relative corrosion behavior of the alloys.

RESULTS

From potentiokinetic polarization curves using the electrochemical hysteresis method, it is possible to obtain the following information. Zero current potential E_o, primary passivation potential E_{p_1} (also referred to as E_{pp}), any secondary passivation potentials E_{p_2}, pitting potential (or rupture potential) E_R, protection potential E_p, and the corresponding current density associated with each potential. This information was obtained for each of the six alloys exposed under the various conditions of exposure referred to in Table II. Tables III through VIII are tabulations of this information for each of the experiments. Figures 5 through 12 show the characteristic configurations of the polarization curves obtained for each of the six alloys.

The variation of the Zero Current Potential, the Passivation Potential, the Rupture Potential and the Protection Potential (where applicable) for four of the alloys as a function of chloride content in solutions of various pHs is shown in Figures 13 through 24.

This information is replotted and summarized on Potential versus pH co-ordinates to show the locus of Zero Current Potentials and Passivation Potentials as a function of chloride content. See Figures 25 through 28. Similar curves on Potential versus pH co-ordinates are shown in Figures 29 through 32 and illustrate the locus of Rupture Potentials and Protection Potentials for solutions of a variety of chloride contents.

The influence of varying chromium content in binary iron-chromium alloys is shown in Figure 33. In this figure, the Zero

Current Potential, the Passivation Potential and the Protection Potential are compared.

Figures 34 through 37 show the effect of chloride ion concentration on the corrosion velocity at the Primary Passivation Potential, E_{pp}, for four alloys of the Binary Fe-Cr series as a function of pH.

Figure 38 shows a family of curves for the six iron-chromium alloys showing the logarithm of the Primary Passivation Current-density for each alloy as a function of the pH of the solution. From this curve, it is possible to construct corrosion velocity contours.

Figures 39 through 44 show the experimental Pourbaix Diagrams for each of six iron-chromium alloys. Corrosion velocities are shown within the general corrosion region as the logarithm of the current density. In the Passive region, Rupture Potentials are shown as a function of chloride ion concentration and pH. In this region, the numbers shown are the logarithms of the chloride ion molarities. Protection Potentials are shown as a range. Protection Potential ranges tend to increase as chromium content increases.

Figure 45 is a group of Schematic, Experimental Pourbaix Diagrams for the six alloys based on data from 0.1M chloride ion solutions. This grouping permits "side-by-side" comparison of the influence of chromium additions on the form of the diagrams.

For comparison, Figures 46 through 48 taken from the "Atlas,"[1] are included showing the equilibrium Pourbaix Diagrams for pure iron, pure chromium in chloride-free solutions and pure chromium in the presence of chlorides.

DISCUSSION OF RESULTS

Foley has summarized the role of chloride ion in the corrosion of iron[10]. The present work adds significantly to the state of knowledge regarding ferrous alloys in saline environments.

For all of the Fe-Cr binary alloys tested, the zero current potential was a function of chromium content and pH but not of chloride content of the solution. See Figures 25 through 28. Increasing chromium content shifted the location of the zero current potential locus in the noble direction (toward the equilibrium hydrogen evolution line on the Pourbaix Diagram), see Figure 33. The crossing of the zero current lines for the 12 Cr and 16.9 Cr alloys is considered open to question at this time.

The immunity potential for an alloy has been assumed to be the potential at which the zero current potential line for that alloy intersects the equilibrium hydrogen evolution line. For thermodynamic reasons, the immunity potential line is drawn horizontally and represents the boundary between general corrosion and non-corrosion. Potentiostatic tests are required to verify the position of the immunity potential locus. Chromium additions above 5% extend the immunity range significantly.

The corrosion velocities at the Zero Current Potential are shown in Figure 49. Although the calculated rates of corrosion are low (at E_o) for all alloys tested, the spread in corrosion rate spans one order of magnitude when comparing 0.5 Cr with the 24.9 Cr alloy, the higher chromium alloy having the lower corrosion rate.

The primary passivation potentials also were functions of chromium content and pH but not of chloride ion concentration. Figure 33

shows the family of passivation lines for the six Fe-Cr alloys tested. The discontinuity in the passivation line for the 0.5 Cr alloy (pH 7.5) is considered questionable at this time. The Passivation Current Density for each alloy was tabulated from the potentiokinetic polarization curves in the various electrolytes. For each alloy, logarithm of the Passivation Current Density was plotted against pH and a straight line was drawn through the data, Figures 34 through 37 inclusive. Except for the 2% Cr alloy for which more scatter occurred, the data show that the current density at the Primary Passivation Potential is independent of chloride content. The "second line" shown on Figure 34 for the 0.5 Cr alloy, is believed to show the tendency for crystalline salt to interfere with the reaction in the saturated solution. Increasing chromium content shifts the position of the passivation line to the left on the Pourbaix Diagram and the slope becomes flatter. Both effects extend the passive region.

Figure 38 compares the corrosion velocities at the Primary Passivation Potential, E_{pp}, of the several alloys at various pHs. As expected, differences in corrosion rate are most dramatically shown at acid pHs where the corrosion rate for the 24.9 Cr alloy is five orders of magnitude less than for the 0.5 Cr alloy at pH 4. In the alkaline solutions the corrosion rates converge to very low values for all alloys tested as would be predicted from inspection of the Pourbaix Diagram for iron. Current densities recorded during potentiokinetic polarization studies are influenced by the scan rate. All experiments were conducted at a rate of 46.7 mv/min. so that the data would be comparable. Calibration of the data us-

ing gravimetric measurements would permit quantitative results. Such calibrations were not included in this investigation since the primary interest in corrosion velocity information was as a basis for comparing alloys of a family.

Figures 29 through 32 inclusive, are experimental Pourbaix Diagrams for four of the alloys showing the Zero Current Potentials and Passivation Potentials (previously shown to be independent of chloride content), the Immunity Potential (assumed to be independent of chloride), the Protection Potential (data points +) and the Rupture Potentials (open circles). Numbers beside the data points indicate the logarithm of the chloride ion molarity. The Protection Potential for all alloys was between minus 0.200 and minus 0.400 volts SHE and was independent of chloride ion concentration. The Protection Potential has significance only in regard to localized forms of corrosion such as pitting[21,22]. Accordingly, those data points in the passive region should be considered as Protection Potentials. Corresponding data points in the general corrosion region show that the Zero Current Potential is the same on the downward potential traverse as on the upward traverse, and that it is insensitive to chloride ion concentration. The potential is seen to be within the scatter band of the protection potential.

The rupture potentials (pitting potentials) for the Fe-Cr alloys are sensitive not only to alloy content and pH, but also are strongly dependent on chloride content of the electrolyte. Increasing chloride content tended to lower the rupture potential. See Figures 39 through 44. The rupture potentials in saturated

solutions approached the protection potential. Scatter was greatest for most dilute solutions. The limit of detection of chloride by titration was slightly better than 10^{-6} molar, therefore, "nil" chloride was plotted as 10^{-6} molar. A number of the rupture potential lines tend to be concave downward (i.e., the curves have a "hump") in the pH range between about 8-9. Pourbaix suggests the likelihood of a restricted region of passivation between pH = 8-9 caused by a film of chromic oxide in the presence of chloride on the diagram for pure chromium in The Atlas. See Figure 48. It is attractive to consider the possibility that the addition of chromium to iron leads to the formation of reaction products containing both chromium and iron oxides. If this is true, perhaps the "humps" in the curves are traceable to this. Comparison of Rupture Potentials for the various alloys shows that E_R shifts in the noble direction as chromium increases. A later phase of the work will be devoted to study of the composition and morphology of the reaction product films using x-ray and SEM.

Apparently the range of variation of values for the protection potential is far less than for the so-called pitting potential. This suggests the possibility that the Protection Potential may be a material property of more practical significance than the Pitting Potential which seems more sensitive to the method and conditions of test.

Figure 50 illustrates an additional use of the corrosion velocity trajectories beyond estimating the corrosion rate. The convergence of the velocity contours may be used to fix the transition pH at which the boundary between General Corrosion and Passivation occurs.

It is of interest to conjecture under what conditions complex ions containing chlorides (e.g., $FeCl^{++}$) may influence the form of the Pourbaix Diagram. Thermodynamic information was not readily available for several of the potential solid species, but information was at hand for $FeCl_2$, $FeCl_3$, $FeCl^{++}$ and Cl^-. From this data, Mr. A. Pourbaix determined that the soluble species $FeCl_2$ and $FeCl_3$ would predominate over Fe^{++} and Fe^{+++} only if the logarithm of the chloride ion molarity exceeds +3.96. Considering that at saturation the logarithm of the chloride ion molarity was only +0.8 for NaCl, it may be concluded that $FeCl_2$and $FeCl_3$ do not predominate. The ionic species $FeCl^{++}$, by contrast, is shown to predominate over $Fe^{+++}$when the logarithm of the chloride ion molarity exceeds -1.48. At lower chloride concentrations the diagram would be the same as for chloride-free solutions. The calculated limits for the region of predominance of $FeCl^{++}$ were established in the classical way used in the construction of diagrams for soluble species[1].

Coexistence Species	0.1M Cl^-	1.0M Cl^-
$Fe^{++}/FeCl^{++}$	+0.791 Volt	+0.682 V
$FeCl^{++}/Fe(OH)^{++}$	pH = 2.92	pH = 3.92
$FeCl^{++}/Fe_2O_3$	pH = 1.92	pH = 4.76*
$FeCl^{++}/Fe(OH)_3$	pH = 2.26	pH = 5.10*

FOR COMPARISON

Fe^{+++}/Fe_2O_3 (in chloride-free solutions) pH = 1.8

$Fe^{+++}/Fe(OH)_3$ (in chloride-free solutions) pH = 4.3

As a result of these calculations it may be assumed that the "corrosion triangle" is unaffected by chloride concentration.

This is consistent with the experimental observation that the Zero Current and Passivation Potentials as well as the corrosion velocities at these potentials were independent of chloride ion concentration.

The pHs marked with an asterisk(*) are within the range of pHs employed in this investigation, but must be considered approximate since the values were not corrected for any ionic interactions. The vertical boundary between General Corrosion and Passivation would be expected to be moved slightly to the right (increasing the domain of General Corrosion somewhat) in chloride solutions having a logarithm of chloride ion molarity greater than -1.48. Mr. Pourbaix's calculations were based on pure iron; therefore, application to Fe-Cr alloys must be made with care. However, they provide important background for interpretation of the experimental results. Further experiments will be required to test these conjectures.

CONCLUSIONS

The following conclusions may be drawn from research to date.

(1) Electrochemical hysteresis methods may be used to construct experimental Pourbaix Diagrams for alloy systems.

(2) The corrosion behavior of several alloys in a family may be compared quickly and directly by use of these methods.

(3) The corrosion rate may be estimated and included on the experimental Pourbaix Diagram. These rates also may be used to determine boundaries of various domains on the diagram.

(4) The Zero Current Potential, Passivation Potentials and Protection Potentials of six Fe-Cr binary alloys were independent of chloride ion concentration from nil to saturated.

(5) The Zero Current Potentials and Passivation Potentials were functions of alloy composition and pH.

(6) The rate of corrosion for these binary Fe-Cr alloys decreases as the chromium content increases (above 5% Cr).

(7) The corrosion rate at the Primary Passivation Potential and the Zero Current Potential is independent of chloride content, but dependent on pH and chromium content.

(8) With increasing chromium content, the locus of Zero Current Potentials moves toward the equilibrium hydrogen line (to more noble values).

(9) With increasing chromium content the loci of Passivation Potentials moves downward and to left and tend to have shallower slopes, all of which restrict the area of the "corrosion triangle" and extend the passive pH range. The greatest improvement is observed between 5 and 12% chromium. The General Cor-

(9) rosion region for alloys containing 16.9% chromium and above is restricted to pHs below 7.

(10) Increasing chromium content tends to extend the Immunity Region to more noble potentials.

(11) The Pitting (or Rupture) Potential is dependent on alloy composition, pH and chloride composition in deaerated solutions.

(12) It is likely that chromium oxide is strongly influential in providing passivation since Rupture Potentials increase with increasing chromium and "humps" appear in E_R curves in the vicinty of pH 8-9.

(13) The concept of the Protection Potential, first proposed by Pourbaix, appears to be of greater practical importance than the pitting (or rupture) potential based on the independence of the Protection Potential to chloride content, pH or chromium content.

FUTURE WORK

In order to complete the study of these alloys so as to maximize the usefulness of the result, several additonal investigations are needed.

Potentiokinetic Studies

(1) Extend the pH range covered to provide additional verification of boundaries of the experimental diagram.

(2) Apply present methods to pure iron, pure chromium and austemtic stainless steels to provide a "bridge" to the thermodynamic data and to other alloys.

(3) Investigate the influence of oxygen, carbon dioxide, etc., on electrochemical behavior.

Potentiostatic Studies

(1) Hold specimens at particular potentials and pHs so as to accumulate sufficient reaction products for analysis.

(2) Verify positions of Immunity Potentials.

(3) Verify limits of Passivation range.

(4) Verify that specimens held at or below the Protection Potential are not subject to localized attack or that pits will "heal."

X-Ray and Scanning Electron Microscropy

(1) Determine chemical analysis and/or chrystalline structure of reaction products. Verify the influence of chromium in providing passivation.

(2) Determine physical character and morphology of reaction products.

Mechanism of Crevice Corrosion and Pitting

(1) Construct simulated "crevices" to determine influence of chromium additions on tendency for crevice corrosion.

(2) Test the predictions of Pourbaix regarding the significance of the Protection Potential by monitoring the potential and pH within the crevice as the exposed portion of the sample is polarized to various potentials.

(3) Develop a test method in which pits (or crevices) could be electrically isolated from the balance of the specimen but could be connected through measuring instrumentation. This would permit measurement of current flow in addition to potential and pH.

LIST OF REFERENCES

1. M. Pourbaix, Atlas of Electrochemical Equilibria in Aqueous Solutions, Translated from the French by James A. Franklin, Pergamon Press (1966).

2. S. Brennert, "Method for Testing the Resistance of Stainless Steels to Local Corrosive Attack," Journal of the Iron and Steel Institute, 135 (1937) 101P - 111P.

3. M. Stern, "The Electrochemical Behavior, Including Hydrogen Overvoltage, of Iron in Acid Environments," Journal of the Electrochemical Soc., 102 (Nov. 1955) 609 - 616.

4. M. Stern and A. L. Geary, "Electrochemical Polarization I. A Theoretical Analysis of the Shape of Polarization Curves," Journal of the Electrochemical Soc., 104 (Jan. 1957) 56 - 63.

5. T. P. Hoar, "On Corrosion - Resistant Materials," Journal of the Electrochemical Soc. (Jan. 1970) 17C - 22C.

6. N. D. Greene, "Predicting Behavior of Corrosion Resistant Alloys by Potentiostatic Polarization Methods," Corrosion, 18 (April 1962) 136t - 142t.

7. R. F. Steigerwald and N. D. Greene, "The Anodic Dissolution of Binary Alloys," Journal of the Electrochemical Soc., 109 (Nov. 1962) 1026 - 1034.

8. M. Pourbaix, L. Klimzack-Mathieiu, C. Mertens, J. Meunier, C. Vanleugenhaghe, L. de Muncky, J. Laureys, L. Neelemans and M. Warzee, "Potentiokinetic and Corrosimetric Investigations of the Corrosion Behavior of Alloy Steels," Corrosion Science, 3 (1963) 239 - 259.

9. M. Pourbaix and F. Vandervelden, "Intensiostatic and Potentiostatic Methods. Their Use to Predetermine the Circumstances for Corrosion or Non-Corrosion of Metals and Alloys," Corrosion Science, 5 (1965) 81 - 111.

10. H. Grubitsch, L. Willfurth and H. Zitter, "Potentiostatische, Potentiokinetische und Intensiokinetische Stromdicte - Potential - Messungen an Austenitischen Crom - Nickel - Stählen," Werkstoffe und Korrosion, Heft 10 (1966) 862 - 869.

11. E. A. Lizlovs and A. P. Bond, "Anodic Polarization of Some Ferritic Stainless Steels in Chloride Media," Journal of the Electrochemical Soc., 116 (May 1969) 574 - 579.

12. M. A. Streicher, "The Time-Factor in Potentiostatic Studies of Intergranular Corrosion of Austenitic Stainless Steels," Corrosion Science, 9 (1969) 53 - 56.

13. M. Pourbaix, Thermodynamique des Solutions Aqueuses Diluées. Représentation Graphique du Rôle du pH et du Potentiel (Thesis Delft, 1945), Reimpression, CEBELCOR (1963).

14. J. R. Myers, "Improved Working - Electrode Assembly for Electrochemical Measurements," Corrosion, 24 (Oct. 1968) 352.

15. W. D. France, Jr., "A Specimen Holder for Precise Electrochemical Polarization Measurements on Metal Sheets and Foils," Journal of the Electrochemical Soc., 114 (August 1967) 818-819.

16. W. D. France, Jr. and R. W. Lietz, Improved Data Recording for Automatic Potentiodynamic Polarization Measurements, Research Laboratories, General Motors Corp., Warren, Michigan (May 3, 1968).

17. Recommended Practice for a Standard Method for Making Potentiostatic and Potentiodynamic Anodic Polarization Measurements, Task Group 2, Potentiostatic and Potentiodynamic Polarization, Section I, Subcommittee XI, ASTM Committee G-1 (April 10, 1968).

18. Proposed Recommended Practice for Conventions Applicable to Electrochemical Measurements in Corrosion Testing, ASTM Designation: G3-.

19. M. Pourbaix, "Corrosion, Passivite et Passivation du Fer . Le Rôle du pH et du Potentiel," (Thesis Brussels, 1945, extrait), Memoires Soc. Roy. Belge Ingénieurs Industriels, No. 1 (Mars 1951).

20. R. T. Foley, "Role of the Chloride Ion in Iron Corrosion," Corrosion, 26 (Feb. 1970) 58 - 70.

21. M. Pourbaix, Significance of Protection Potential in Pitting and Intergranular Corrosion, Paper presented at the 1970 Corrosion Research Conference of NACE, Philadelphia (March 2 - 4, 1970).

22. C. Vanleugenhaghe, L. Klimczak-Mathieu, J. Meunier et M. Pourbaix, "Influence de Chlorures et D'oxydants sur le Comportement D'aciers Inoxydables en Solution Bicarbonique," Corrosion Science, 2 (1962) 29 - 35.

LIST OF GENERAL REFERENCES

A. M. Pourbaix, Atlas of Electrochemical Equilibria in Aqueous Solutions, Translated from the French by James A. Franklin, Pergamon Press (1966).

B. J. O'M. Bockris and B. E. Conway, Modern Aspects of Electrochemistry, Plenum Press (1969).

C. K. J. Vetter, Electrochemical Kinetics. Theoretical and Experimental Aspects, Translated by Scripta Technica, Inc., Academic Press (1967).

D. P. Delahay, Double Layer and Electrode Kinetics, Interscience Publishers (1966).

E. D. J. G. Ives, Reference Electrodes. Theory and Practice, Academic Press (1961).

F. R. F. Steigerwald, "Electrochemistry of Corrosion," Corrosion, 24 (Jan. 1968) 1 - 10.

G. M. Stern, "Fundamentals of Electrode Processes in Corrosion," Corrosion, 13 (Nov. 1957) 775t - 782t.

H. N. D. Greene, Experimental Electrode Kinetics, Rensselaer Polytechnic Institute, Troy, New York (1965).

I. M. Pourbaix, Lectures on Electrochemical Corrosion, Translated from the French by J. A. S. Green, Prepublication of a work to be published by Plenum Press, CEBELCOR (April 1967).

J. H. H. Uhlig, Corrosion and Corrosion Control, John Wiley and Sons, Inc. (1964).

K. C. E. Wicks and F. E. Block, Thermodynamic Properties of 65 Elements - Their Oxides, Halides, Carbides and Nitrides, Bulletin 605, Bureau of Mines (1963).

L. O. Kubaschewski and E. LL. Evans, Metallurgical Thermochemistry, Pergamon Press (1958).

M. Andre J. de Bethune and Nancy A. Swendeman Loud, Standard Aqueous Electrode Potentials and Temperature Coefficients at 25°C, Clifford A. Hampel, Skokie, Illinois (1964).

APPENDIX

LIST OF TABLES

LIST OF FIGURES

LIST OF FIGURES (Cont'd.)

LIST OF FIGURES (Cont'd.)

LIST OF FIGURES (Cont'd.)

TABLE I

Compositions of Binary Iron-Chromium Alloys Under Test

Alloy	C	Mn	P	S	Si	Cu	Ni	Cr	Source
1	0.15	1.3	0.011	0.037	0.22	0.09	0.12	0.5	USS
2	0.16	1.4	0.008	0.022	----	0.09	0.03	2.0	USS
3	0.16	1.4	0.010	0.022	0.19	0.09	0.04	5.0	USS
4	0.15 .20	--	NA	NA	NA	NA	----	12-13	NRL
5	0.17	1.3	0.014	0.018	0.17	0.09	0.11	16.9	USS
6	0.09	0.82	0.020	0.015	0.22	0.08	0.29	24.9	USS

USS - United States Steel Corporation, Monroeville, Pennsylvania

NRL - Naval Research Laboratory, Washington, D.C.

TABLE II

Test Solutions

Concentrations of Chloride ion (as NaCl) tested at each pH.

Nil, 10^{-4}, 10^{-3}, 10^{-2}, 10^{-1}, 10°, Saturated

pH	Buffer
4.5	0.0160M NaOH + .0740M $KHC_8H_4O_4$
5.5	0.0380M NaOH + 0.0520M $KHC_8H_4O_4$
7.0	0.0455M NaOH + 0.0455M $KHC_8H_4O_4$
8.9	0.1000M $NaHCO_3$
9.4	0.0020M NaOH + 0.0220M $Na_2B_4O_7.10H_2O$
11.0	0.0215M NaOH + 0.0100M $Na_2B_4O_7.10H_2O$
11.0	0.0012M NaOH

TABLE III

ALLOY Fe - 0.5 Cr - 0.15 C

Run No.	Log [Cl^-] (Log Molarity)	pH	E_o (Volts vs SCE)	E_{p_1} E_{pp} (Volts vs SCE)	Log i_{p_1} (i in amps/cm^2)	E_{p_2} (Volts vs SCE)	E_R (Volts vs SCE)	E_p (Volts vs SCE)
C-68	-6.0	5.5	-0.660	+0.200	-2.13	------	+1.240	-0.660
C-79	-6.0	5.5	-0.690	+0.260	-2.10	------	+1.240	-0.690
C-66	-6.0	8.7	-0.815	-0.640	-4.10	------	+0.960	+0.620
C-67	-6.0	8.7	-0.820	-0.640	-4.10	------	+0.960	+0.820
C-75	-6.0	10.8	-0.650	-0.420	-5.57	------	+0.820	-0.580
C-76	-6.0	10.8	-0.800	-0.410	-5.41	------	-0.820	+0.600
C-92	-3.0	5.5	-0.685	+0.320	-2.17	------	+0.330	-0.690
C-93	-3.0	5.5	-0.690	+0.230	-2.21	------	+0.250	-0.690
C-87	-3.0	8.7	-0.830	-0.640	-4.12	-0.270	+0.180	-0.310
C-88	-3.0	8.7	-0.810	-0.610	-4.00	-0.240	+0.230	-0.220
C-84	-3.0	10.7	-0.520	-0.410	-5.41	------	-0.190	-0.660
C-85	-3.0	10.7	-0.520	-0.440	-5.60	------	-0.200	-0.670
C-57	-2.0	5.5	-0.665	------	-----	------	------	-0.670
C-58	-2.0	5.5	-0.685	------	-----	------	------	-0.680
C-59	-2.0	8.7	-0.650	-0.610	-4.00	-0.215	-0.005	-0.270
C-60	-2.0	8.7	-0.675	-0.620	-4.17	-0.300	-0.035	-0.230
C-61	-2.0	11.0	-0.440	-0.380	-6.08	------	-0.240	-0.690
C-63	-2.0	11.0	-0.480	-0.440	-5.52	------	-0.270	-0.680
C-29	-1.0	4.5	-0.675	------	-----	------	------	-0.615
C-30	-1.0	4.5	-0.665	------	-----	------	------	-0.620
C-27	-1.0	5.5	-0.670	------	-----	------	------	-0.670
C-28	-1.0	5.5	-0.670	------	-----	------	------	-0.680
C-25	-1.0	7.0	-0.745	-0.370	-2.85	------	-0.230	-0.720
C-26	-1.0	7.0	-0.770	-0.370	-2.85	------	-0.230	-0.730
C-23	-1.0	8.9	-0.750	-0.580	-3.83	------	-0.410	-0.565
C-24	-1.0	8.9	-0.790	-0.650	-4.35	------	-0.425	-0.525
C-16	-1.0	9.3	-0.820	-0.675	-5.00	------	-0.240	-0.600
C-18	-1.0	9.3	-0.840	-0.640	-5.02	------	-0 240	-0.570
C-31	-1.0	11.0	-0.845	-0.775	-5.48	-0.455	-0.385	-0.760
C-32	-1.0	11.0	-0.900	-0.755	-5.15	-0.470	-0.410	-0.770

Continued

TABLE III (Continued)

ALLOY Fe - 0.5 Cr - 0.15 C

Run No.	Log [Cl^-] (Log Molarity)	pH	E_o (Volts vs SCE)	E_{p_1} E_{pp} (Volts vs SCE)	Log i_{p_1} (i in amps/cm^2)	E_{p_2} (Volts vs SCE)	E_R (Volts vs SCE)	E_P (Volts vs SCE)
C-100	0.0	4.9	-0.650	------	-----	------	------	-0.650
C-101	0.0	4.9	-0.650	------	-----	------	------	-0.650
C-96	0.0	8.3	-0.800	-0.610	-3.75	------	-0.440	-0.745
C-97	0.0	8.3	-0.790	-0.610	-4.10	------	-0.460	-0.760
C-103	0.0	10.6	-0.470	------	-----	------	------	-0.745
C-104	0.0	10.6	-0.525	------	-----	------	------	-0.680
C-119	0.8	4.6	-0.645	------	-----	------	------	-0.630
C-120	0.8	4.6	-0.640	------	-----	------	------	-0.630
C-110	0.8	7.6	-0.760	-0.595	-4.05	------	-0.410	-0.580
C-111	0.8	7.6	-0.775	-0.605	-4.15	------	-0.425	-0.550
C-117	0.8	10.6	-0.875	-0.735	-5.69	------	-0.495	-0.765
C-118	0.8	10.6	-0.840	-0.670	-5.69	------	-0.510	-0.720

TABLE IV

ALLOY Fe - 2.0 Cr - 0.16 C

Run No.	Log [Cl^-] (Log Molarity)	pH	E_o (Volts vs SCE)	E_{p_1} E_{pp} (Volts vs SCE)	Log i_{p_1} (i in amps/cm^2)	E_{p_2} (Volts vs SCE)	E_R (Volts vs SCE)	E_p (Volts vs SCE)
C-70	-6.0	5.5	-0.690	-0.050	-3.58	+0.520	+1.020	+0.150
C-72	-6.0	5.5	-0.660	-0.110	-3.54	+0.540	+0.990	+0.090
C-64	-6.0	8.7	-0.780	-0.610	-5.67	-0.260	+0.880	+0.370
C-65	-6.0	8.7	-0.800	-0.610	-5.72	-0.270	+0.850	+0.430
C-55	-6.0	11.0	-0.420	-0.410	-7.81	------	+0.810	-0.560
C-56	-6.0	11.0	-0.500	-0.410	-6.48	------	+0.770	-0.620
C-89	-3.0	5.5	-0.660	+0.020	-3.57	------	+0.040	-0.660
C-90	-3.0	5.5	-0.660	-0.010	-3.56	------	+0.080	-0.660
C-78	-3.0	8.8	-0.800	-0.610	-5.61	------	+0.900	-0.110
C-79	-3.0	8.8	-0.810	-0.640	-5.68	------	+0.900	------
C-82	-3.0	10.8	-0.470	-0.410	-6.36	------	-0.120	-0.640
C-86	-3.0	10.8	-0.470	-0.410	-6.36	------	-0.120	-0.640
C-49	-2.0	5.5	-0.660	-0.080	-3.60	------	-0.060	-0.670
C-50	-2.0	5.5	-0.670	-0.090	-3.59	------	-0.075	-0.670
C-52	-2.0	8.7	-0.780	-0.640	-5.61	-0.240	-0.070	-0.285
C-53	-2.0	8.7	-0.760	-0.610	-5.71	-0.205	-0.005	-0.330
C-80	-2.0	10.8	-0.720	-0.410	-6.70	------	-0.250	-0.720
C-81	-2.0	10.8	-0.520	-0.410	-6.74	------	-0.270	-0.660
C-37	-1.0	4.5	-0.635	+0.050	-1.90	------	+0.050	-0.620
C-38	-1.0	4.5	-0.635	+0.075	-1.90	------	+0.075	-0.620
C-35	-1.0	5.4	-0.663	-0.180	-2.25	------	-0.130	-0.660
C-36	-1.0	5.4	-0.670	-0.160	-2.30	------	-0.155	-0.670
C-33	-1.0	6.9	-0.720	-0.390	-3.05	------	-0.195	-0.735
C-34	-1.0	6.9	-0.730	-0.400	-3.15	------	-0.200	-0.700
C-39	-1.0	8.8	-0.820	-0.635	-4.45	------	-0.355	-0.560
C-40	-1.0	8.8	-0.820	-0.650	-4.35	------	-0.385	-0.545
C-41	-1.0	9.3	-0.735	-0.620	-5.35	------	-0.230	-0.580
C-42	-1.0	9.3	-0.775	-0.620	-5.15	------	-0.230	-0.580
C-47	-1.0	11.0	-0.790	-0.475	-5.35	------	-0.370	-0.705
C-48	-1.0	11.0	-0.690	-0.440	-5.35	------	-0.370	-0.760

Continued

TABLE IV (Continued)

ALLOY Fe - 2.0 Cr - 0.16 C

Run No.	Log [Cl^-] (Log Molarity)	pH	E_o (Volts vs SCE)	E_{p_1} E_{pp} (Volts vs SCE)	Log i_{p_1} (i in amps/cm^2)	E_{p_2} (Volts vs SCE)	E_R (Volts vs SCE)	E_P (Volts vs SCE)
C-98	0.0	4.9	-0.640	------	-----	------	------	-0.640
C-99	0.0	4.9	-0.640	------	-----	------	------	-0.640
C-94	0.0	8.2	-0.800	-0.585	-4.04	------	-0.425	-0.640
C-95	0.0	8.2	-0.800	-0.595	-4.00	------	-0.440	-0.765
C-106	0.0	10.6	-0.775	-0.450	-5.25	------	-0.440	-0.700
C-107	0.0	10.6	-0.800	-0.455	-6.95	------	-0.425	-0.750
C-112	0.8	4.5	-0.620	------	-----	------	------	-0.620
C-113	0.8	4.5	-0.635	------	-----	------	------	-0.635
C-108	0.8	7.6	-0.755	-0.610	-5.60	------	-0.435	-0.580
C-109	0.8	7.6	-0.760	-0.610	-5.51	------	-0.455	-0.610
C-115	0.8	10.6	-0.710	------	-----	------	-0.495	-0.765
C-116	0.8	10.6	-0.710	------	-----	------	-0.525	-0.760

TABLE V

ALLOY Fe - 5 Cr - 0.16 C

Run No.	Log [Cl^-] (Log Molarity)	pH	E_o (Volts vs SCE)	E_{p_1} E_{pp} (Volts vs SCE)	Log i_{p_1} (i in amps/cm^2)	E_{p_2} (Volts vs SCE)	E_R (Volts vs SCE)	E_P (Volts vs SCE)
J-8	-1.0	4.5	-0.645	-0.315	-2.88	------	-0.205	-0.630
J-9	-1.0	4.4	-0.665	-0.290	-2.74	------	-0.195	-0.620
J-10	-1.0	5.5	-0.665	-0.380	-3.08	------	-0.230	-0.675
J-11	-1.0	5.4	-0.675	-0.385	-3.10	------	-0.230	-0.675
J-12	-1.0	6.9	-0.740	-0.500	-3.68	------	-0.155	-0.730
J-13	-1.0	6.9	-0.725	-0.490	-3.74	------	-0.235	-0.695
J-14	-1.0	8.9	-0.800	-0.650	-4.86	------	-0.180	-0.570
J-15	-1.0	8.9	-0.810	-0.630	-4.79	------	-0.200	-0.510
J-16	-1.0	9.4	-0.710	-0.460	-5.42	------	-0.285	-0.460
J-17	-1.0	9.4	------	------	-----	------	------	-0.550
J-18	-1.0	9.4	-0.500	-0.325	-5.13	------	-0.280	-0.530
J-19	-1.0	9.3	-0.785	-0.450	-5.47	------	-0.135	-0.525
J-20	-1.0	11.1	-0.390	------	-----	------	-0.075	-0.610
J-21	-1.0	11.1	-0.535	-0.490	-5.22	------	-0.075	-0.610

TABLE VI

ALLOY Fe - 12 Cr - 0.15 C

Run No.	Log [Cl^-] (Log Molarity)	pH	E_o (Volts vs SCE)	E_{p_i} E_{pp} (Volts vs SCE)	Log i_{p_1} (i in amps/cm^2)	E_{p_2} (Volts vs SCE)	E_R (Volts vs SCE)	E_P (Volts vs SCE)
S-36	-6.0	5.4	-0.610	-0.500	-4.84	------	+1.140	+1.120
S-37	-6.0	5.4	-0.610	-0.490	-4.84	------	+1.160	+1.120
S-34	-6.0	8.6	-0.800	-0.660	-5.00	-0.360	+0.920	+0.900
S-35	-6.0	8.7	-0.790	-0.640	-5.07	-0.380	+0.840	+0.760
S-38	-6.0	10.8	-0.680	-0.450	-5.57	------	+0.780	+0.770
S-39	-6.0	10.8	-0.550	-0.440	-5.55	------	+0.780	+0.740
S-44	-3.0	5.4	-0.630	-0.510	-4.72	------	+1.170	+1.130
S-45	-3.0	5.4	-0.630	-0.500	-4.72	------	+1.180	+1.120
S-42	-3.0	8.7	-0.800	-0.660	-5.03	-0.320	+0.920	+0.900
S-43	-3.0	8.7	-0.800	-0.640	-5.00	-0.300	+0.960	+0.920
S-40	-3.0	10.7	-0.660	-0.460	-5.48	------	+0.640	-0.510
S-41	-3.0	10.7	-0.720	-0.460	-5.52	------	+0.600	-0.480
S-28	-2.0	5.5	-0.610	-0.470	-4.88	------	+0.310	-0.200
S-29	-2.0	5.5	-0.630	-0.510	-4.59	------	+0.315	-0.190
S-32	-2.0	8.7	-0.800	-0.660	-5.07	-0.300	+0.900	+0.900
S-33	-2.0	8.7	-0.800	-0.660	-5.01	-0.300	+0.900	+0.900
S-30	-2.0	10.6	-0.580	-0.450	-5.33	------	+0.220	-0.530
S-31	-2.0	10.7	-0.560	-0.460	-5.40	------	+0.360	-0.540
S-20	-2.0	10.9	-0.780	-0.480	-5.42	------	+0.600	-0.470
S-21	-2.0	10.9	-0.480	-0.450	-5.96	------	+0.600	-0.520
S-14	-1.0	4.6	-0.580	-0.420	-4.62	------	-0.040	-0.350
S-15	-1.0	4.6	-0.580	-0.430	-4.65	------	-0.040	-0.230
S-12	-1.0	5.4	-0.610	-0.470	-4.74	------	+0.010	-0.220
S-13	-1.0	5.4	-0.600	-0.470	-4.87	------	+0.020	-0.180
S-11	-1.0	6.8	-0.700	-0.560	-4.96	------	+0.060	-0.145
S-8	-1.0	6.9	-0.700	-0.550	-4.90	------	+0.010	-0.220
S-9	-1.0	6.9	-0.695	-0.550	-4.90	------	+0.060	-0.130
S-10	-1.0	6.9	-0.340	------	-----	------	+0.020	-0.200
S-18	-1.0	8.9	-0.740	-0.600	-5.70	-0.180	+0.175	-0.440

Continued

TABLE VI (Continued)

ALLOY Fe - 12 Cr - 0.15 C

Run No.	Log [Cl^-] (Log Molarity)	pH	E_o (Volts vs SCE)	E_{p_1} E_{pp} (Volts vs SCE)	Log i_{p_1} (i in amps/cm^2)	E_{p_2} (Volts vs SCE)	E_R (Volts vs SCE)	E_p (Volts vs SCE)
S-19	-1.0	8.9	-0.725	-0.620	-5.55	-0.290	+0.145	-0.425
S-3	-1.0	9.2	-0.570	-0.330	-5.55	------	+0.080	-0.460
S-7	-1.0	9.2	-0.740	-0.320	-5.36	------	+0.060	-0.400
S-1	-1.0	9.3	-0.660	-0.330	-5.46	------	+0.120	-0.420
S-2	-1.0	9.3	-0.510	-0.345	-5.46	------	+0.020	-0.480
S-4	-1.0	10.7	-0.800	-0.445	-5.27	------	+0.210	-0.450
S-5	-1.0	10.7	-0.720	-0.460	-5.24	------	-0.040	-0.540
S-6	-1.0	10.7	-0.830	-0.470	-5.37	------	+0.120	-0.580
S-48	0.0	4.9	-0.590	-0.420	-4.72	------	-0.210	-0.480
S-49	0.0	4.9	-0.590	-0.420	-4.68	------	-0.170	-0.480
S-47	0.0	8.2	-0.775	-0.650	-5.00	------	+0.050	-0.530
S-46	0.0	8.3	-0.785	-0.650	-4.99	------	+0.140	-0.350
S-50	0.0	10.3	-0.840	-0.450	-5.00	------	-0.120	-0.845
S-51	0.0	10.4	-0.780	-0.450	-5.30	------	-0.140	-0.700
S-55	0.78	4.3	-0.565	------	-----	------	-0.345	-0.510
S-56	0.78	4.3	-0.575	------	-----	------	-0.365	-0.535
S-52	0.78	7.7	-0.810	-0.660	-4.53	------	-0.240	-0.550
S-53	0.78	7.7	-0.780	-0.600	-5.00	------	-0.175	-0.405
S-54	0.78	7.7	-0.760	-0.570	-5.16	------	-0.130	-0.540
S-57	0.78	10.4	-0.900	-0.450	-4.98	------	-0.215	-0.620
S-58	0.78	10.4	-0.870	-0.450	-5.25	------	-0.230	-0.705

TABLE VII

ALLOY Fe - 16.9 Cr - 0.17 C

Run No.	Log [Cl^-] (Log Molarity)	pH	E_o (Volts vs SCE)	E_{p_1} E_{pp} (Volts vs SCE)	Log i_{p_1} (i in amps/cm^2)	E_{p_2} (Volts vs SCE)	E_R (Volts vs SCE)	E_P (Volts vs SCE)
J-50	-6.0	5.4	-0.600	-0.530	-5.03	+0.900	+1.000	+0.830
J-51	-6.0	5.4	-0.620	-0.540	-5.04	+0.900	+1.000	+0.810
J-48	-6.0	8.7	-0.760	-0.640	-5.32	+0.760	+0.900	+0.560
J-49	-6.0	8.7	-0.780	-0.660	-5.24	+0.760	+0.920	+0.560
J-46	-6.0	10.8	-0.680	-0.460	-5.48	+0.520	+0.560	+0.400
J-47	-6.0	10.8	-0.520	-0.440	-5.50	+0.530	+0.560	+0.460
J-52	-3.0	5.4	-0.610	-0.540	-5.03	+0.920	+1.03	+0.840
J-53	-3.0	5.4	-0.630	-0.550	-5.00	+0.890	+0.990	+0.770
J-54	-3.0	8.8	-0.730	-0.630	-5.60	+0.760	+0.920	+0.570
J-55	-3.0	8.8	-0.740	-0.650	-5.50	+0.780	+0.940	+0.580
J-56	-3.0	10.8	-0.530	-0.450	-5.57	------	+0.400	-0.280
J-57	-3.0	10.7	-0.480	-0.430	-5.62	------	+0.340	-0.220
J-58	-3.0	10.8	-0.470	-0.410	-5.58	------	+0.400	-0.120
J-38	-2.0	5.4	-0.640	-0.550	-5.14	------	+0.570	+0.070
J-39	-2.0	5.4	-0.620	-0.520	-5.08	------	+0.650	-0.010
J-40	-2.0	8.8	-0.490	-0.280	-5.33	------	+0.470	+0.510
J-41	-2.0	8.9	-0.800	-0.650	-5.25	------	+0.380	+0.520
J-42	-2.0	8.9	-0.790	-0.680	-5.30	+0.730	+0.860	+0.500
J-43	-2.0	10.7	-0.520	-0.460	-5.33	------	+0.160	-0.080
J-44	-2.0	10.7	-0.540	-0.480	-5.40	------	+0.050	-0.390
J-45	-2.0	10.8	-0.530	-0.470	-5.45	------	+0.360	-0.080
J-26	-1.0	4.4	-0.610	-0.560	-4.76	------	+0.140	-0.220
J-27	-1.0	4.4	-0.590	-0.510	-4.88	------	+0.170	-0.160
J-28	-1.0	5.4	-0.660	-0.600	-4.87	------	+0.140	-0.080
J-29	-1.0	5.4	-0.630	-0.570	-5.06	------	+0.130	-0.105
J-30	-1.0	7.0	-0.690	-0.560	-5.18	------	+0.010	-0.100
J-31	-1.0	7.0	-0.710	-0.570	-5.07	------	+0.020	-0.080
J-32	-1.0	8.8	-0.710	0.690	-5.81	-0.280	+0.090	-0.280

Continued

TABLE VII (Continued)

ALLOY Fe - 16.9 Cr - 0.17 C

Run No.	Log [Cl^-] (Log Molarity)	pH	E_o (Volts vs SCE)	E_{p_1} E_{pp} (Volts vs SCE)	Log i_{p_1} (i in amps/cm^2)	E_{p_2} (Volts vs SCE)	E_R (Volts vs SCE)	E_P (Volts vs SCE)
J-33	-1.0	8.8	-0.770	-0.660	-5.31	-0.300	+0.090	-0.280
J-34	-1.0	9.5	-0.670	-0.360	-5.38	------	+0.120	-0.320
J-35	-1.0	9.5	-0.680	-0.370	-5.39	------	+0.160	-0.300
J-36	-1.0	10.9	-0.540	-0.480	-5.30	------	+0.210	-0.060
J-37	-1.0	10.9	-0.680	-0.500	-5.26	------	+0.200	+0.020
J-59	0.0	4.9	-0.610	-0.530	-5.00	------	-0.040	-0.250
J-60	0.0	4.9	-0.580	-0.520	-5.30	------	-0.060	-0.220
J-61	0.0	8.2	-0.690	-0.630	-5.87	-0.260	-0.060	-0.220

TABLE VIII

ALLOY Fe - 24.9 Cr - 0.09 C

Run No.	Log [Cl^-] (Log Molarity)	pH	E_o (Volts vs SCE)	E_{p_1} E_{pp} (Volts vs SCE)	Log i_{p_1} (i in amps/cm^2)	E_{p_2} (Volts vs SCE)	E_R (Volts vs SCE)	E_p (Volts vs SCE)
E-1	-1.0	4.6	-0.550	-0.480	-5.34	------	+0.330	+0.140
E-2	-1.0	4.6	-0.550	-0.420	-5.42	------	+0.350	-0.050
E-3	-1.0	5.3	-0.590	-0.490	-5.42	------	+0.320	+0.070
E-4	-1.0	5.3	-0.550	-0.280	-5.41	------	+0.330	+0.090
E-5	-1.0	6.9	-0.470	-0.230	-5.62	------	+0.350	-0.050
E-6	-1.0	6.9	-0.560	-0.230	-5.55	------	+0.270	-0.030
E-7	-1.0	8.9	-0.440	-0.330	-5.85	------	+0.420	+0.050
E-8	-1.0	8.9	-0.530	-0.350	-5.57	------	+0.440	-0.150
E-9	-1.0	9.3	-0.550	-0.380	-5.70	------	+0.300	-0.300
E-10	-1.0	9.3	-0.530	-0.360	-5.77	------	+0.400	-0.350
E-11	-1.0	11.1	-0.650	-0.510	-5.85	------	+0.430	-0.370
E-12	-1.0	11.1	-0.510	-0.430	-5.89	------	+0.420	-0.340

TABLE IX

1. Magna Anatrol Potentiostat Model 4700M with attached Linear-Scan Model 4510.
2. Hewlett-Packard Sanborn Differential Amplifier Model 8875A.
3. Hewlett-Packard Logarithmic Converter Model 7561A.
4. Varian X - Y Recorder Model F110 (X - Y).
5. Leeds and Northrup Standard 1191-31 Calomel Reference Electrode.
6. Keithley Electrometer Model 602.
7. Keithley pH Electrode Adapter Model 6013.
8. Hewlett-Packard Moseley Model 680 Strip Chart Recorder.
9. E/MC Corporation Ultrasonic Cleaner Model BP-1.
10. Duo Seal Vacuum Pump Model 1405H.

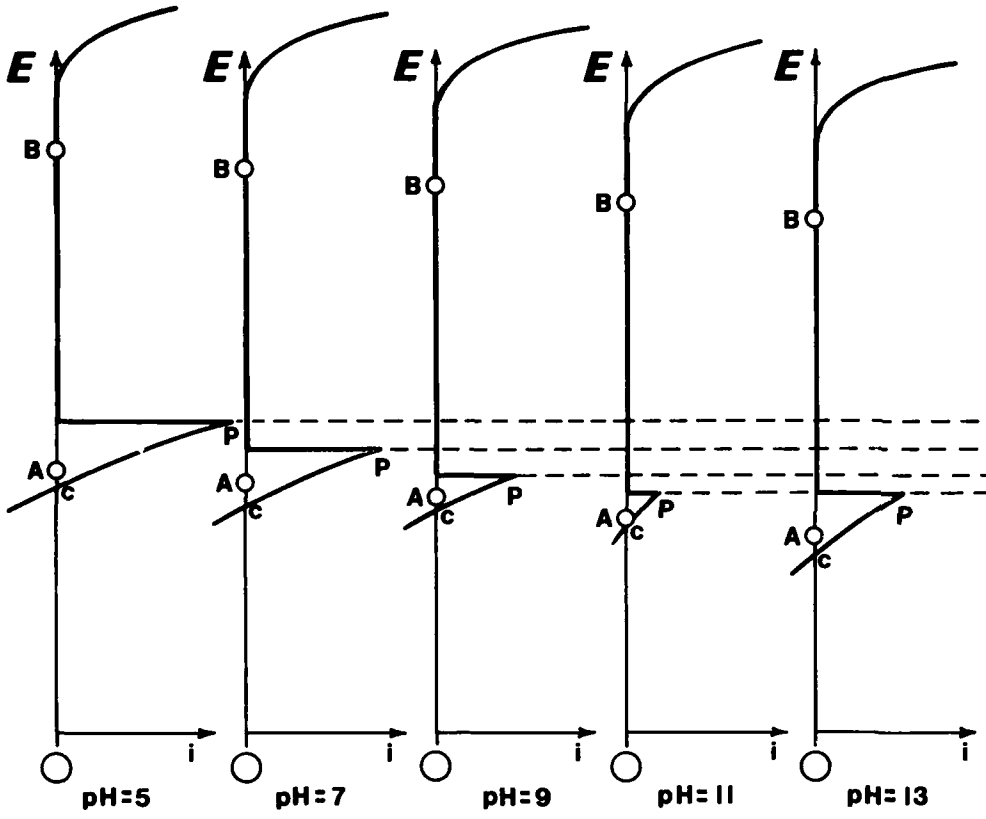

FIGURE 1a: Standard Potentiokinetic Polarization Curves for Armco Iron in Chloride Free Solutions of Various pHs.

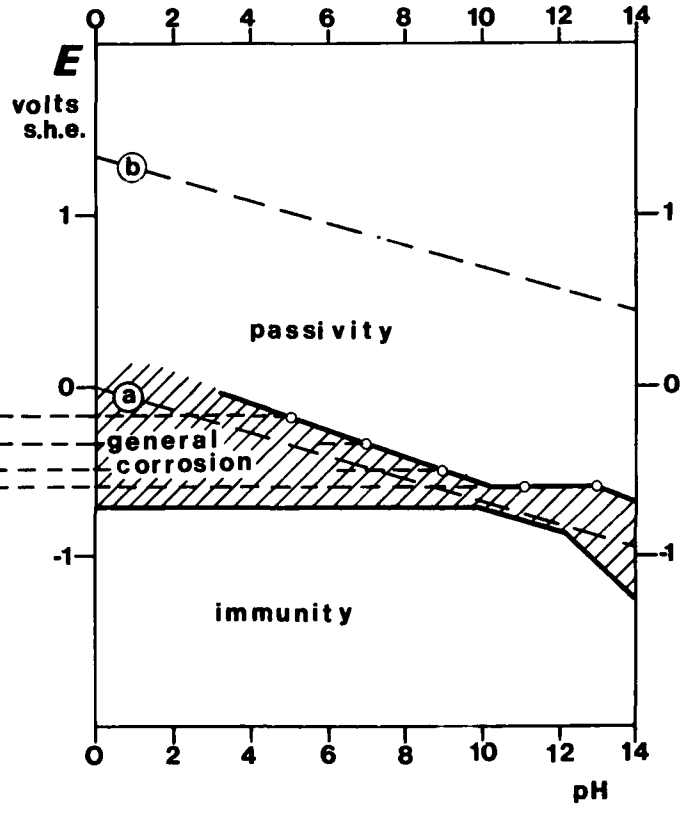

FIGURE 1b: Experimental Pourbaix Diagram Constructed from Data in Figure 1a.

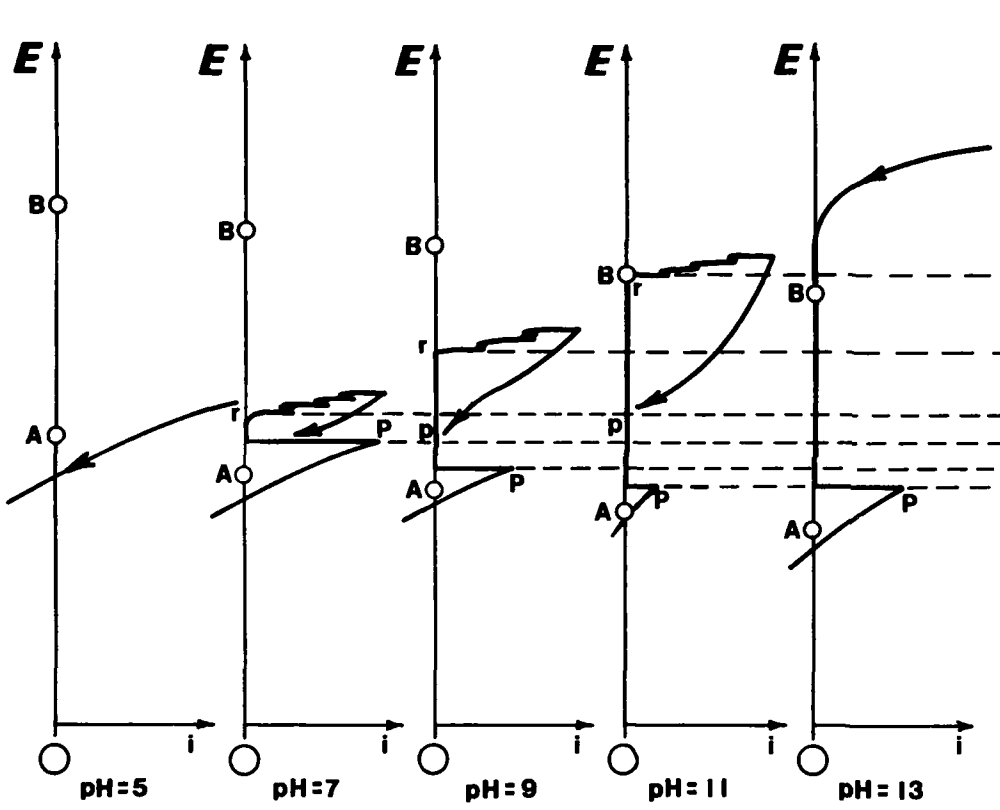

FIGURE 2a: Potentiokinetic Polarization Curves Using Electrochemical Hysteresis Method for Armco Iron in 10^{-2} Molar Chloride Solutions of Various pHs.

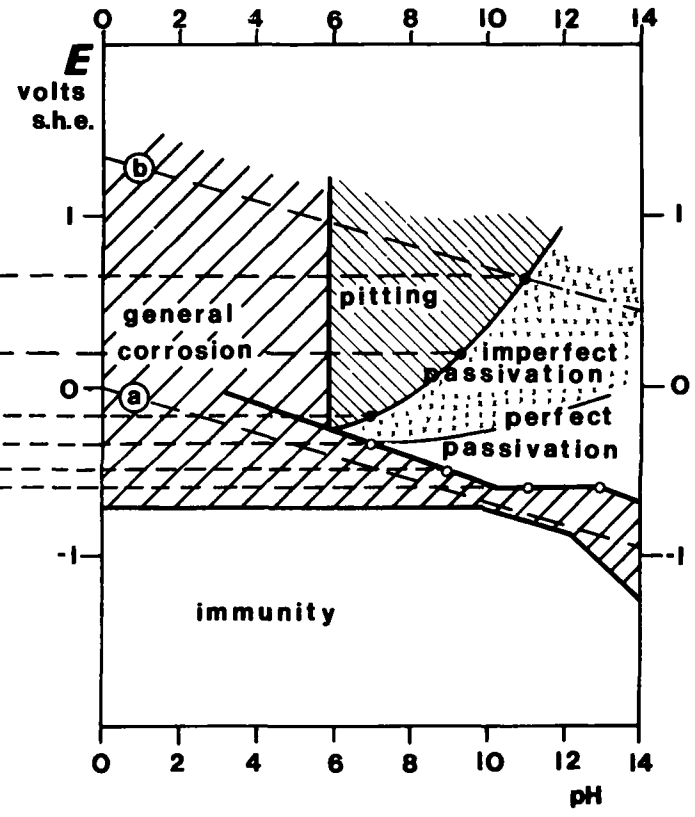

FIGURE 2b: Experimental Pourbaix Diagram Constructed from Electrochemical Hysteresis Data in Figure 2a.

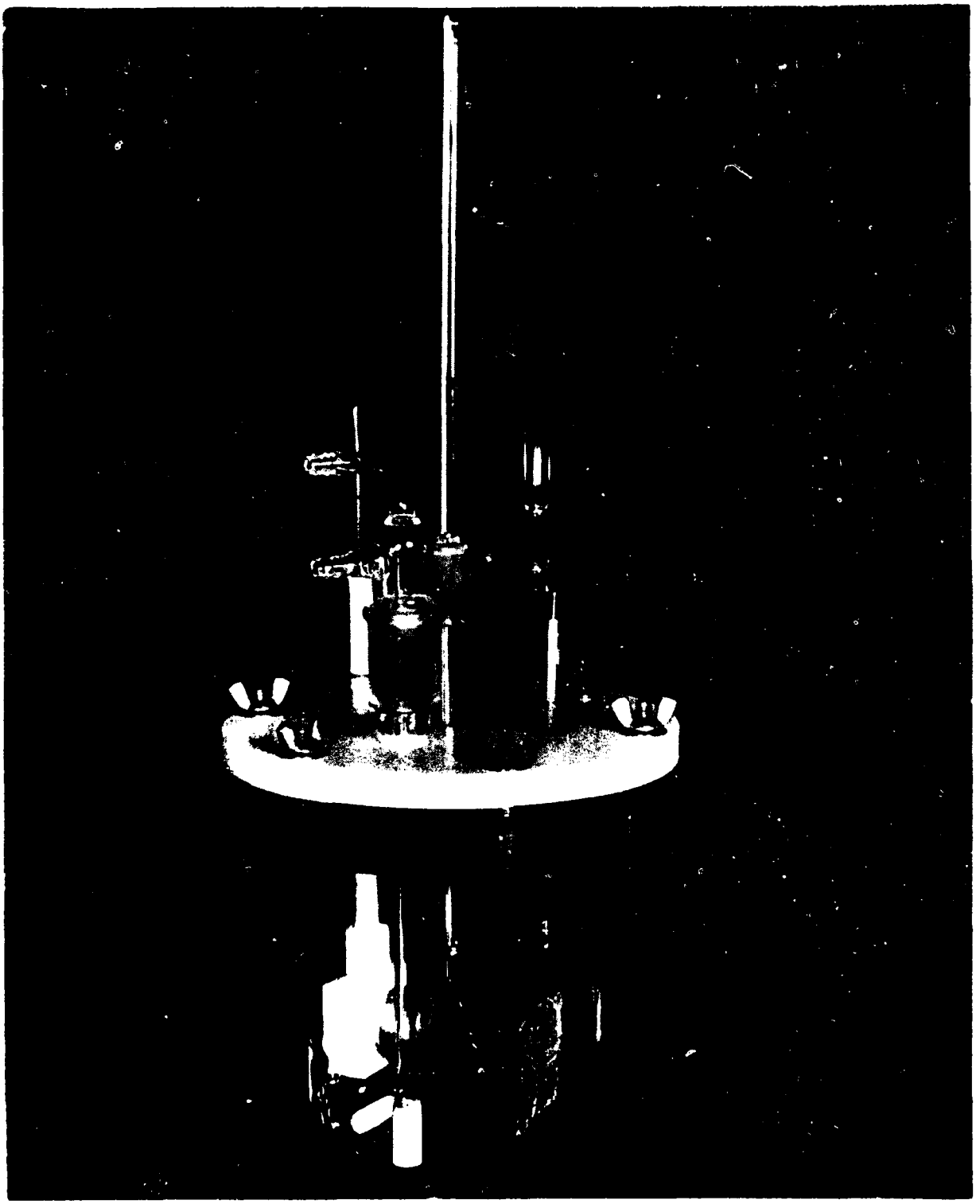

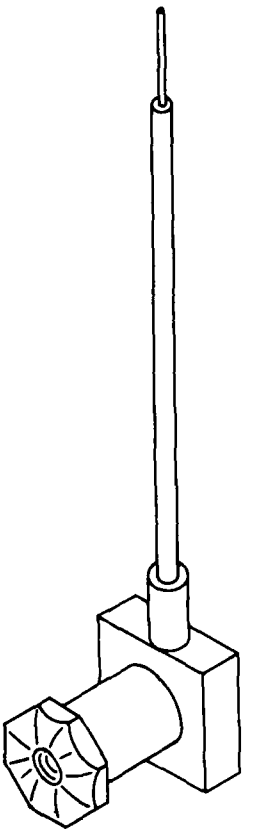

DISK SPECIMEN HOLDER

FIGURE 3b: Assembled View of Specimen Holder.

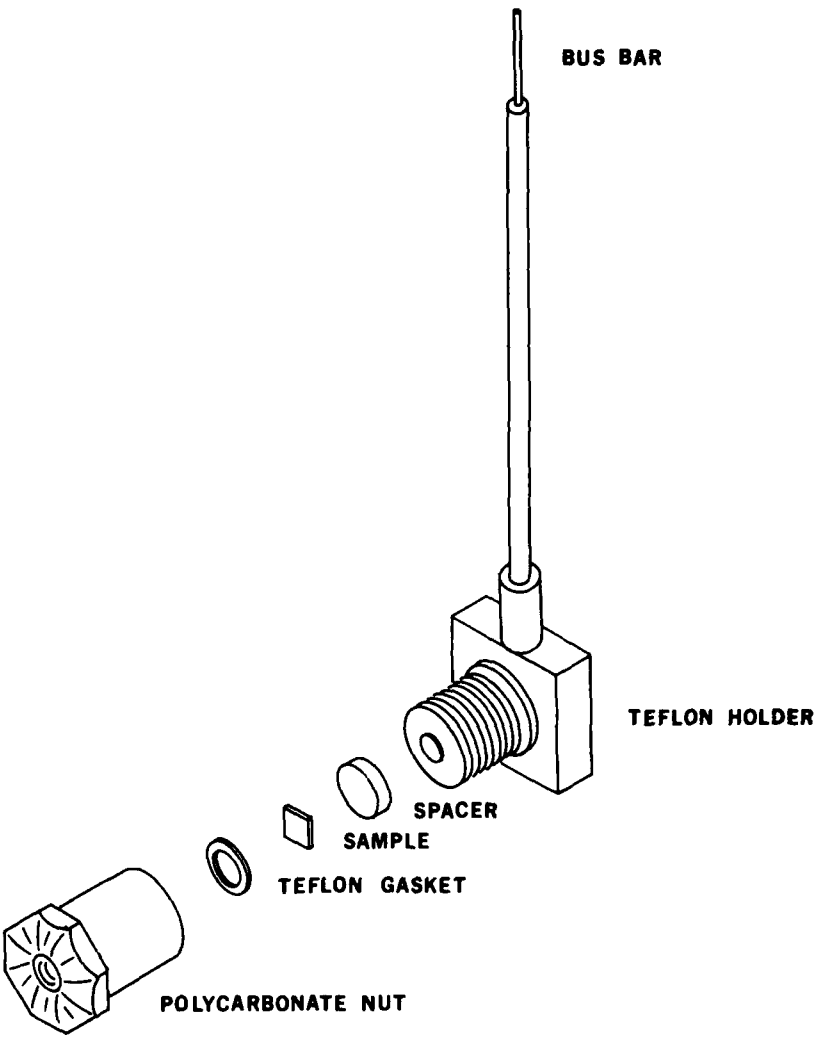

FIGURE 3c: Exploded View of Specimen Holder.

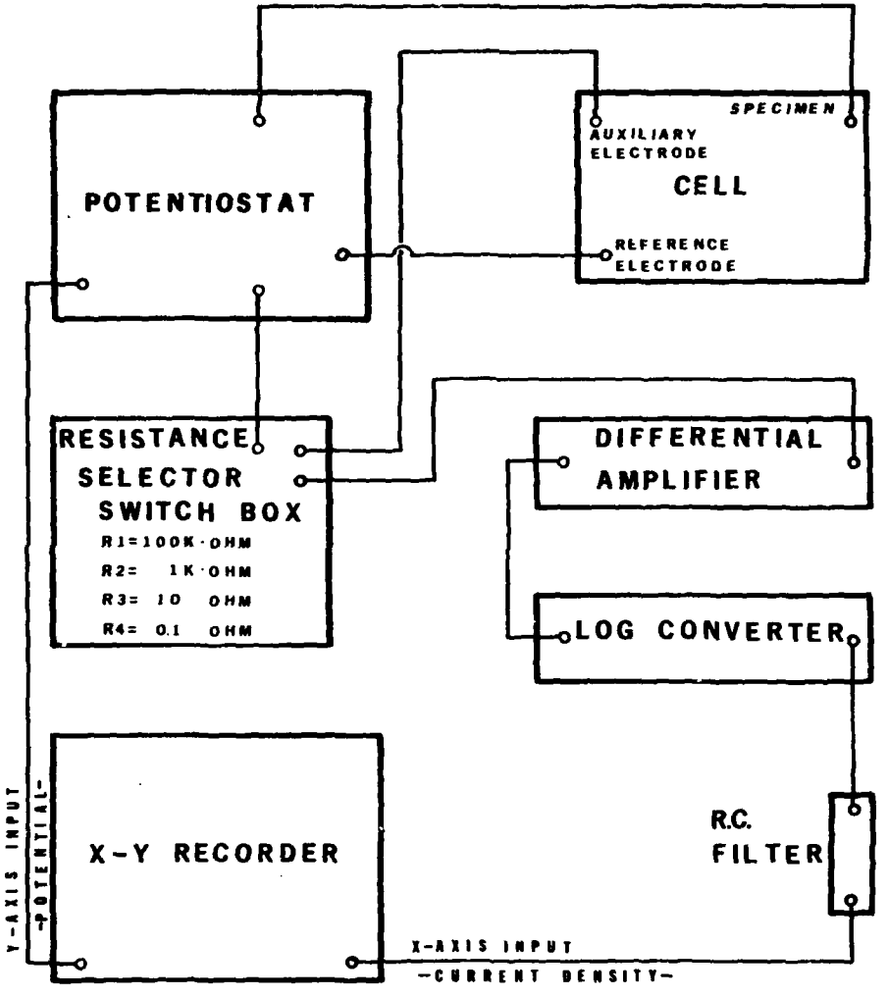

FIGURE 4: Schematic Diagram of Equipment Used.

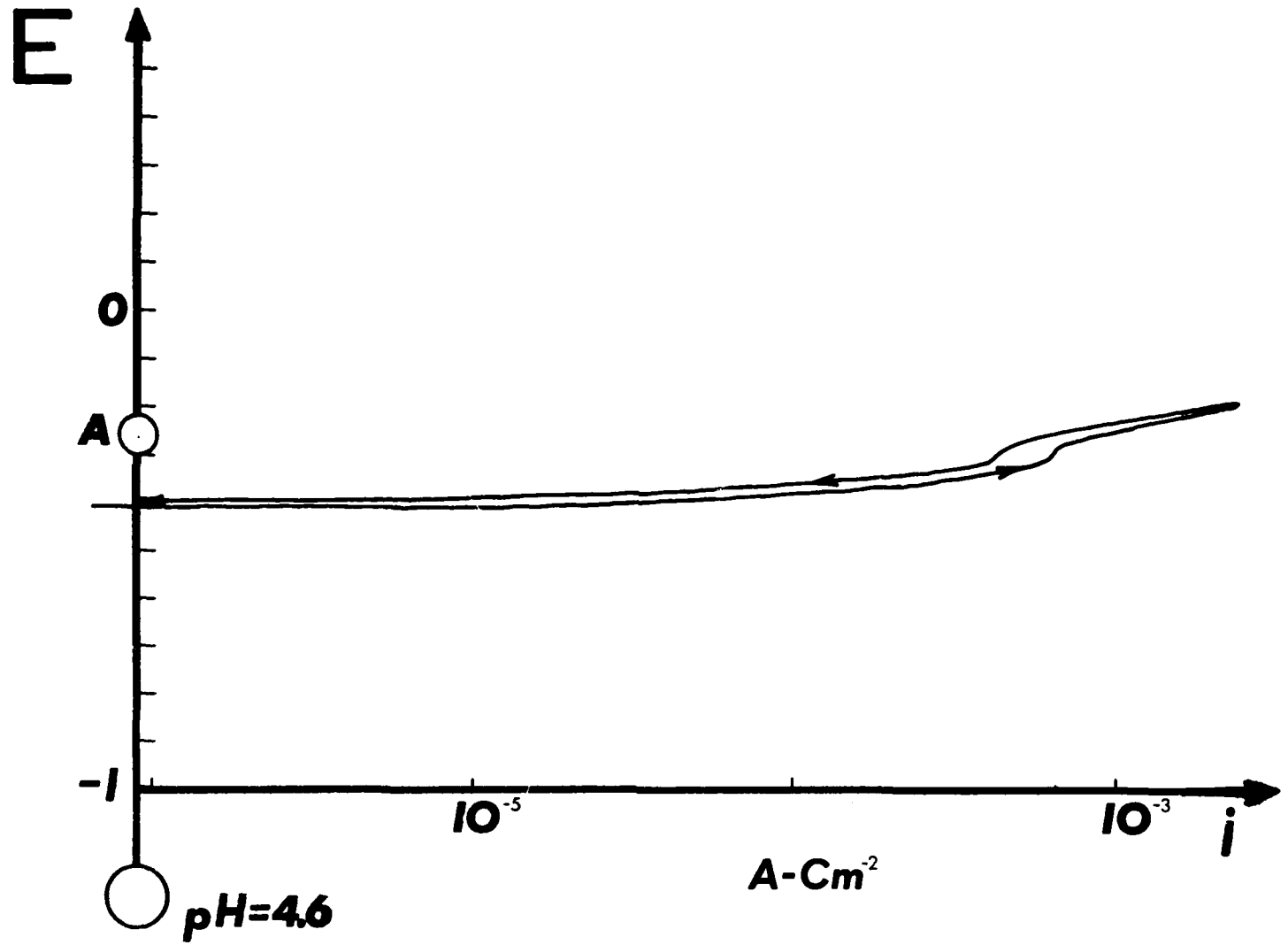

FIGURE 5: Potentiokinetic Curve (Potential versus Current Density) 0.5% Chromium Alloy, pH = 4.6.

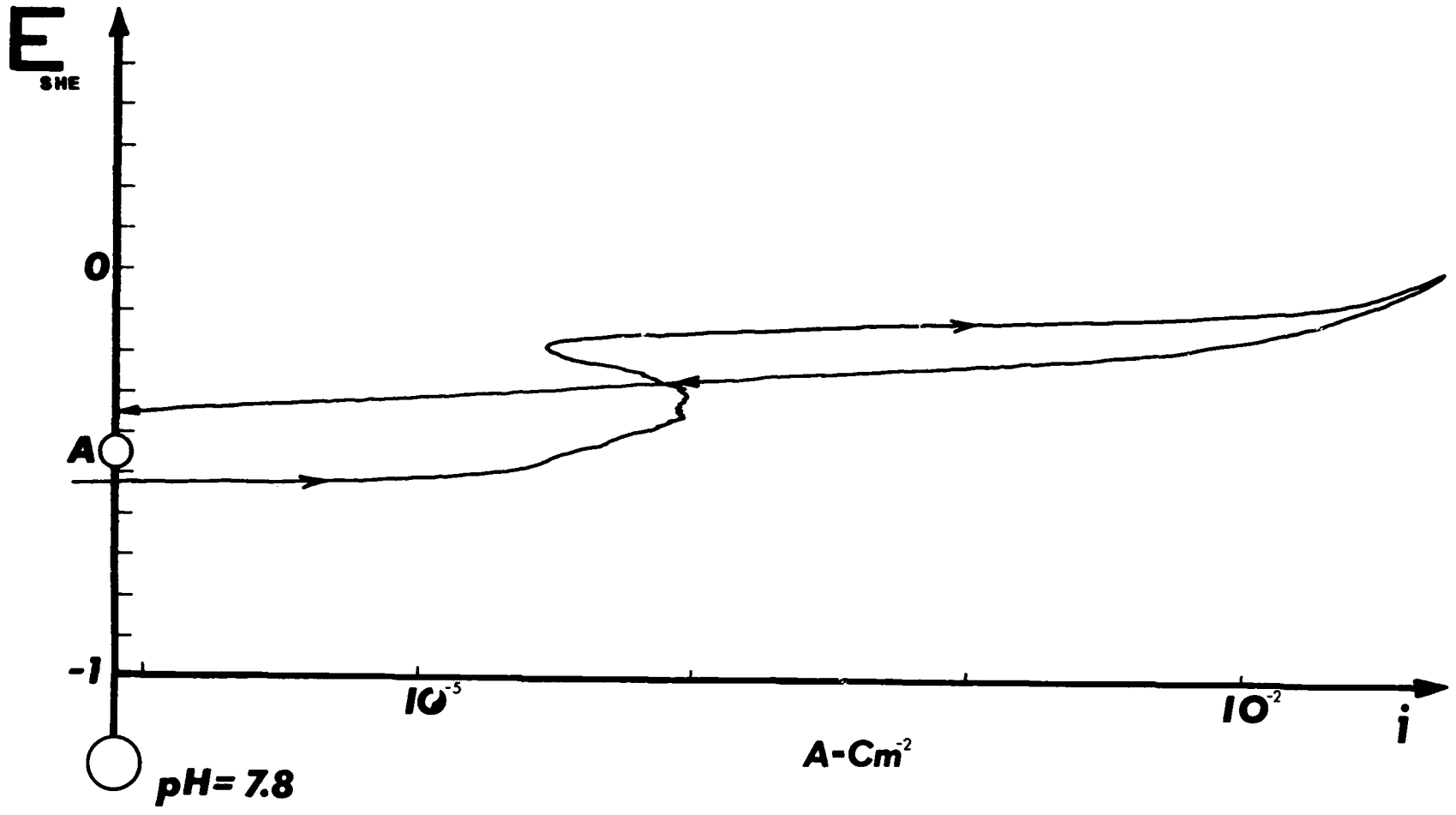

FIGURE 6: Potentiokinetic Curve (Potential versus Current Density) 0.5% Chromium Alloy, pH = 7.8.

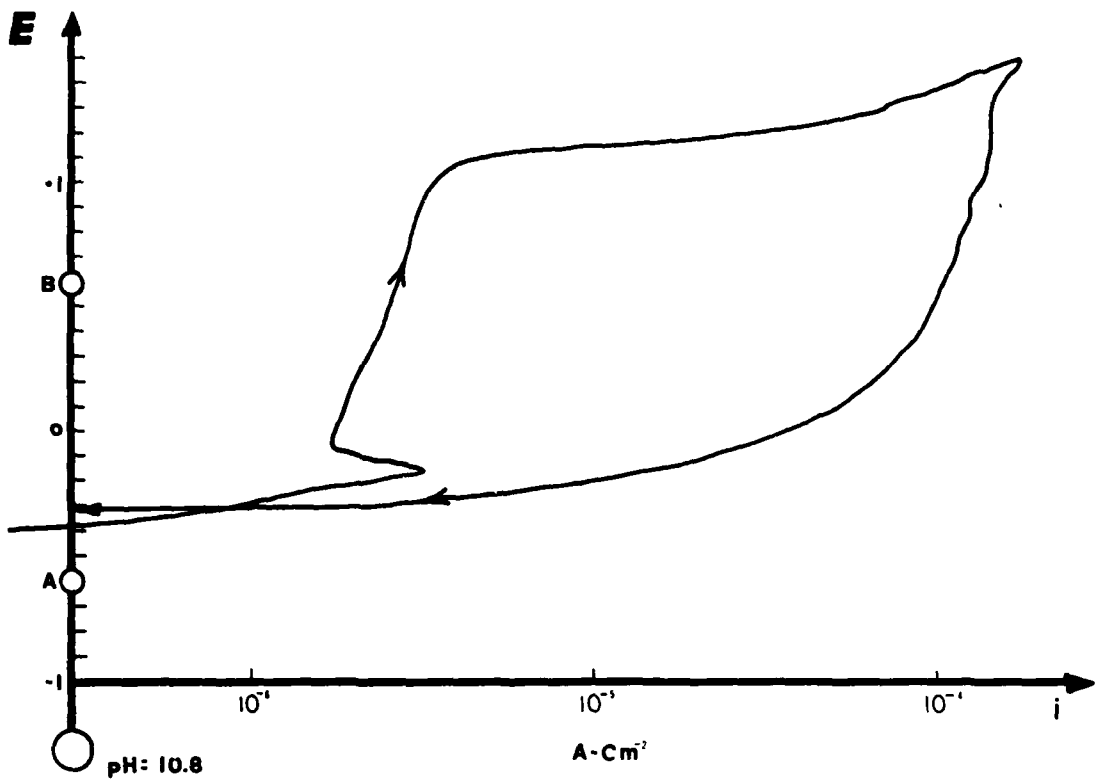

FIGURE 7: Potentiokinetic Curve (Potential versus Current Density). 0.5% Chromium Alloy, pH = 10.8.

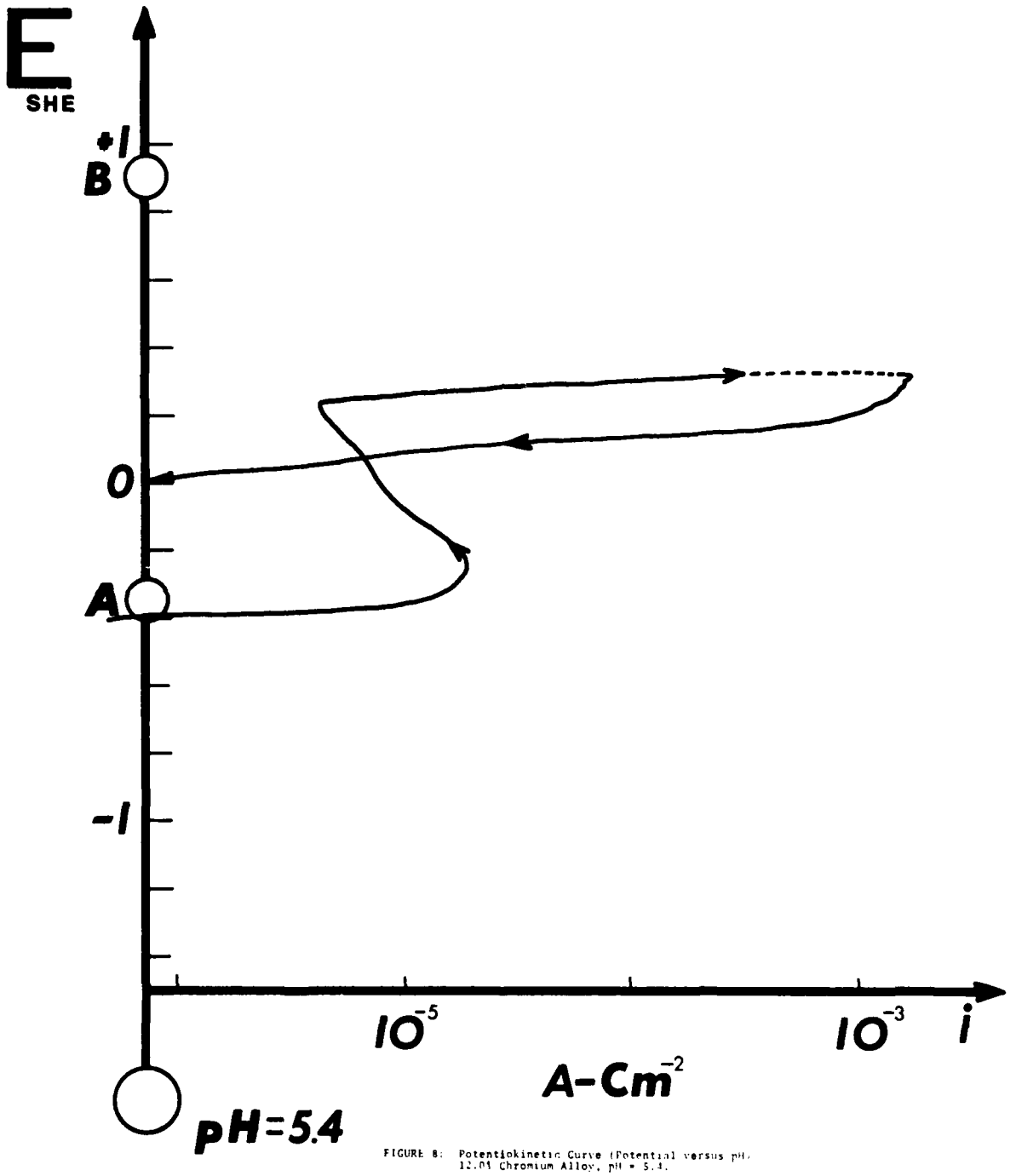

FIGURE 8: Potentiokinetic Curve (Potential versus pH) 12.0% Chromium Alloy, pH = 5.4.

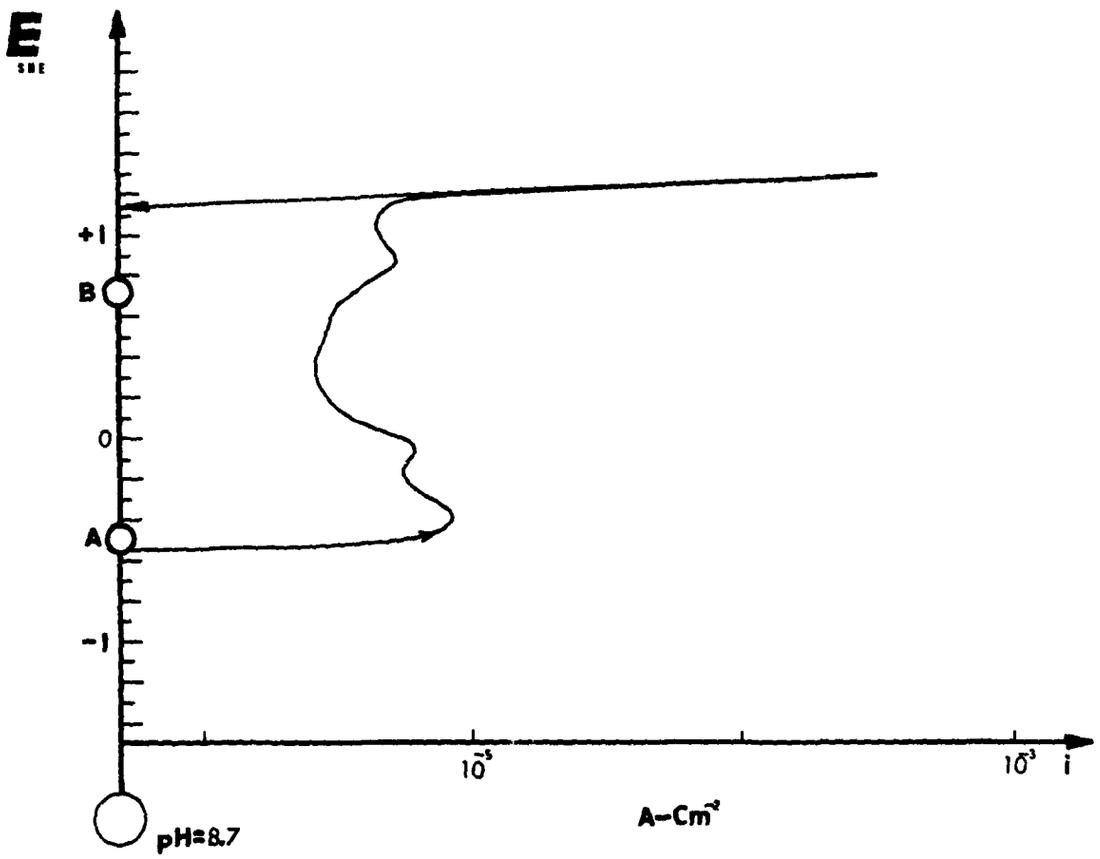

FIGURE 9: Potentiokinetic Curve (Potential versus pH) 12.0% Chromium Alloy, pH = 8.7.

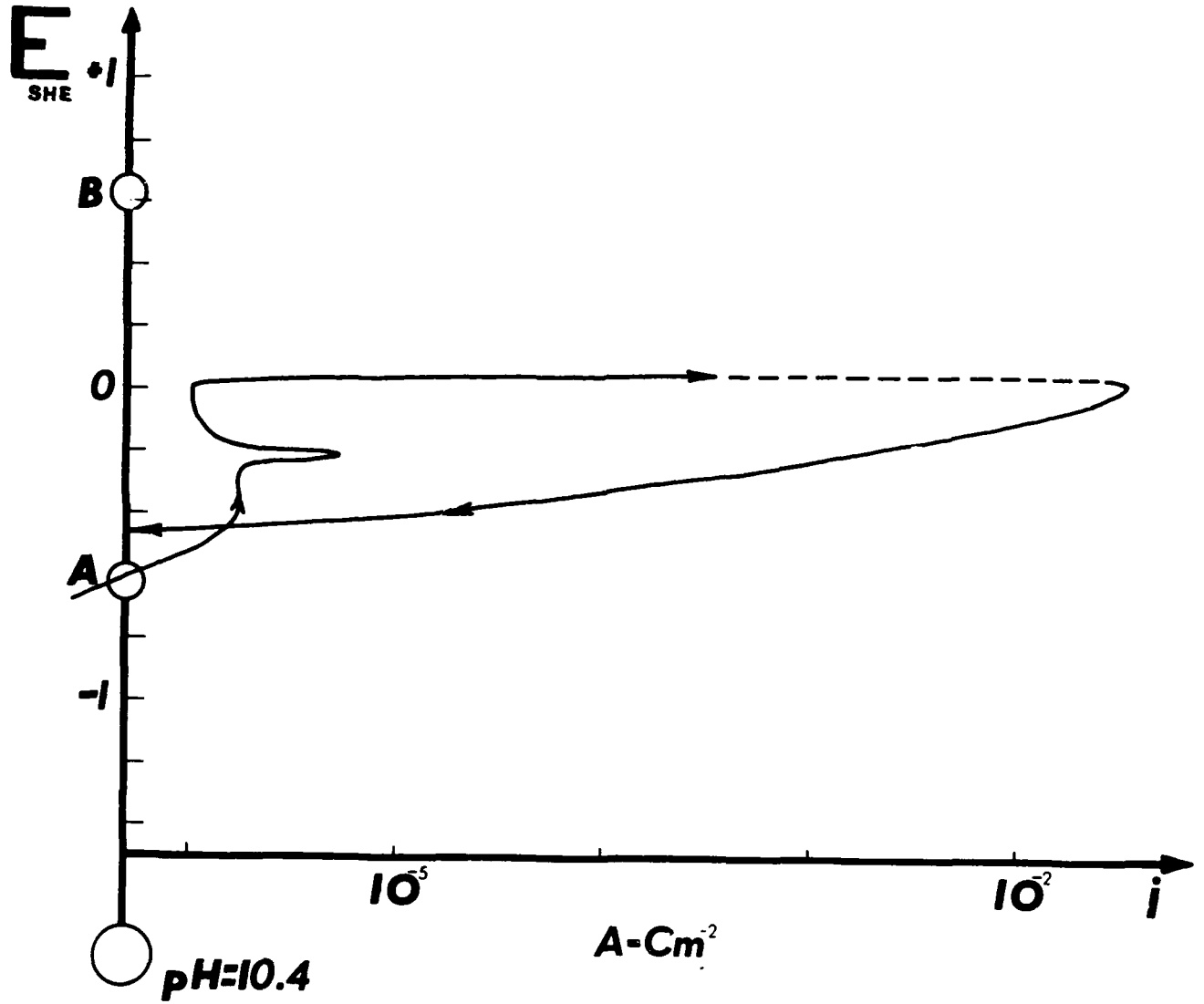

FIGURE 10: Potentiokinetic Curve (Potential versus pH) 12.0% Chromium Alloy, pH = 10.4.

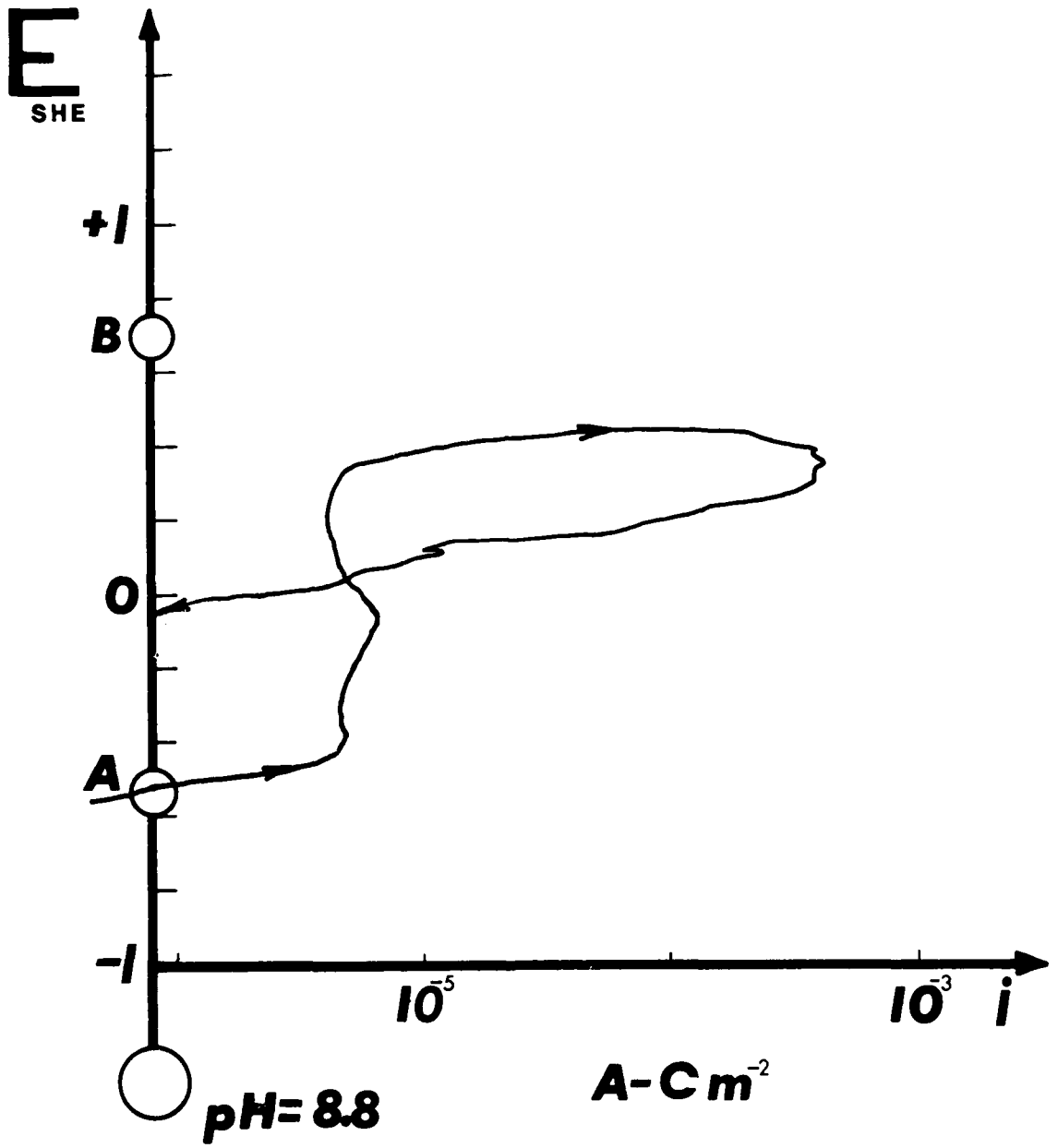

FIGURE 11 Potentiokinetic curve (Potential versus pH) for Chromium Alloy, pH = 8.8.

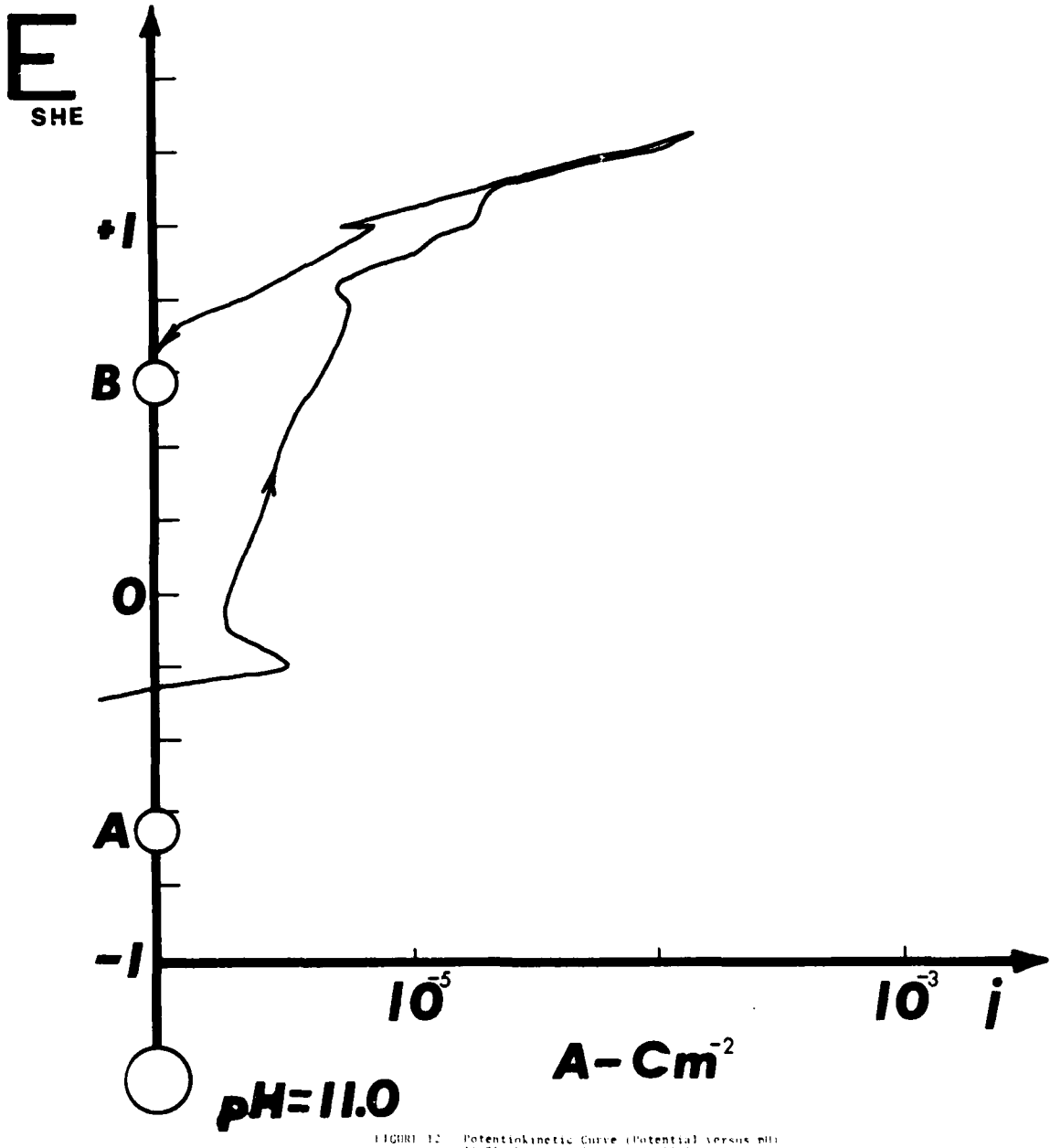

FIGURE 12 Potentiokinetic Curve (Potential versus pH) 16.9% Chromium Alloy, pH = 11.0.

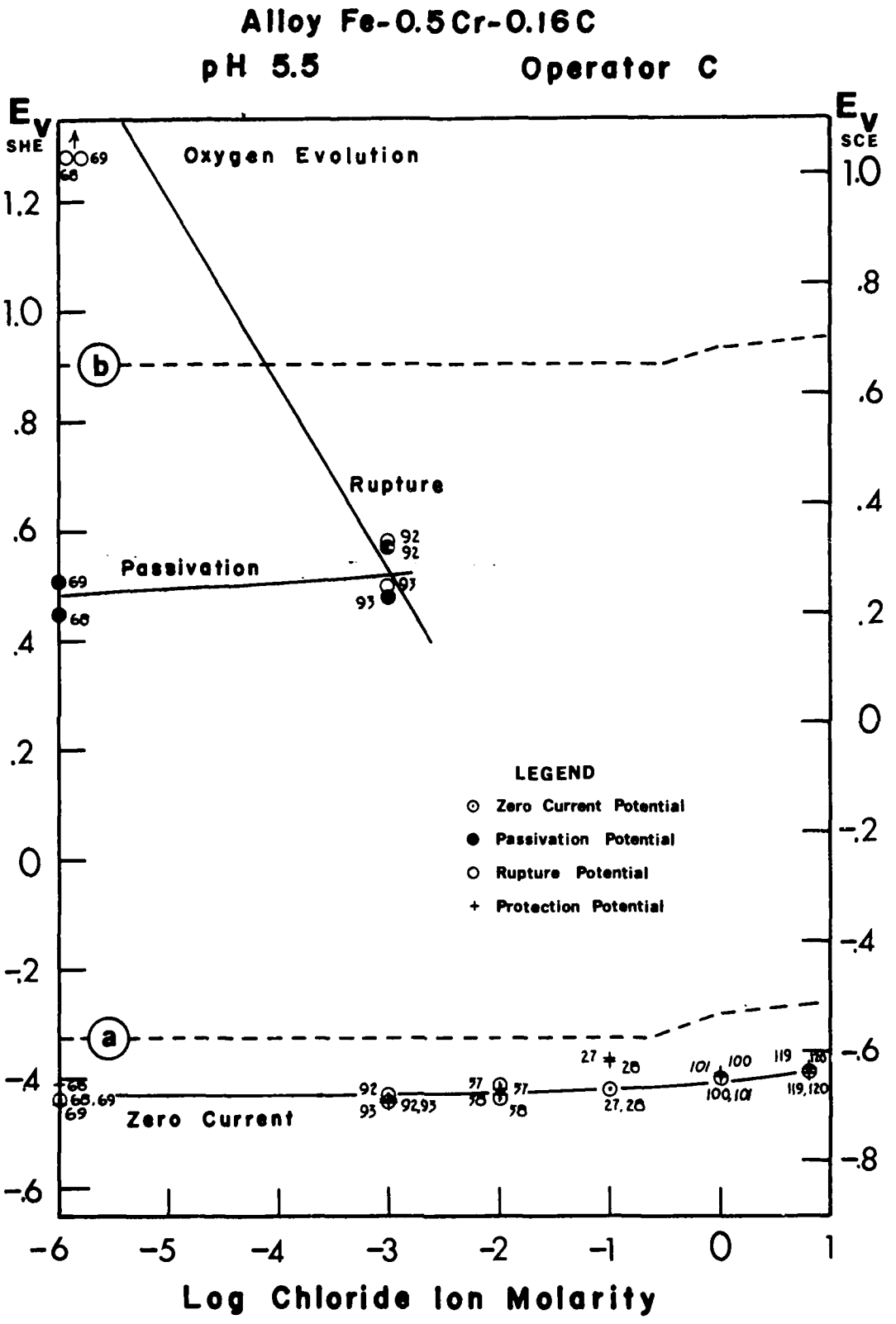

FIGURE 13: Potential versus Log Chloride Ion Molarity. 0.5% Chromium Alloy, pH = 5.5.

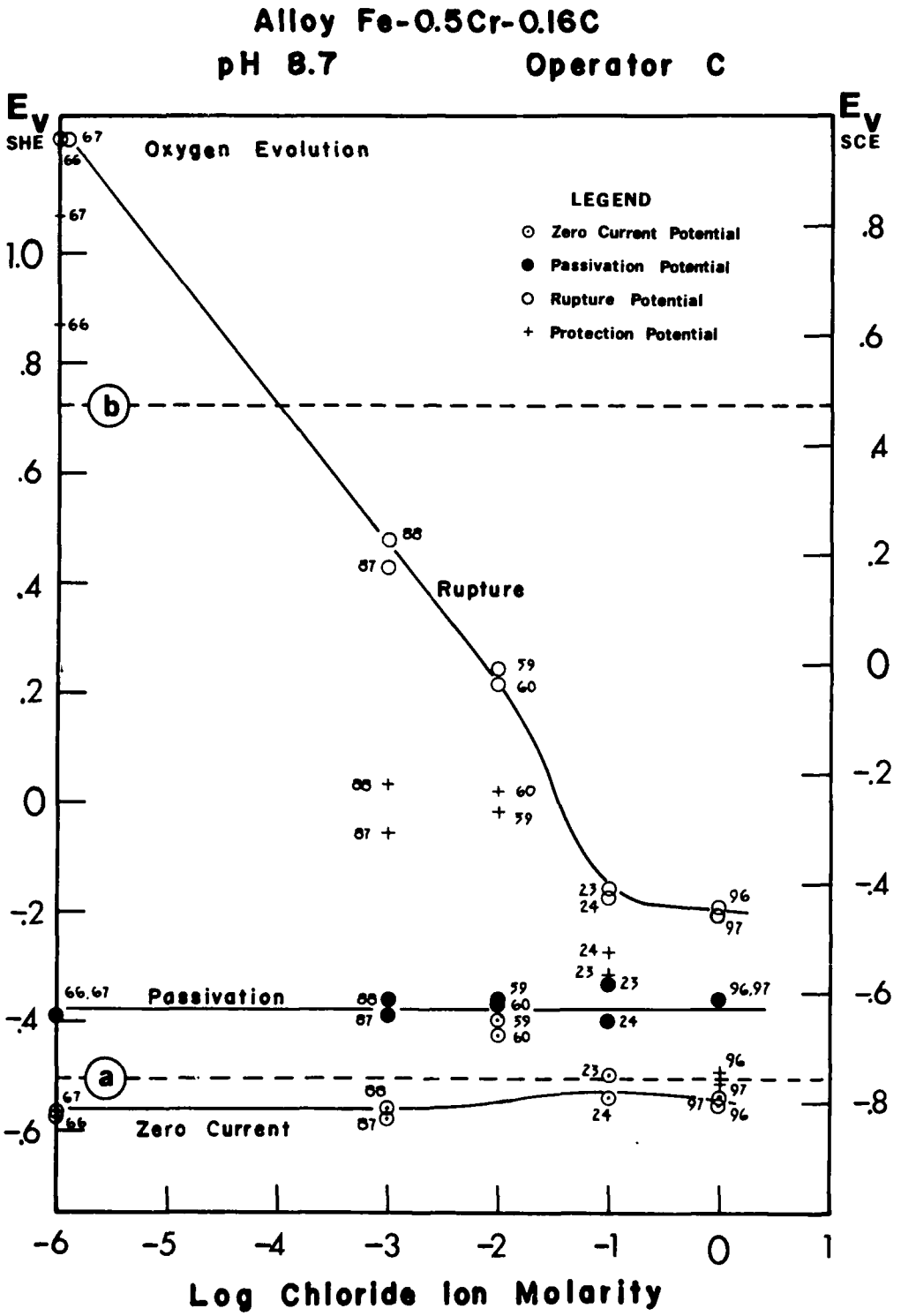

FIGURE 14: Potential versus Log Chloride Ion Molarity 0.5% Chromium Alloy, pH = 8.7.

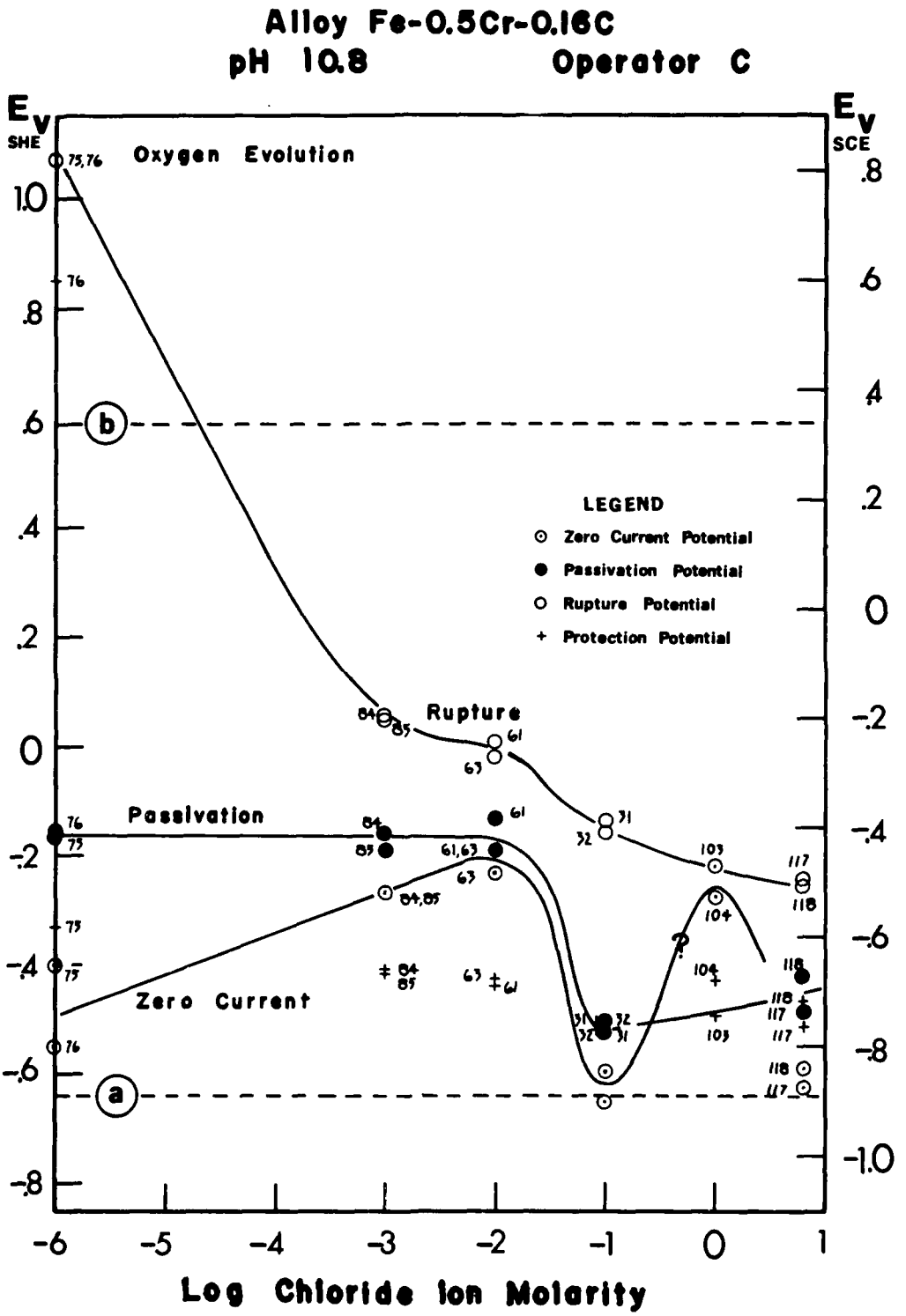

FIGURE 15: Potential versus Log Chloride Ion Molarity 0.5% Chromium Alloy, pH = 10.8.

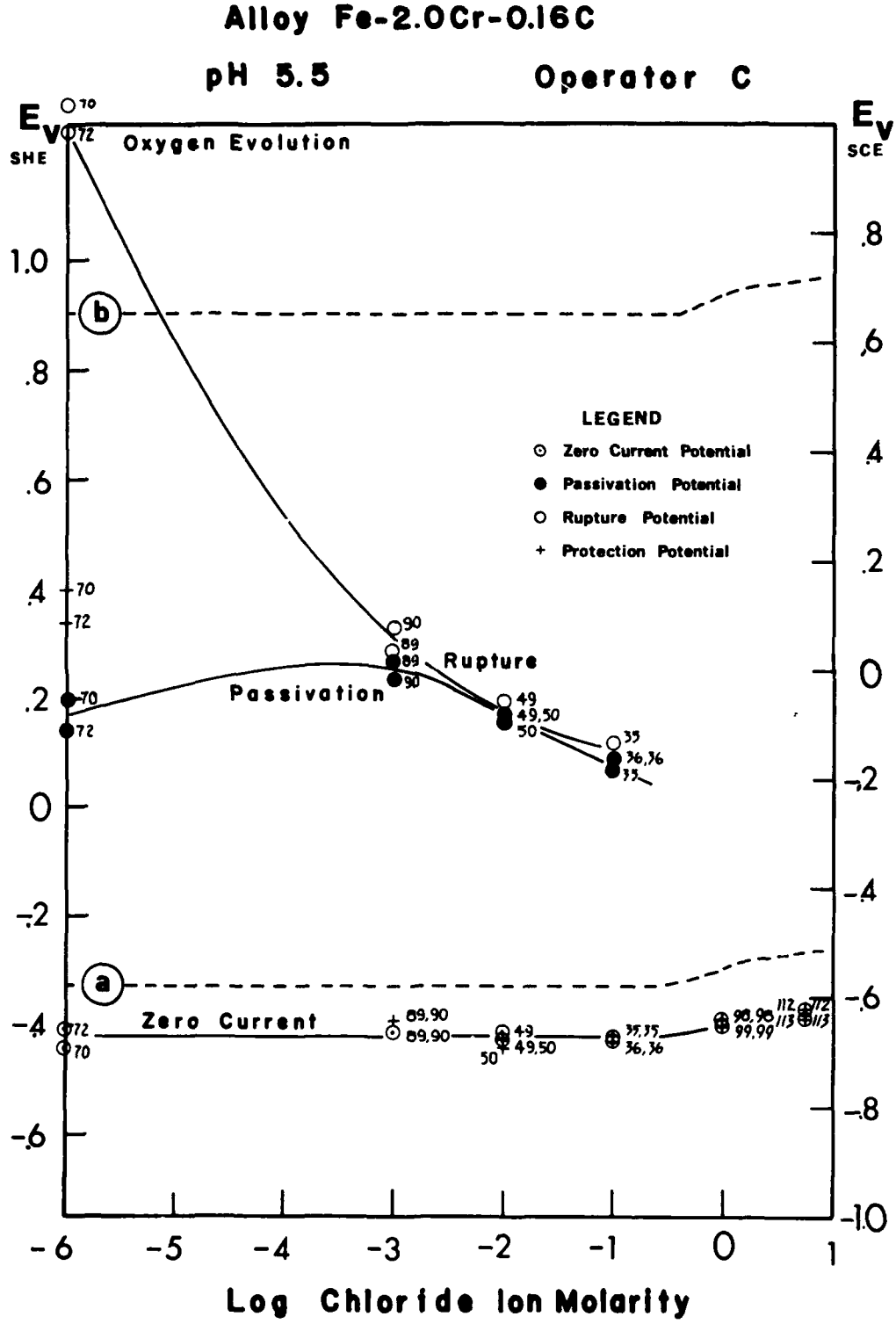

FIGURE 16: Potential versus Log Chloride Ion Molarity
2.0% Chromium Alloy, pH = 5.5.

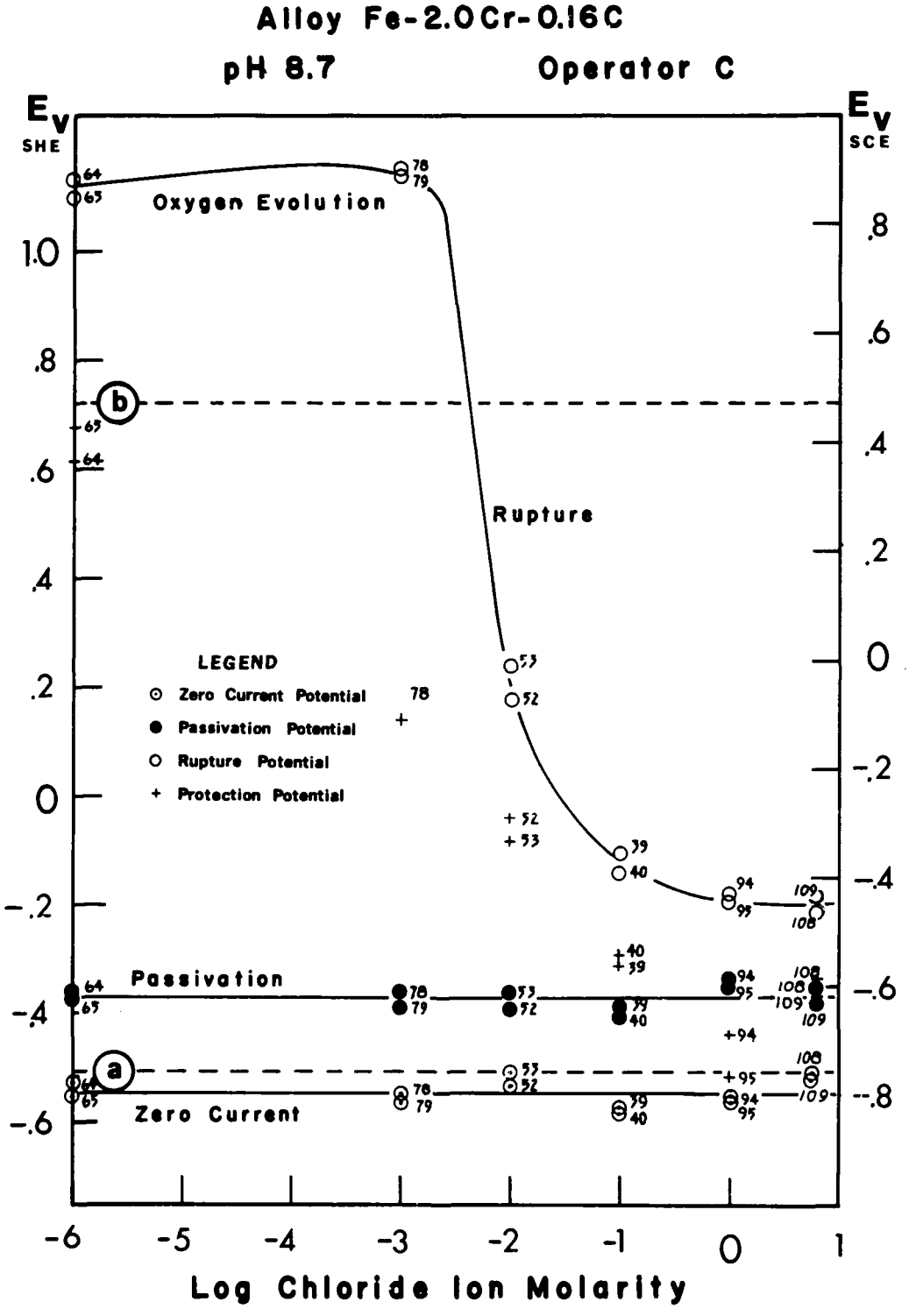

FIGURE 17: Potential versus Log Chloride Ion Molarity
2.0% Chromium Alloy, pH = 8.7.

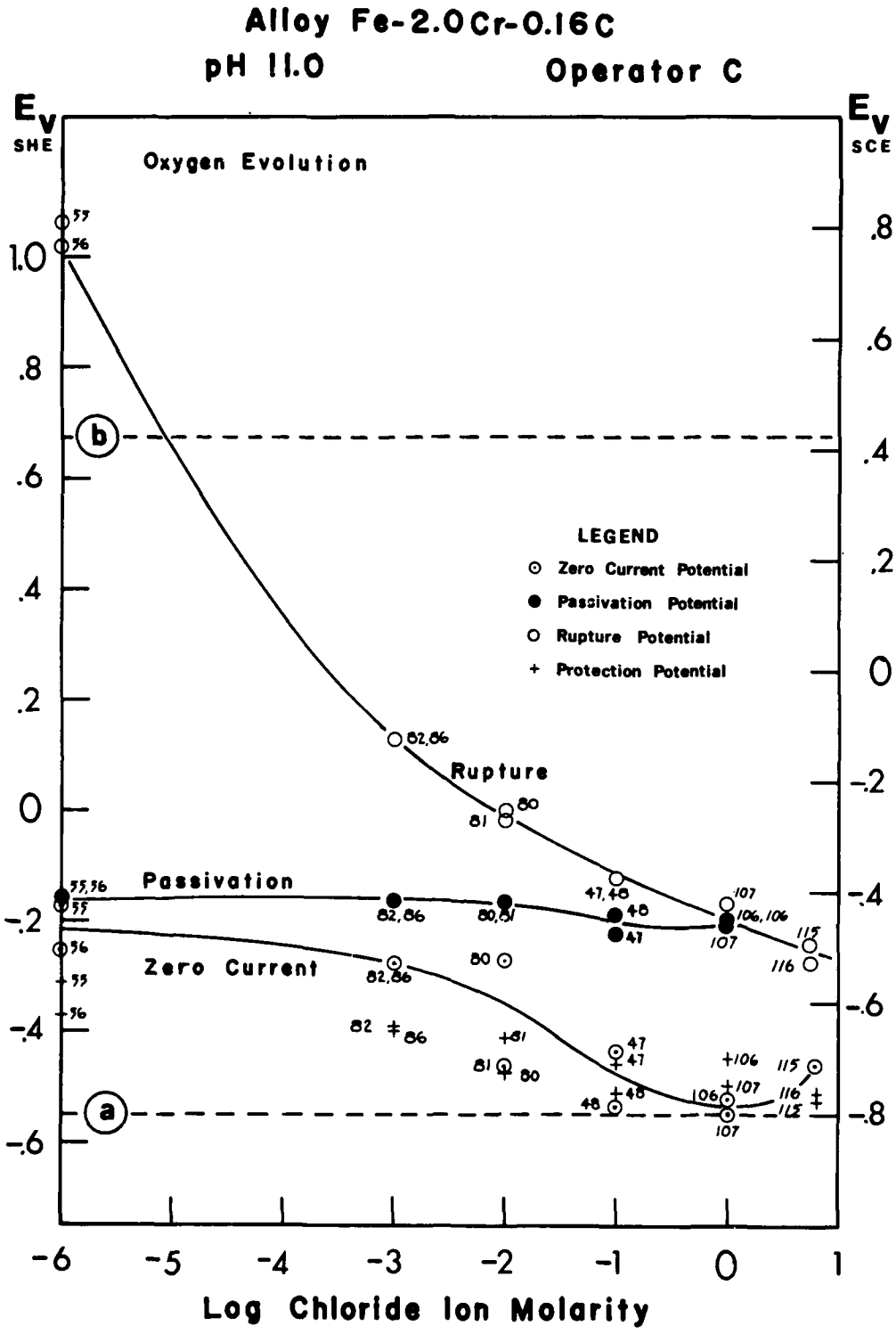

FIGURE 18: Potential versus Log Chloride Ion Molarity 2.0% Chromium Alloy, pH = 11.0.

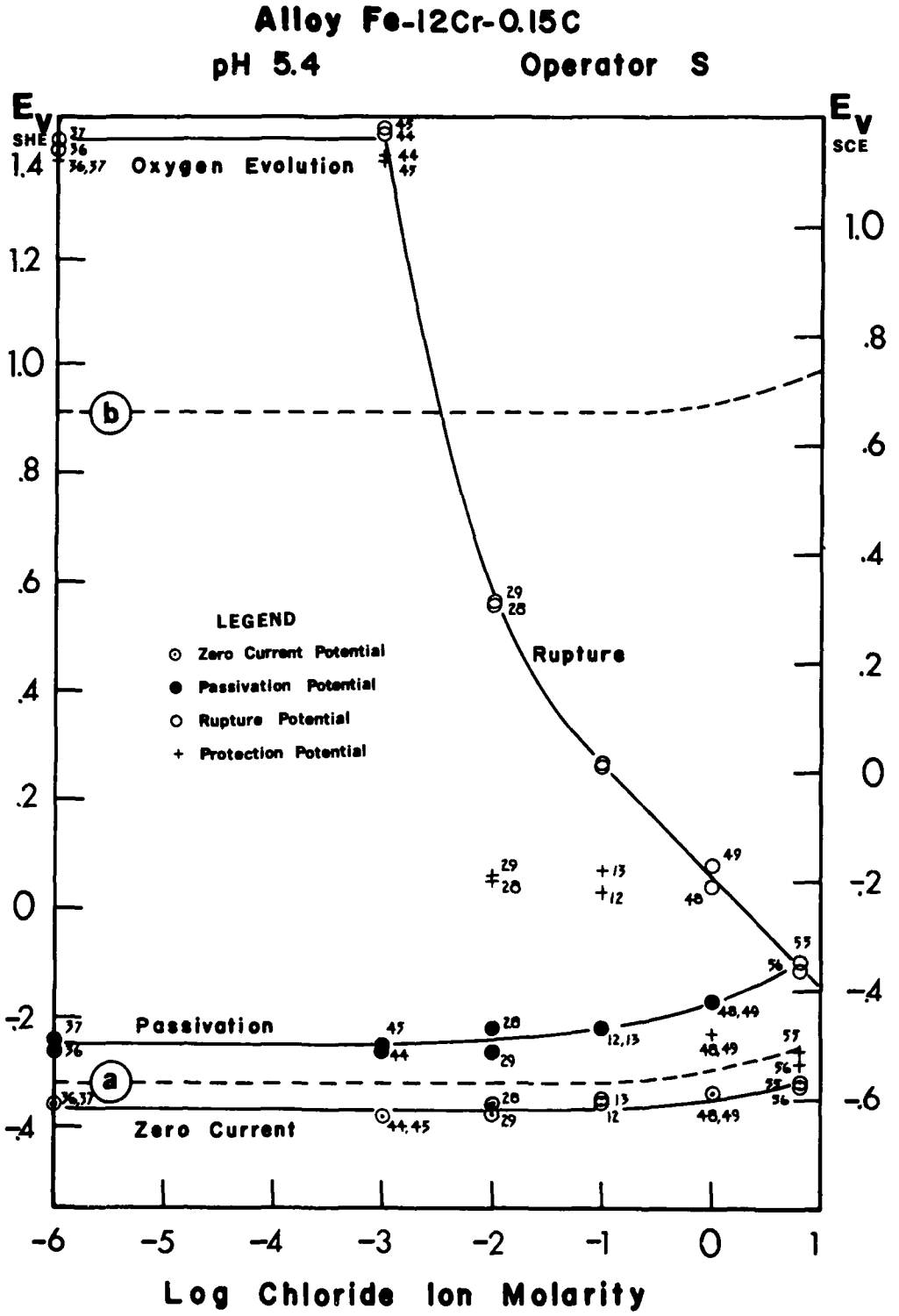

FIGURE 19: Potential versus Log Chloride Ion Molarity
12.0% Chromium Alloy, pH = 5.4.

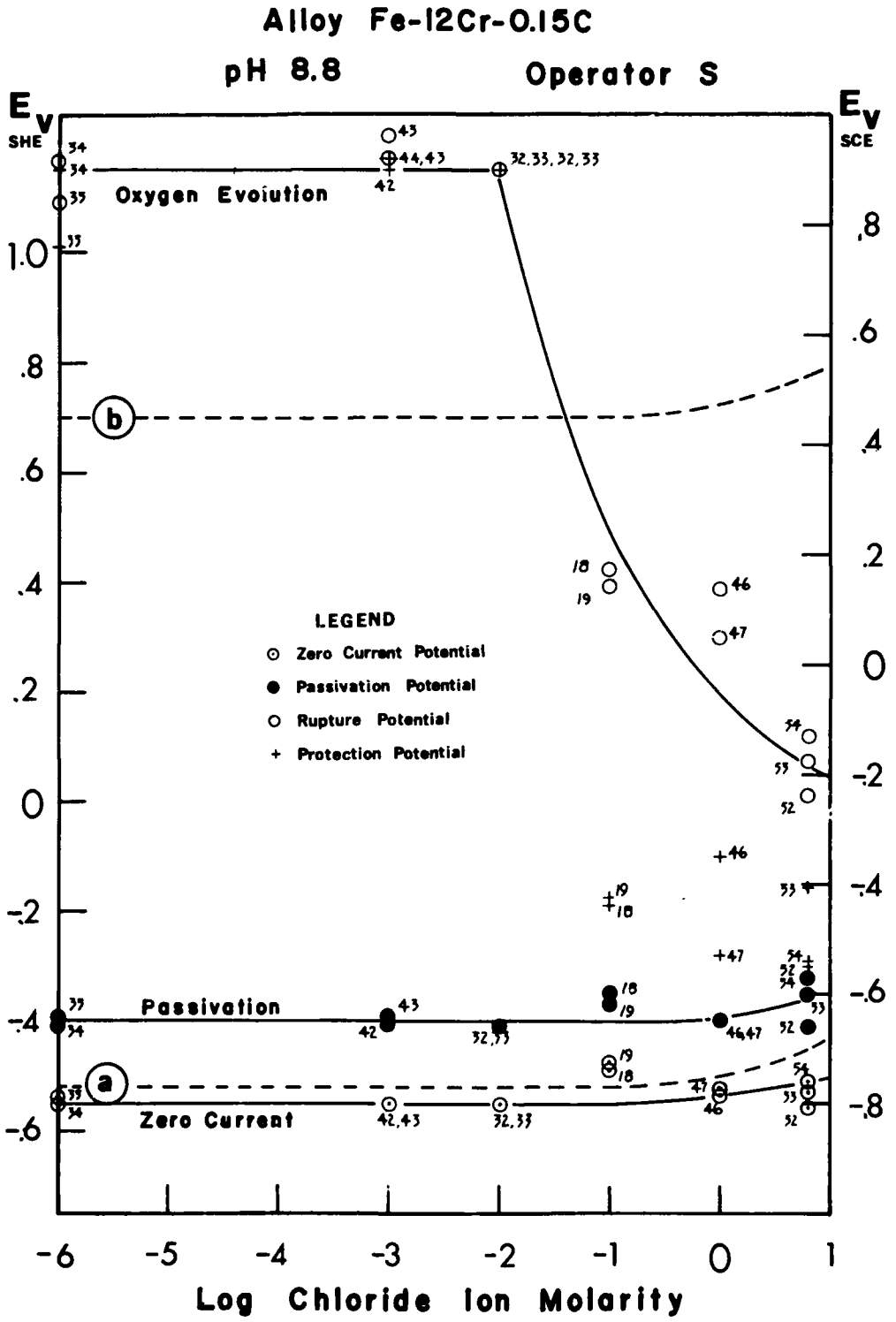

FIGURE 20: Potential versus Log Chloride Ion Molarity 12.0% Chromium Alloy, pH = 8.8.

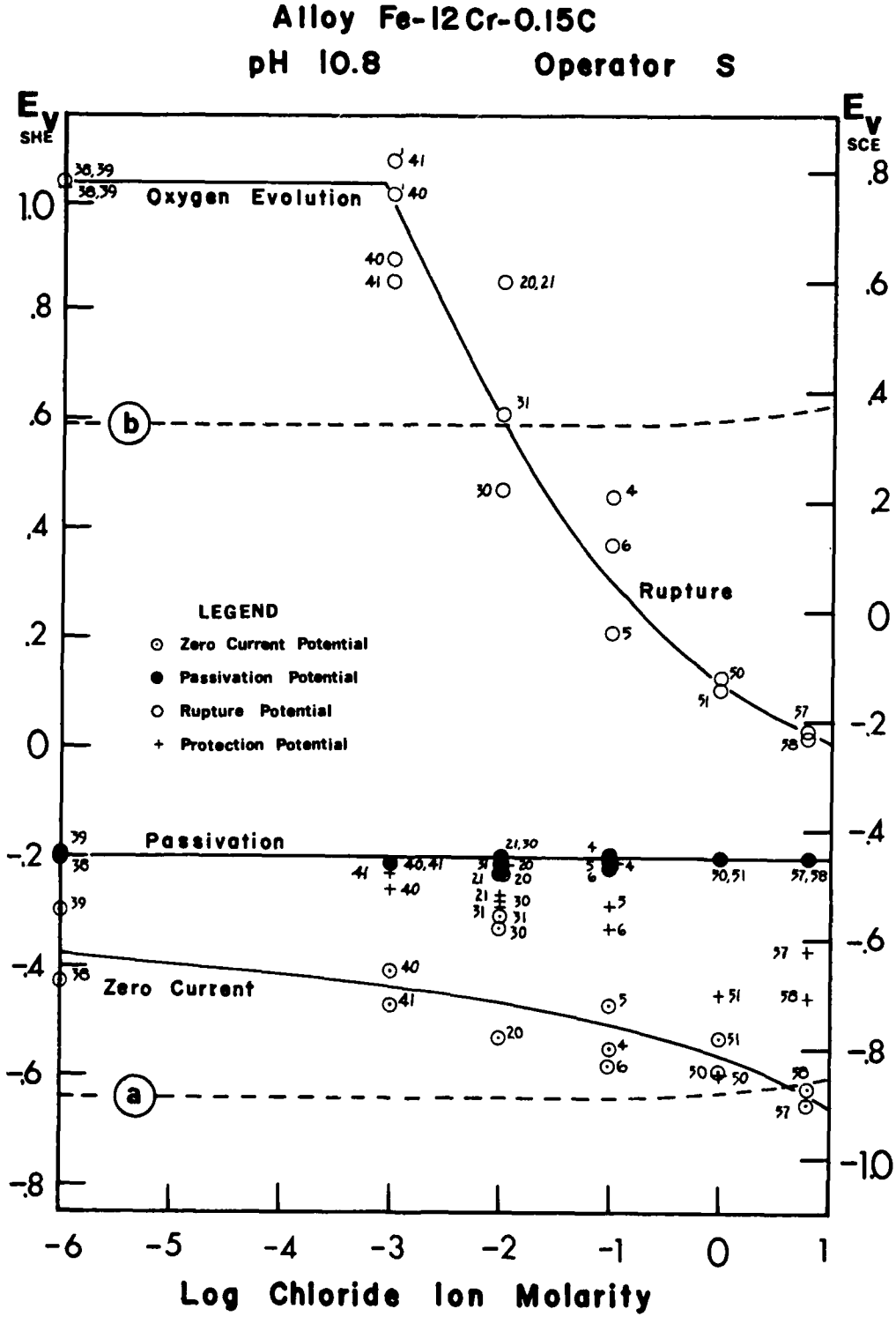

FIGURE 21: Potential versus Log Chloride Ion Molarity 12.0% Chromium Alloy, pH = 10.8.

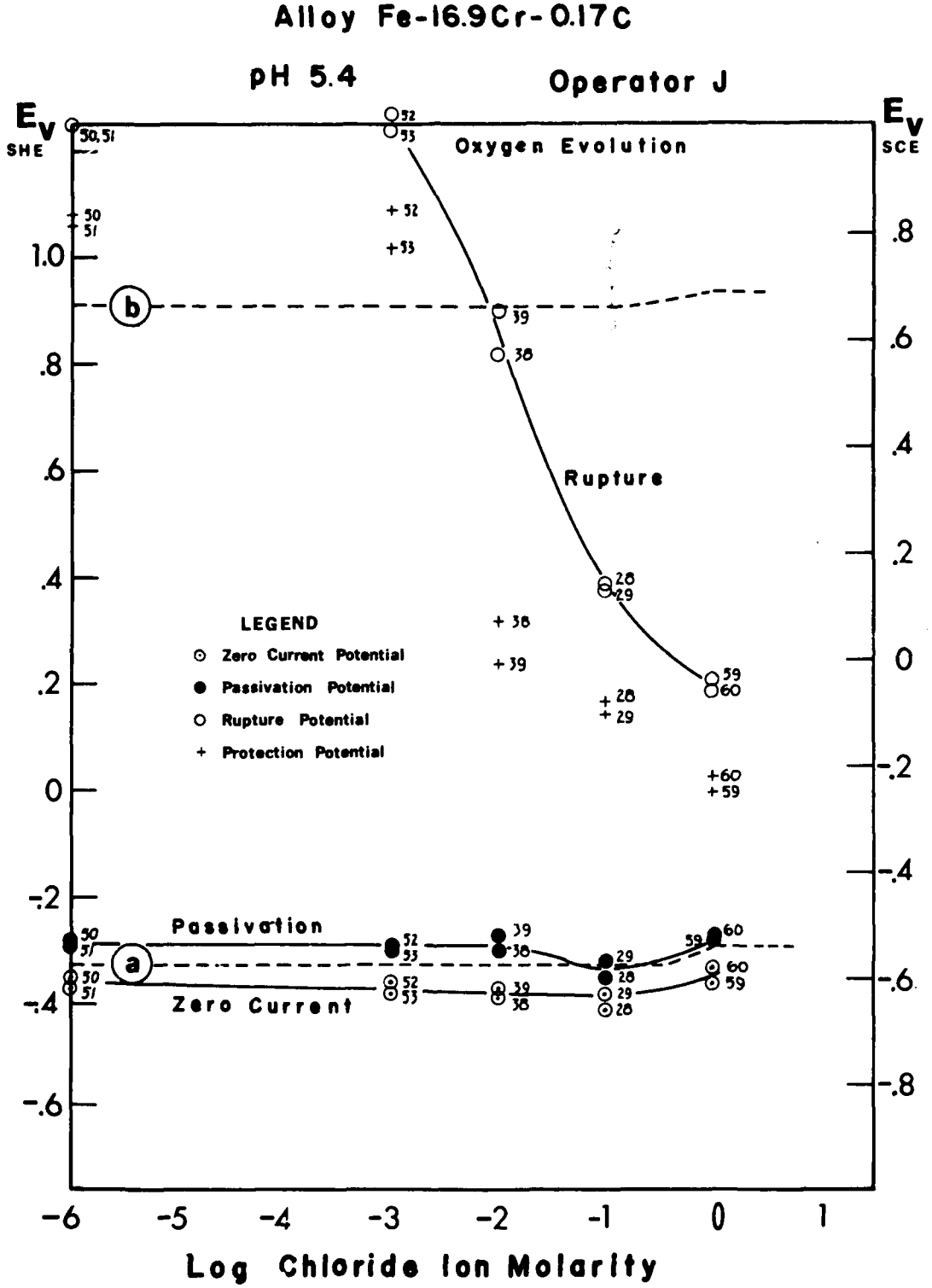

FIGURE 22: Potential versus Log Chloride Ion Molarity 16.9% Chromium Alloy, pH = 5.4.

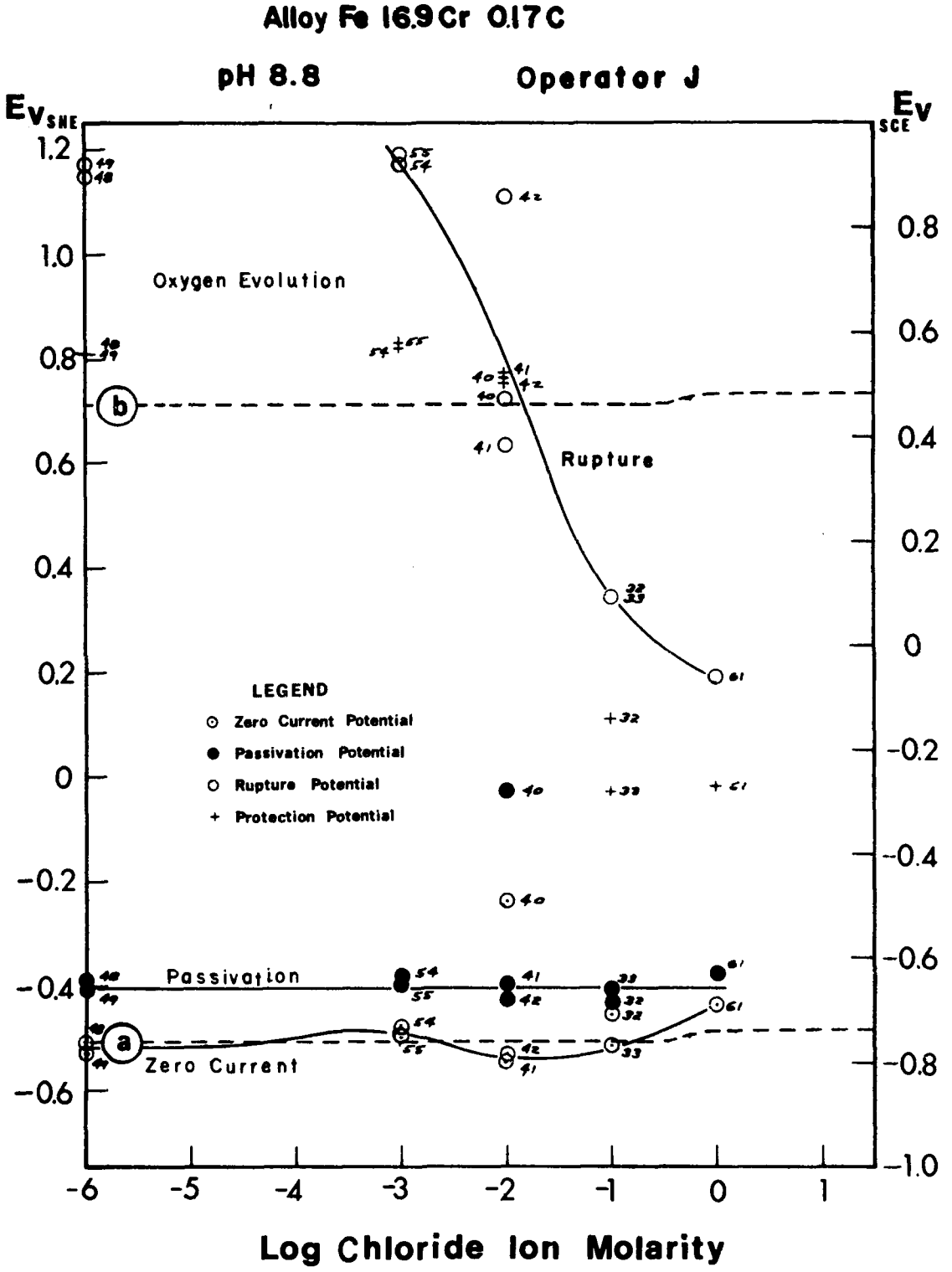

FIGURE 23: Potential versus Log Chloride Ion Molarity 16.9% Chromium Alloy, pH = 8.8.

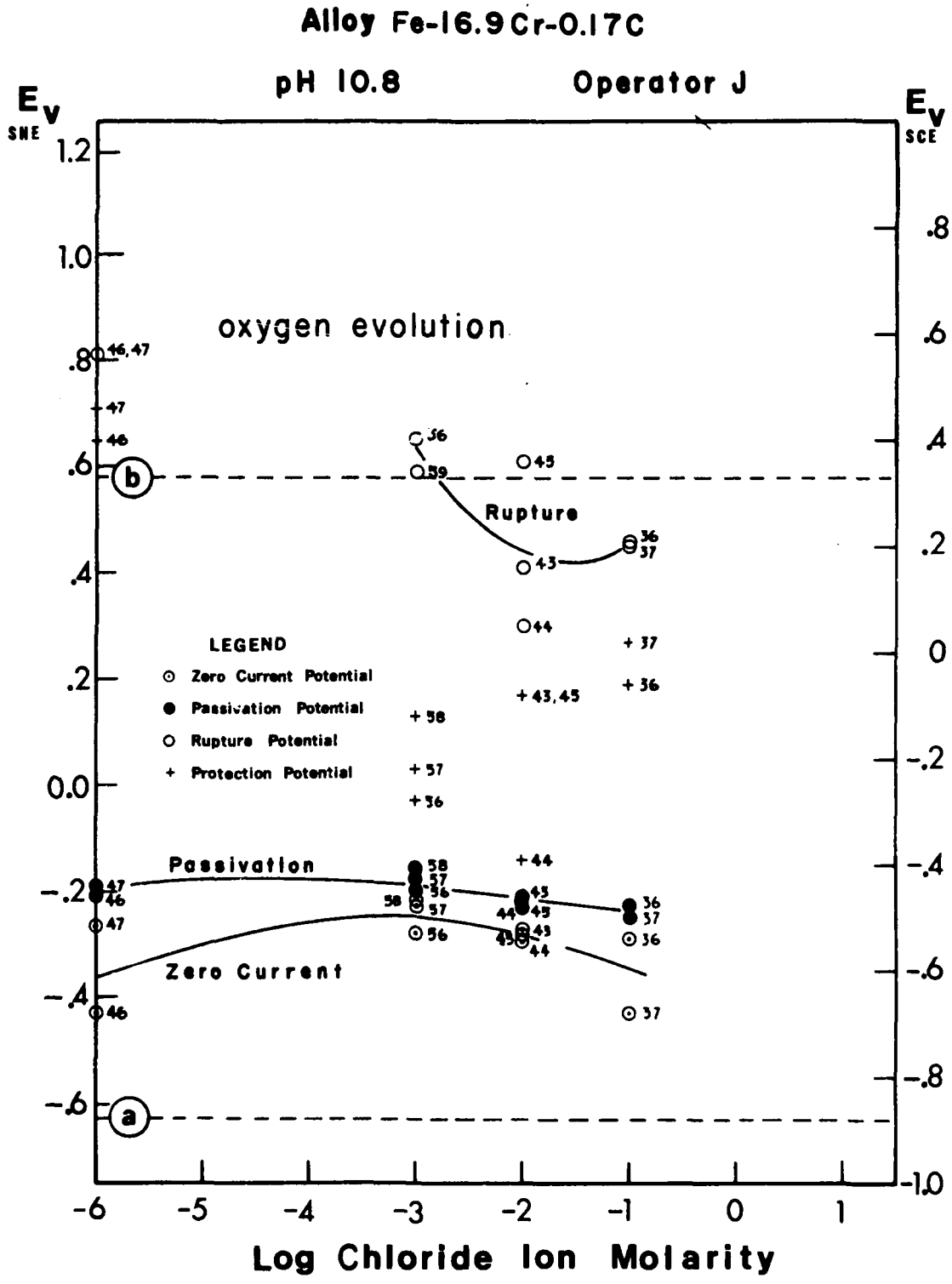

FIGURE 24: Potential versus Log Chloride Ion Molarity 16.9% Chromium Alloy, pH = 10.8.

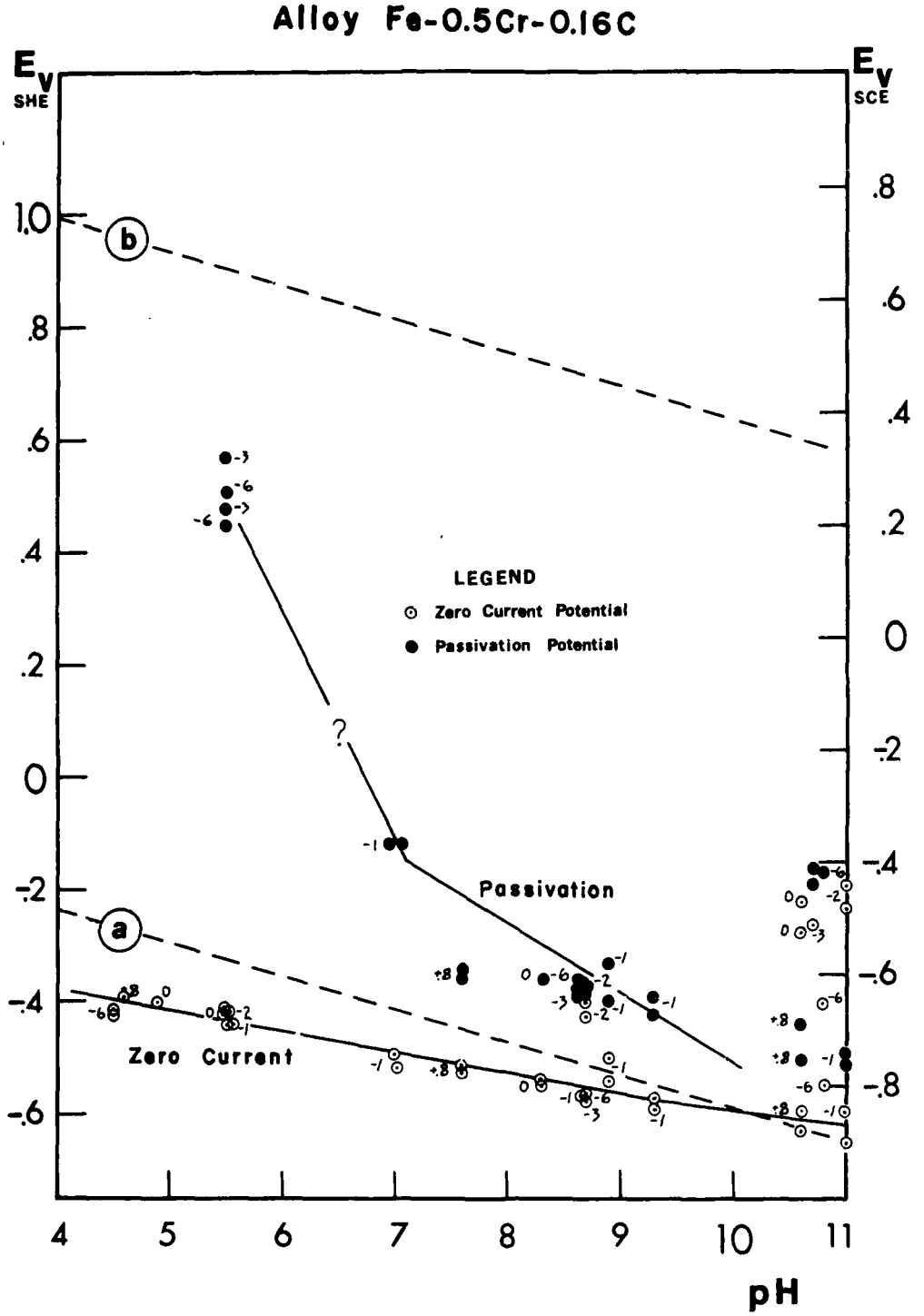

FIGURE 25: Influence of chloride ion molarity on the Passivation Potential and zero current potential as a function of pH for the Fe-Cr alloy containing 0.5% chromium. Numbers by data points indicate the logarithm of the chloride ion molarity.

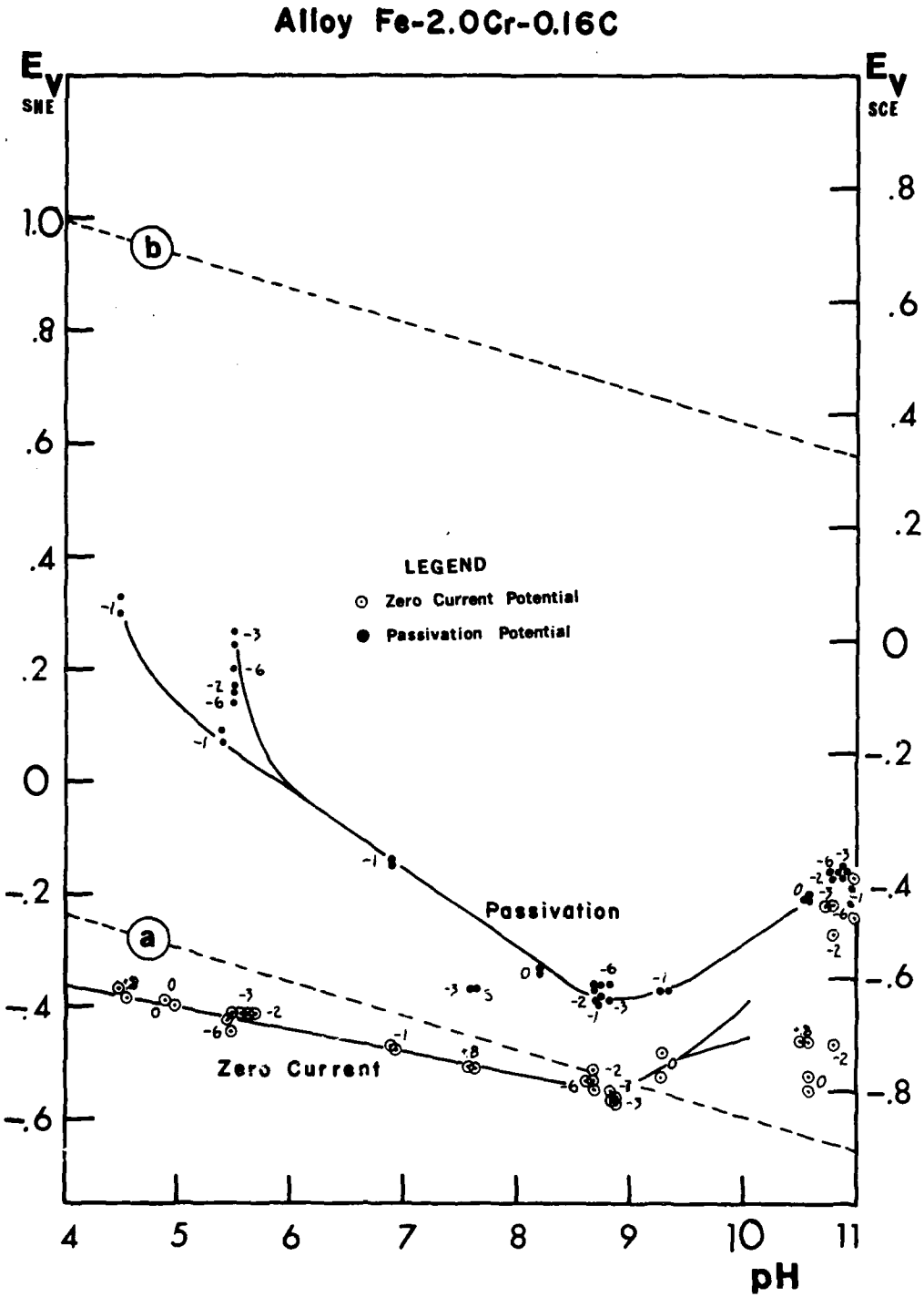

FIGURE 26: Influence of chloride ion molarity on the Passivation Potential and zero current potential as a function of pH for the Fe-Cr alloy containing 2.0% chromium. Numbers by data points indicate the logarithm of the chloride ion molarity.

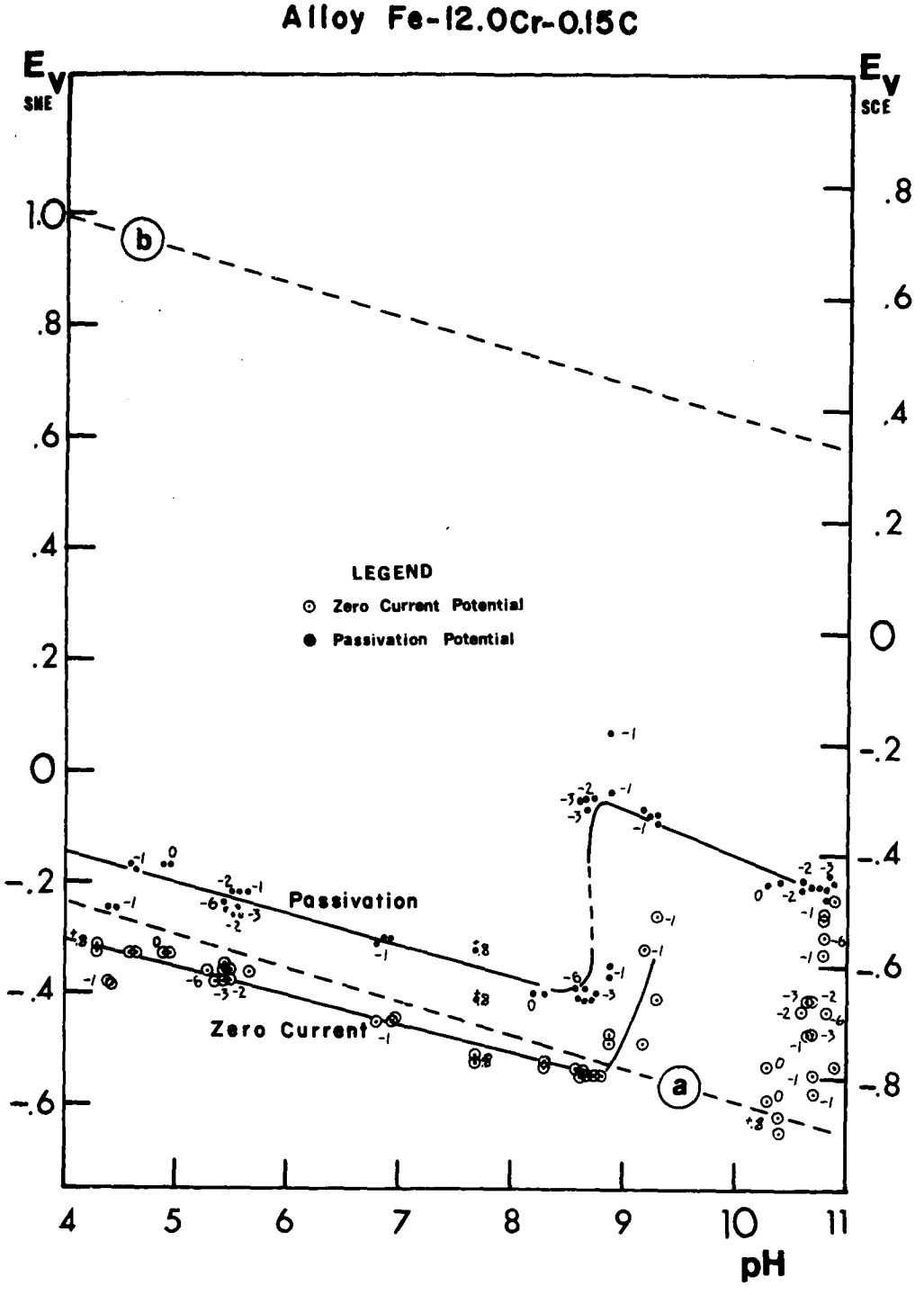

FIGURE 27: Influence of chloride ion molarity on the Passivation Potential and zero current potential as a function of pH for the Fe-Cr alloy containing 12.0% chromium. Numbers by data points indicate the logarithm of the chloride ion molarity.

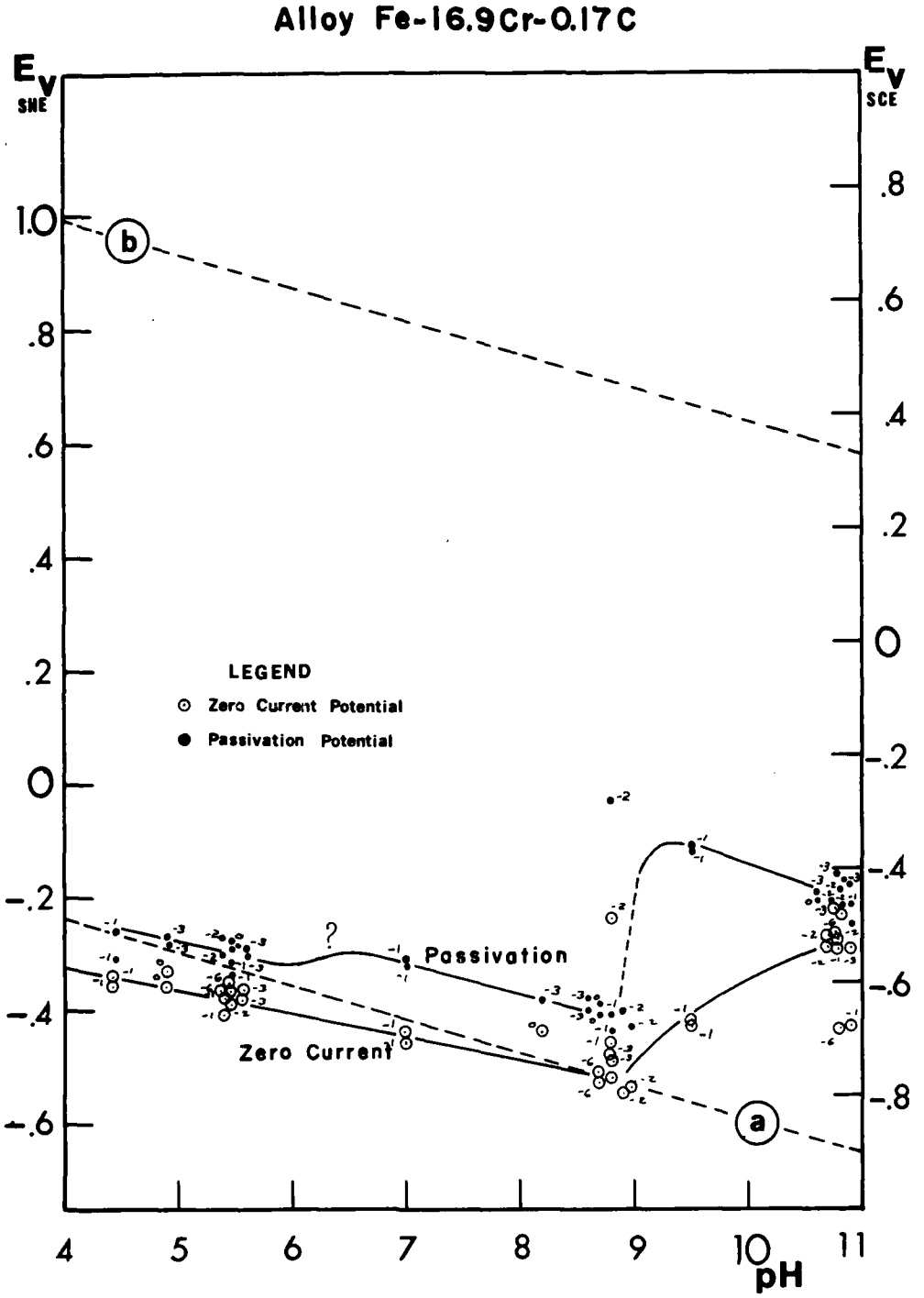

FIGURE 28: Influence of chloride ion molarity on the Passivation Potential and zero current potential as a function of pH for the Fe-Cr alloy containing 16.9% chromium. Numbers by data points indicate the logarithm of the chloride ion molarity.

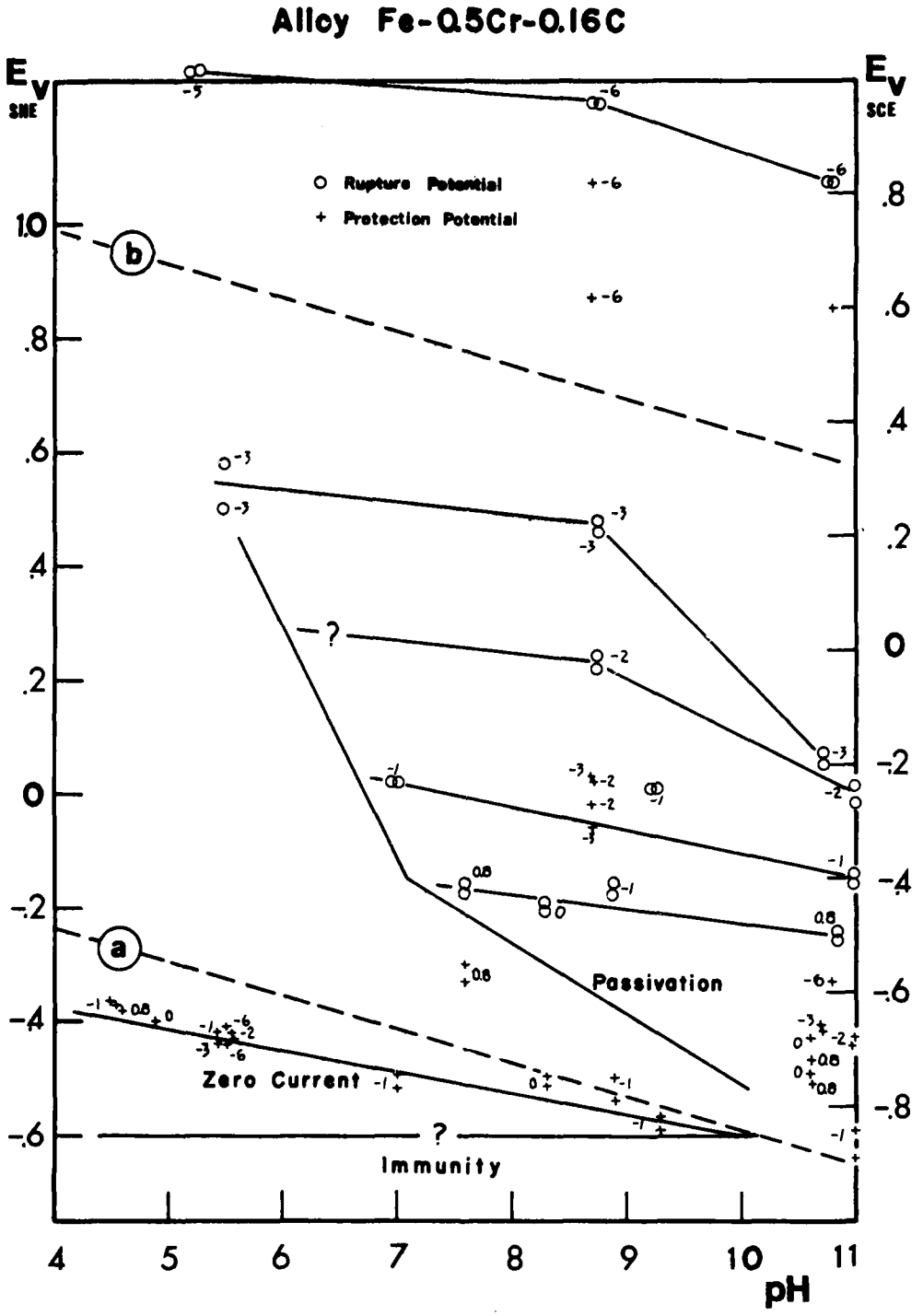

FIGURE 29: Effect of Chloride Ion Concentration on the Rupture Potential and Protection Potential as a Function of pH for the Fe-Cr Alloy Containing 0.5% Chromium. Numbers next to Data Points are Logarithms of the Chloride Ion Molarity.

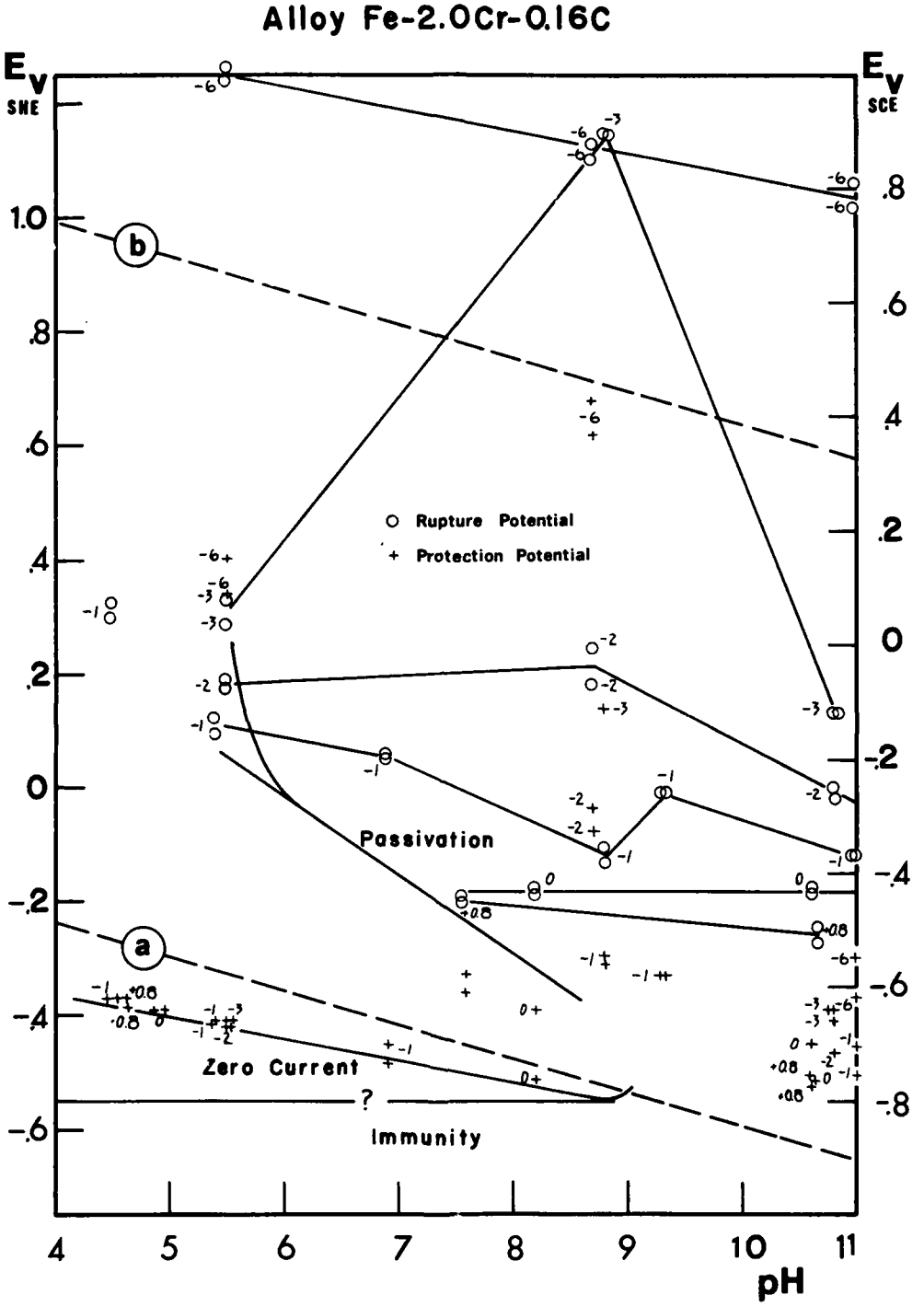

FIGURE 30: Effect of Chloride Ion Concentration on the Rupture Potential and Protection Potential as a Function of pH for the Fe-Cr Alloy Containing 2.0% Chromium. Numbers next to Data Points are Logarithms of the Chloride Ion Molarity.

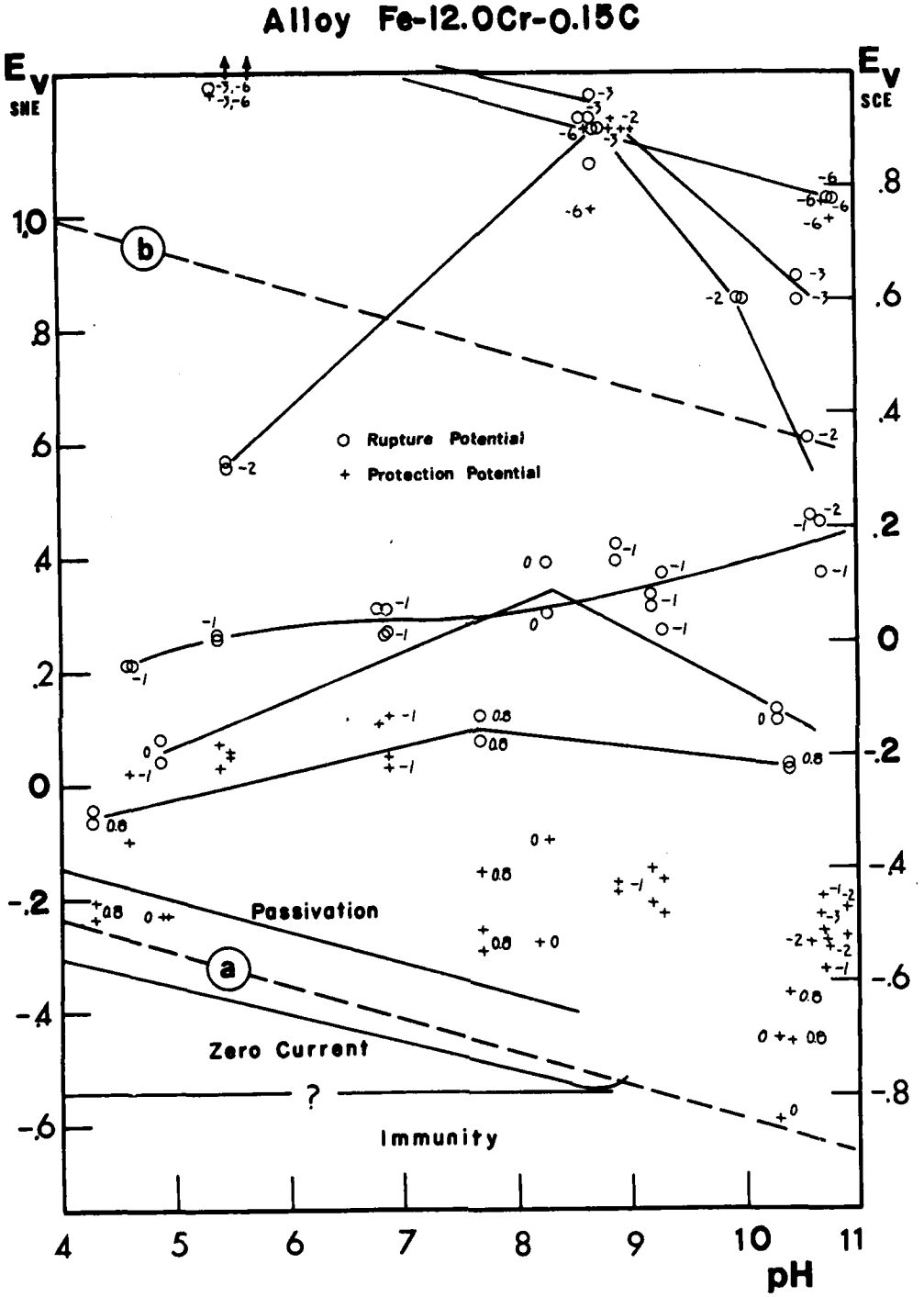

FIGURE 31: Effect of Chloride Ion Concentration on the Rupture Potential and Protection Potential as a Function of pH for the Fe-Cr Alloy Containing 12.0% Chromium. Numbers next to Data Points are Logarithms of the Chloride Ion Molarity.

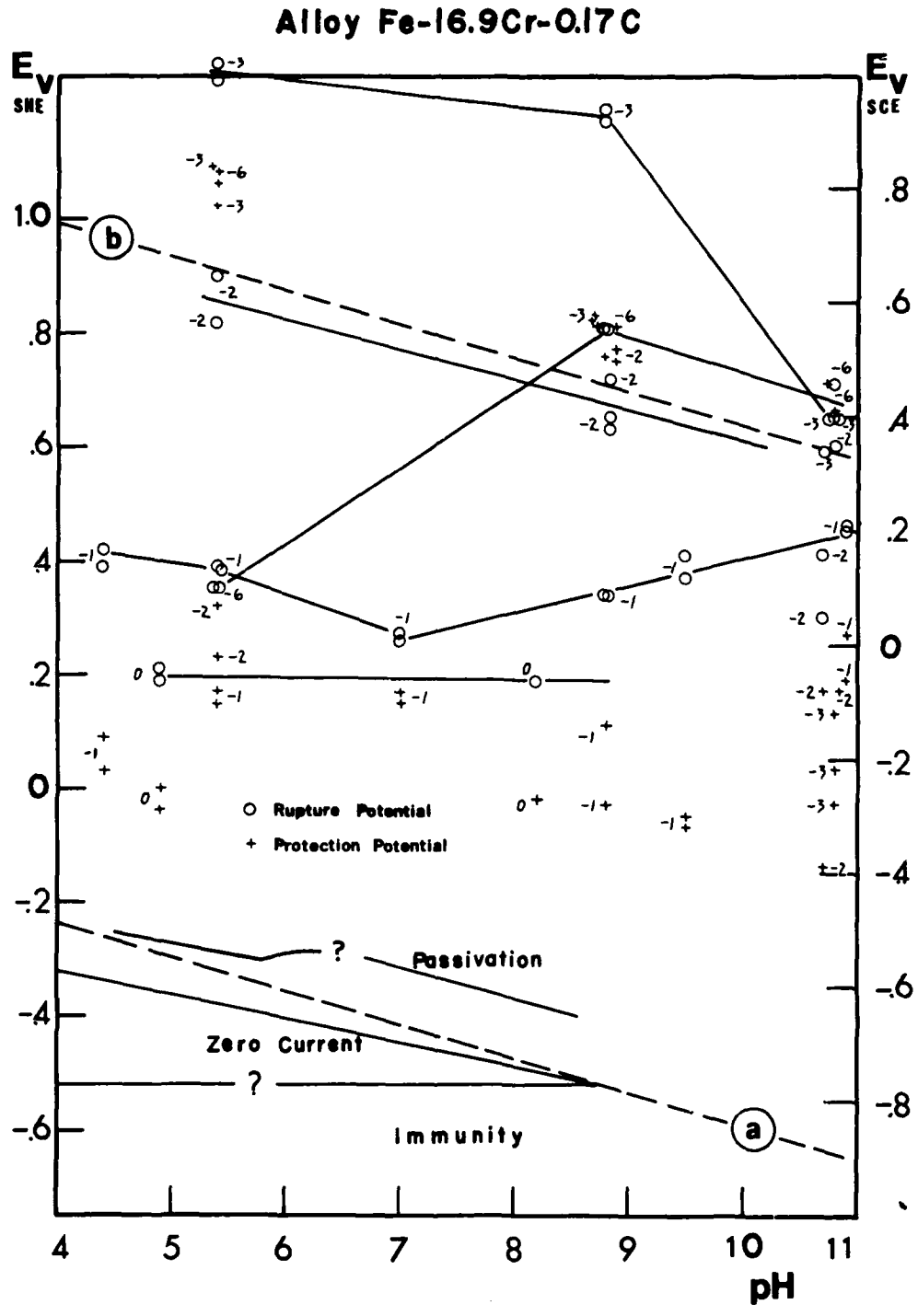

FIGURE 32: Effect of Chloride Ion Concentration on the Rupture Potential and Protection Potential as a Function of pH for the Fe-Cr Alloy Containing 16.9% Chromium. Numbers next to Data Points are Logarithms of the Chloride Ion Molarity.

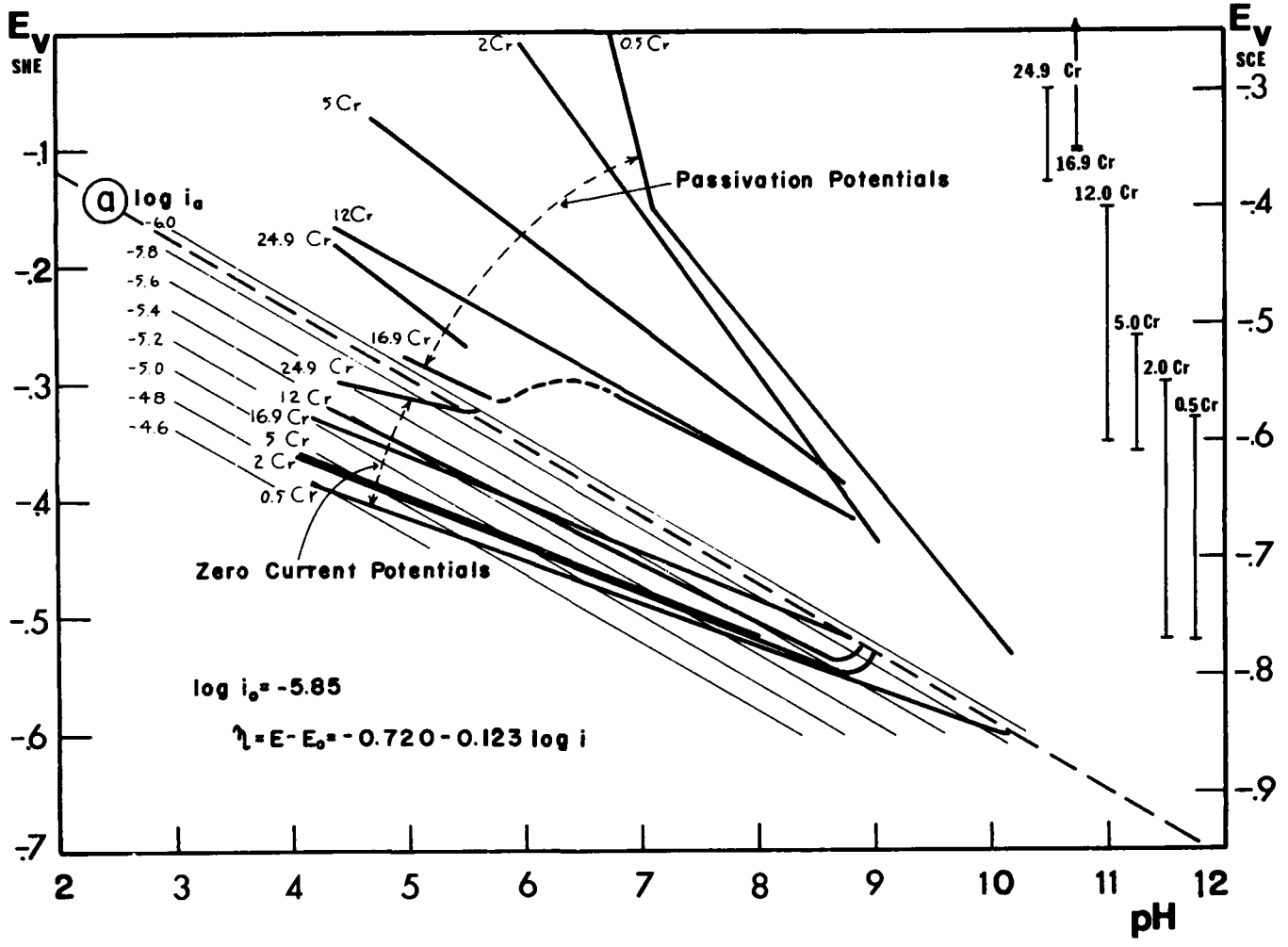

FIGURE 33: Effect of Chromium Content on Passivation Potentials and Zero Current Potentials for a Series of Binary Fe-Cr Alloys as a Function of pH.

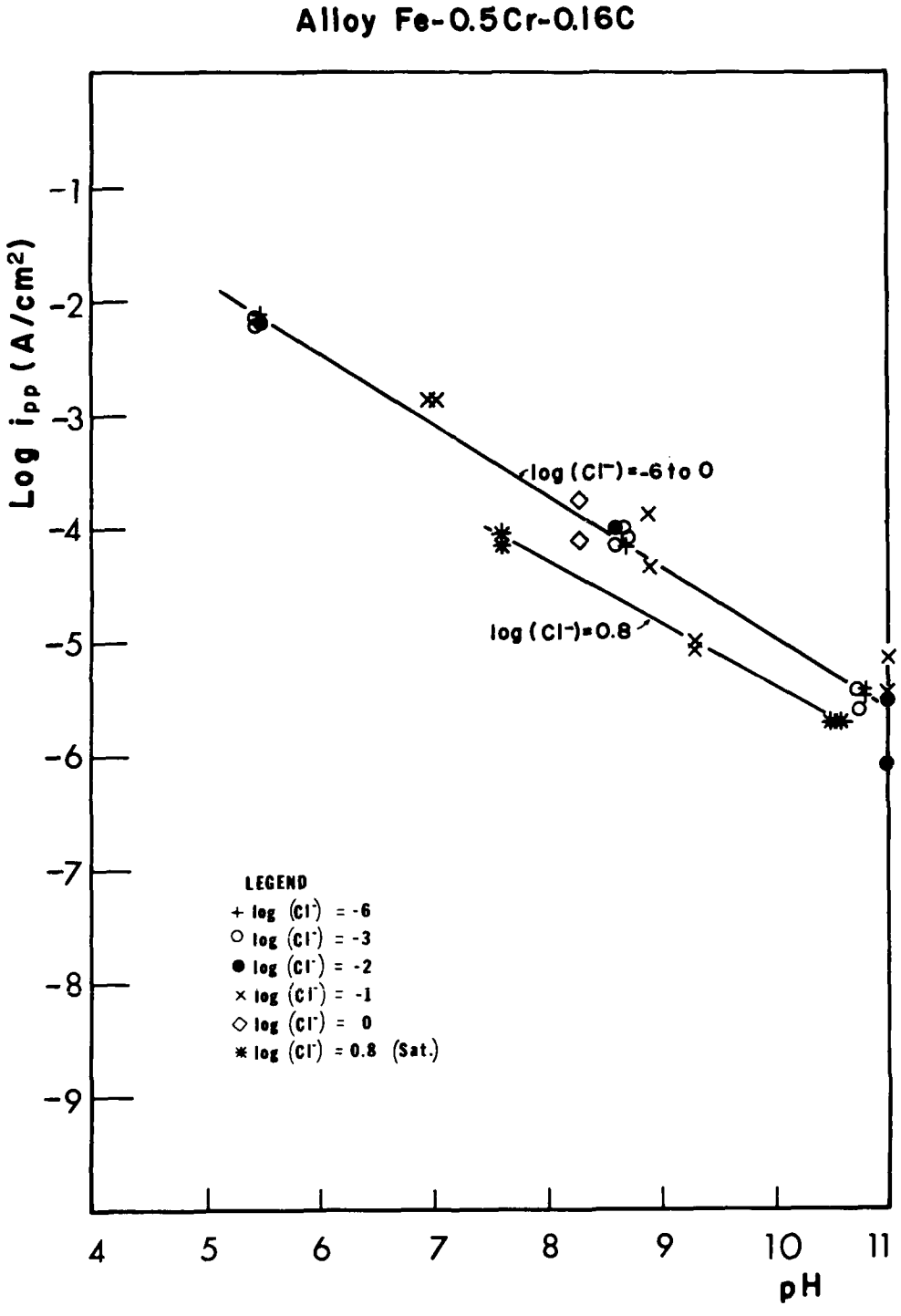

FIGURE 34: Effect of Chloride Ion Concentration on the Corrosion Velocity at the Primary Passivation Potential as a Function of pH. Fe-Cr Alloy Containing 0.5% Chromium.

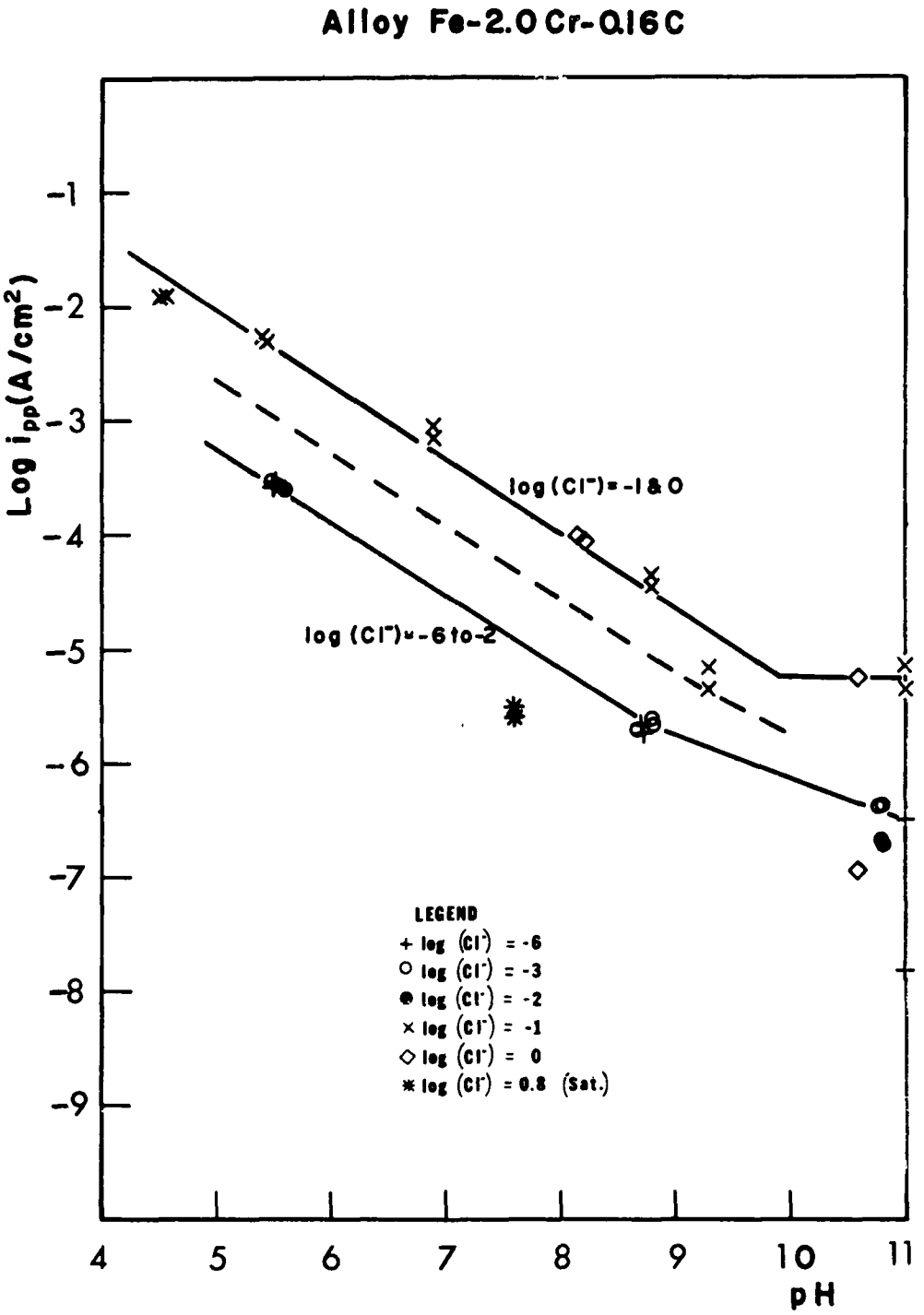

FIGURE 35: Effect of Chloride Ion Concentration on the Corrosion Velocity at the Primary Passivation Potential as a Function of pH. Fe-Cr Alloy Containing 2.0% Chromium.

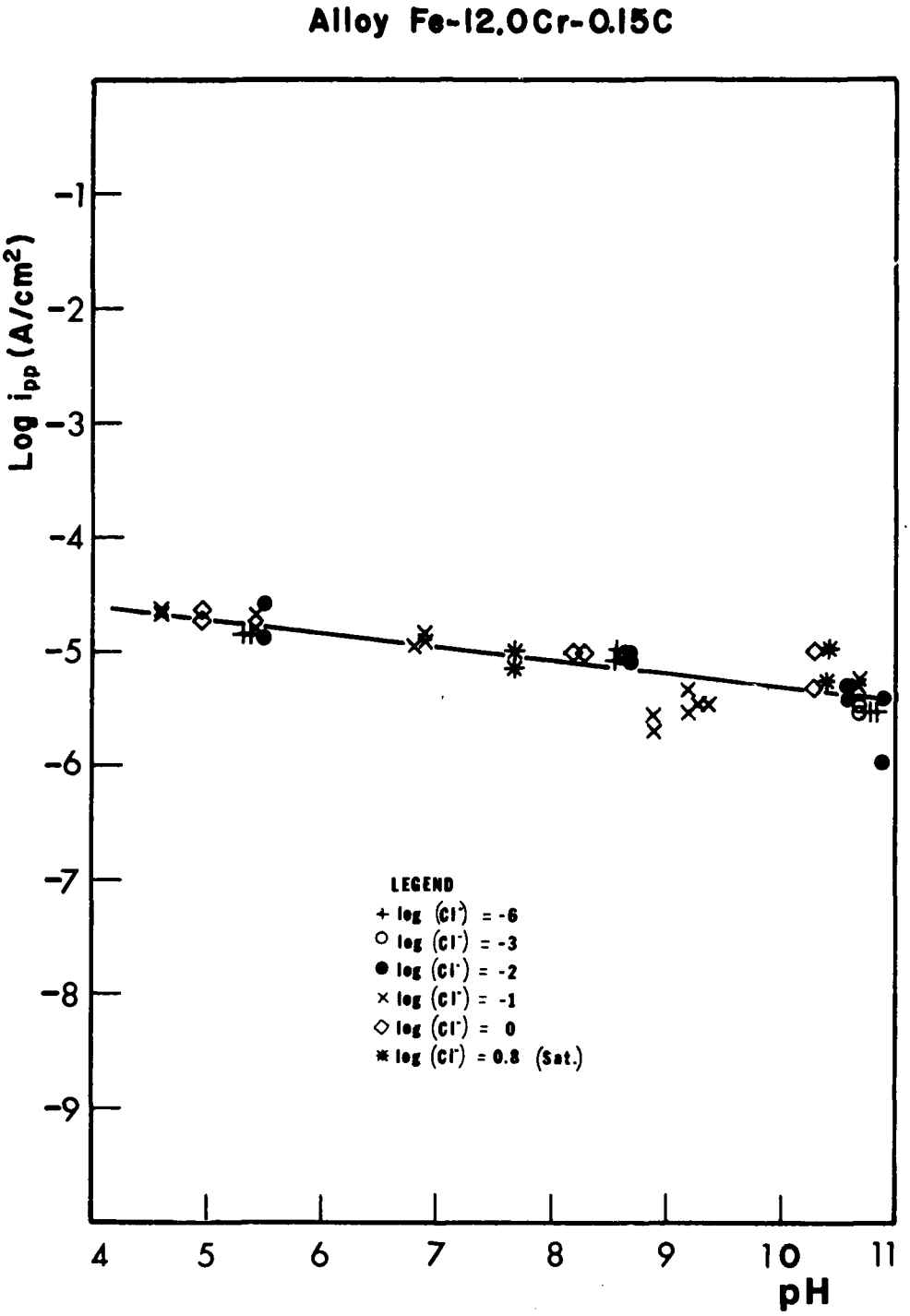

FIGURE 36: Effect of Chloride Ion Concentration on the Corrosion Velocity at the Primary Passivation Potential as a Function of pH. Fe-Cr Alloy Containing 12.0% Chromium.

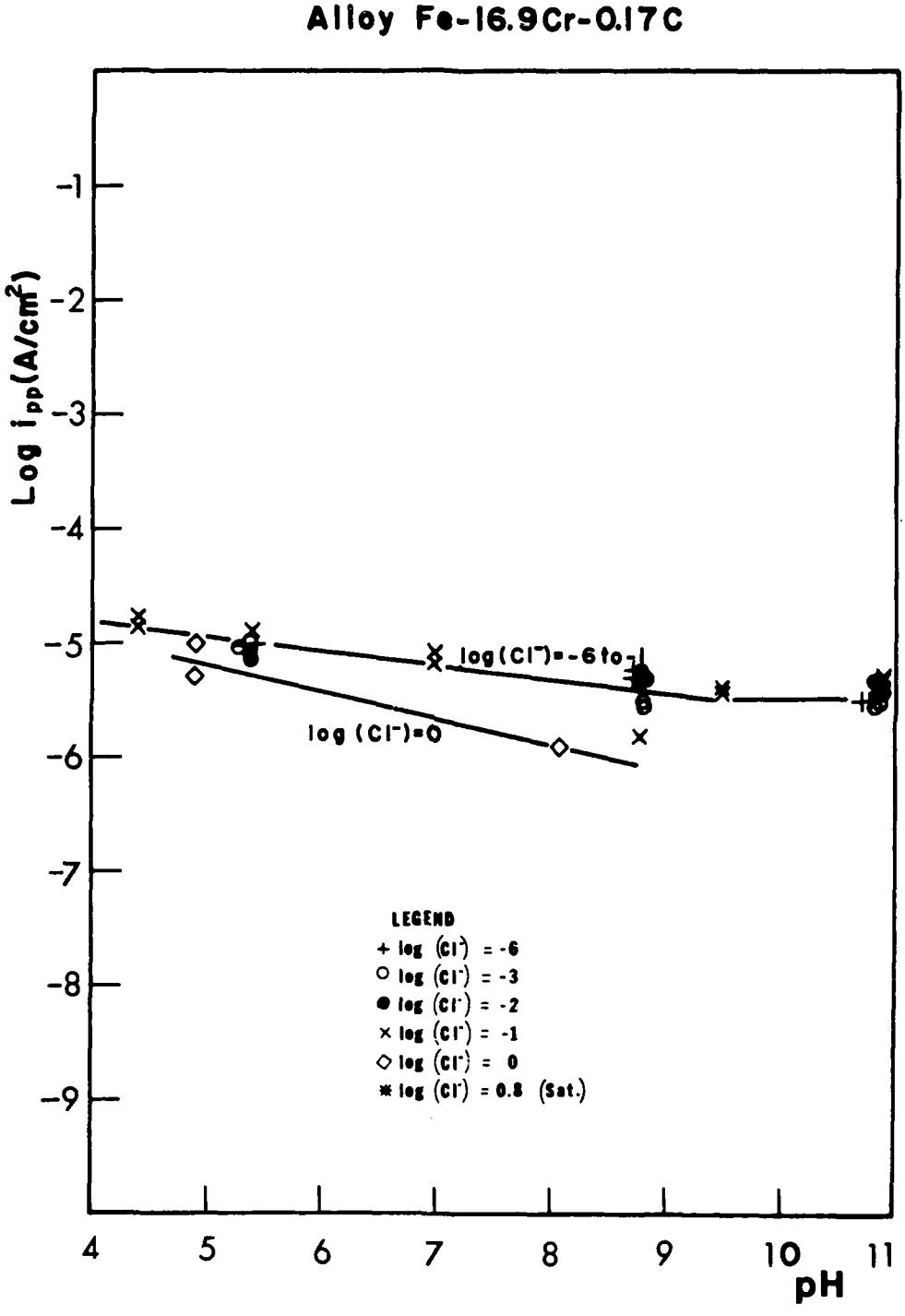

FIGURE 37: Effect of Chloride Ion Concentration on the Corrosion Velocity at the Primary Passivation Potential as a Function of pH. Fe-Cr Alloy Containing 16.9% Chromium.

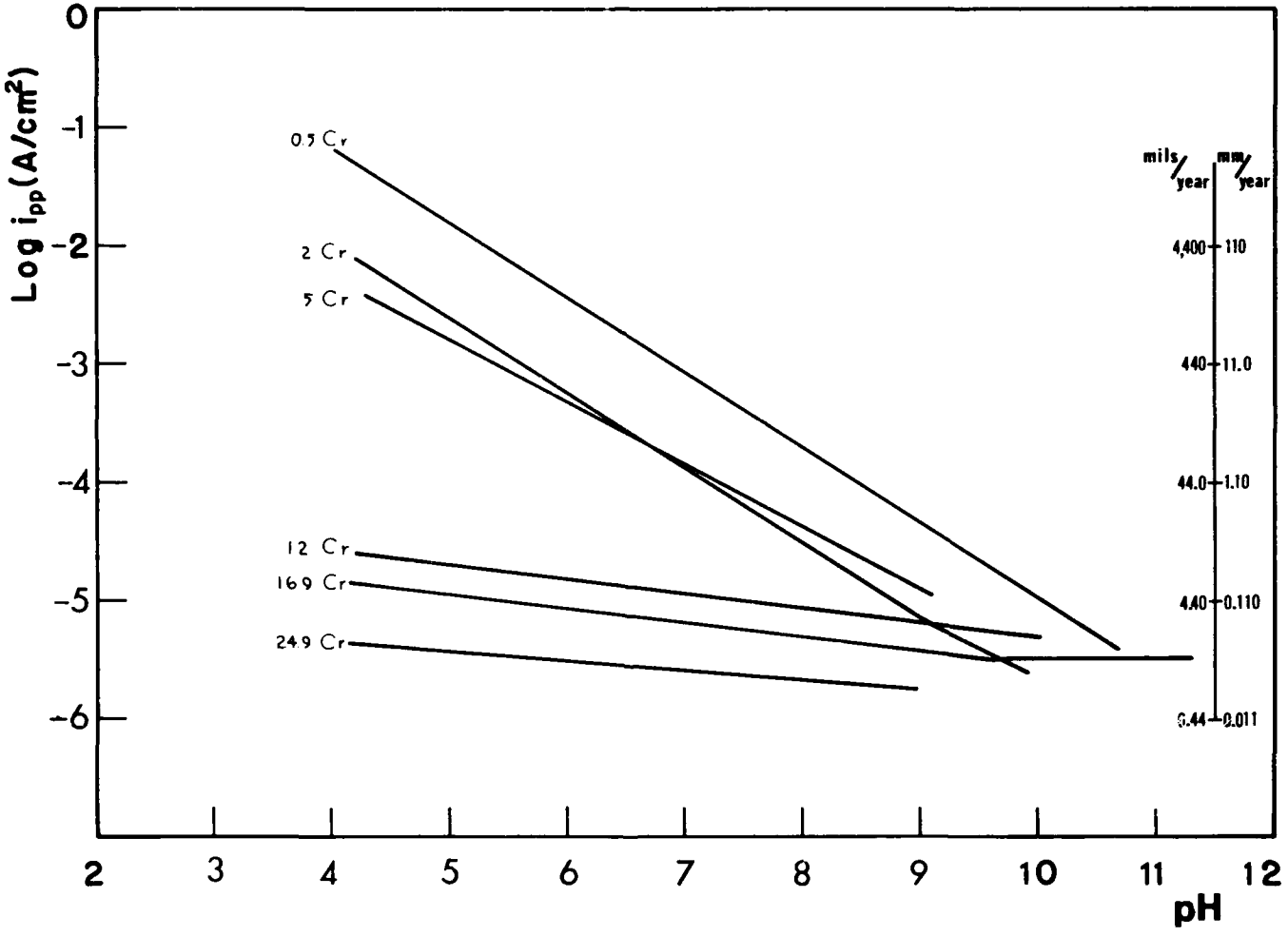

FIGURE 58: Comparison of Corrosion Velocities for the Six Binary Fe-Cr Alloys at the Primary Passivation Potential as a Function of pH.

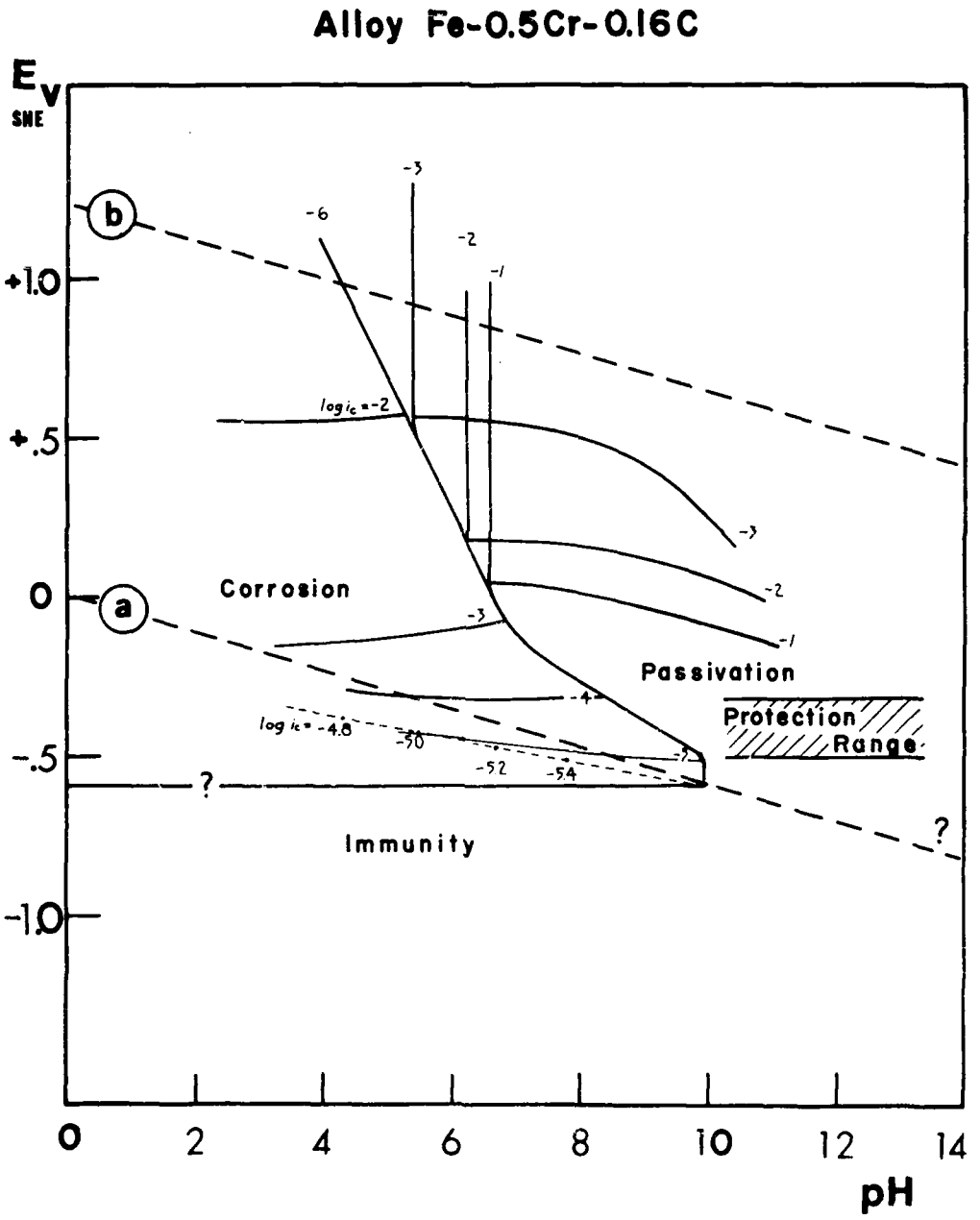

FIGURE 39: Experimental Pourbaix Diagram for Binary Fe-Cr Alloy Containing 0.5 Chromium. Rupture Potential and Protection Potential Range are Superimposed.

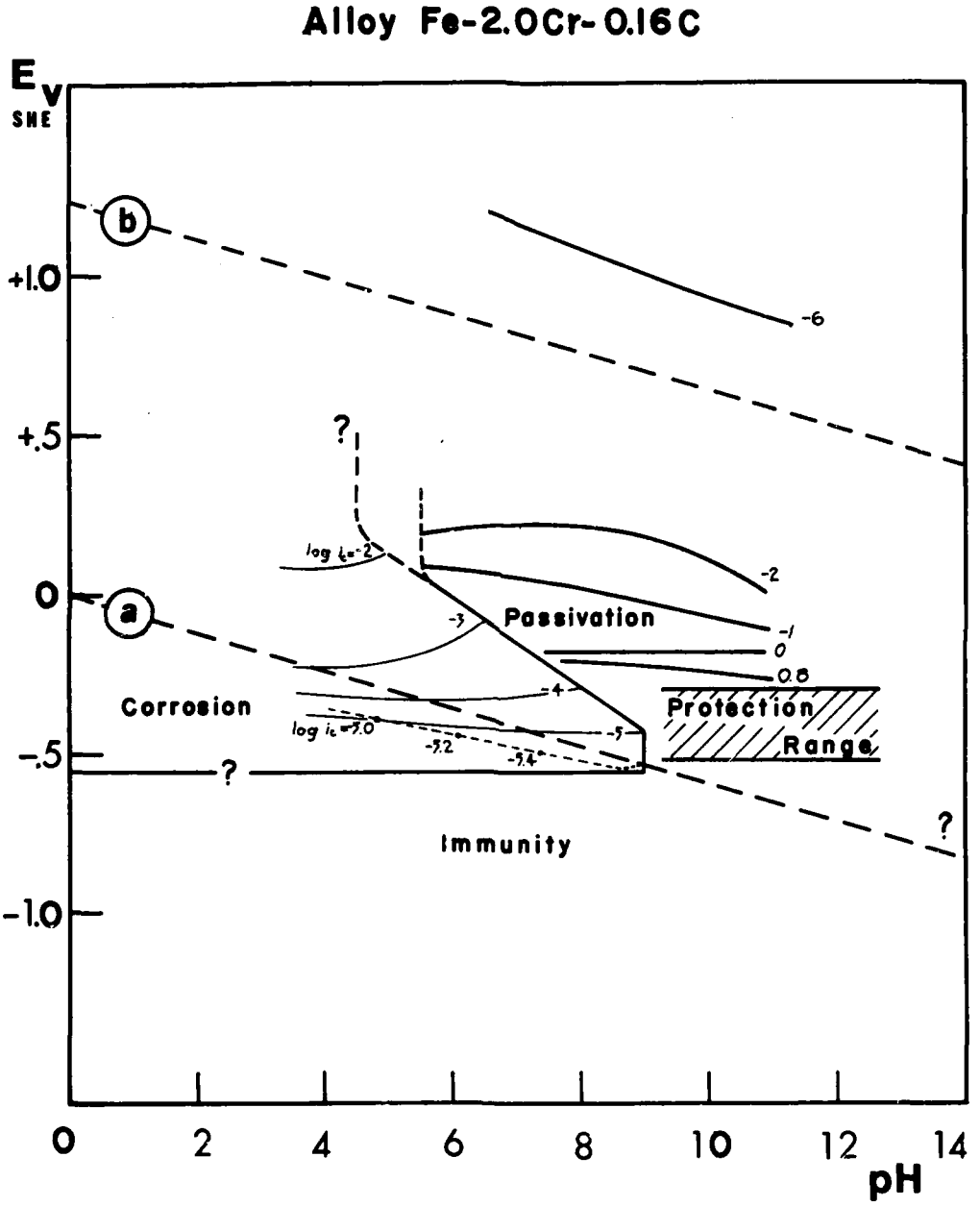

FIGURE 40: Experimental Pourbaix Diagram for Binary Fe-Cr Alloy Containing 2.0% Chromium. Rupture Potential and Protection Potential Range are Superimposed.

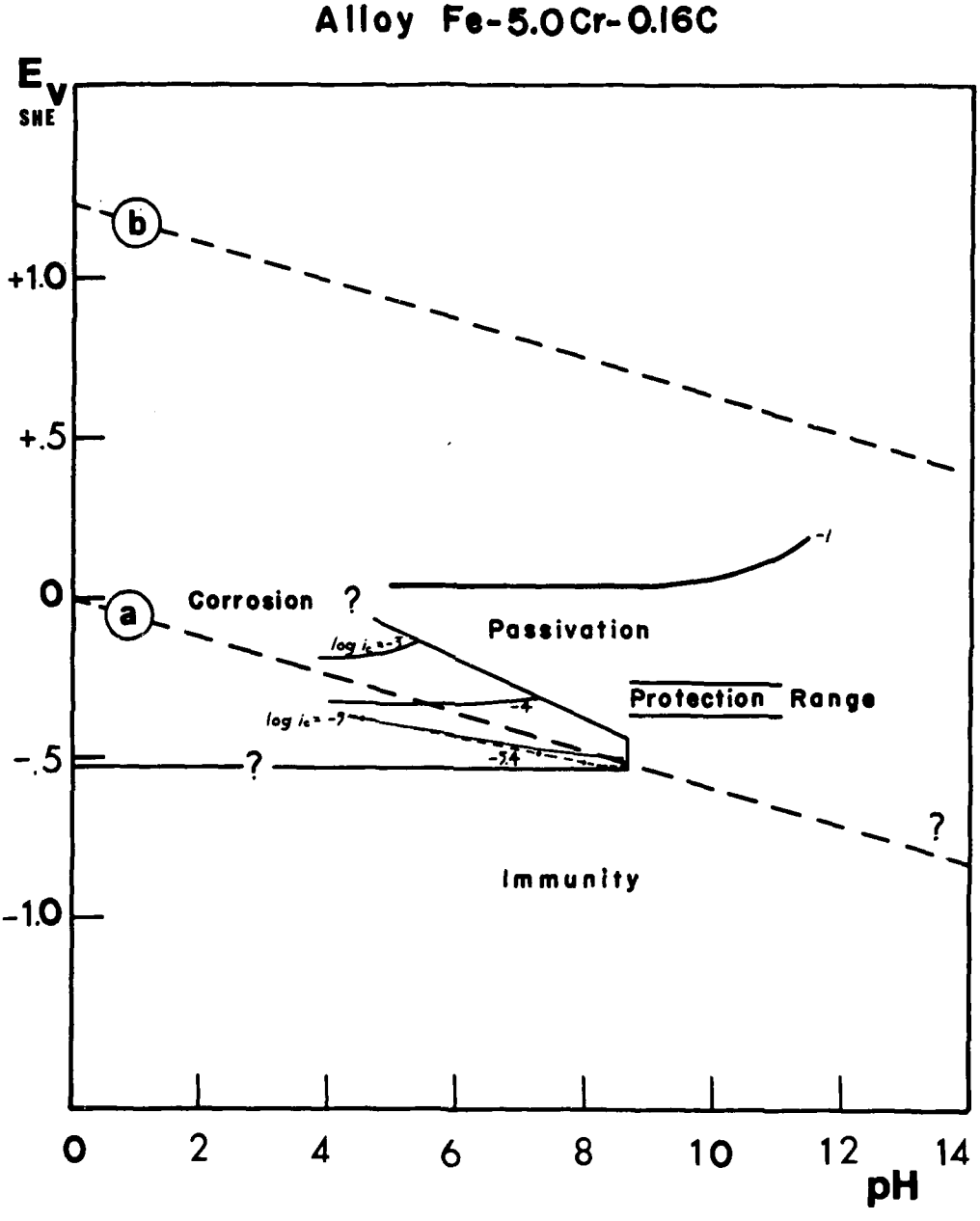

FIGURE 41: Experimental Pourbaix Diagram for Binary Fe-Cr Alloy Containing 5.0% Chromium. Rupture Potential and Protection Potential Range are Superimposed.

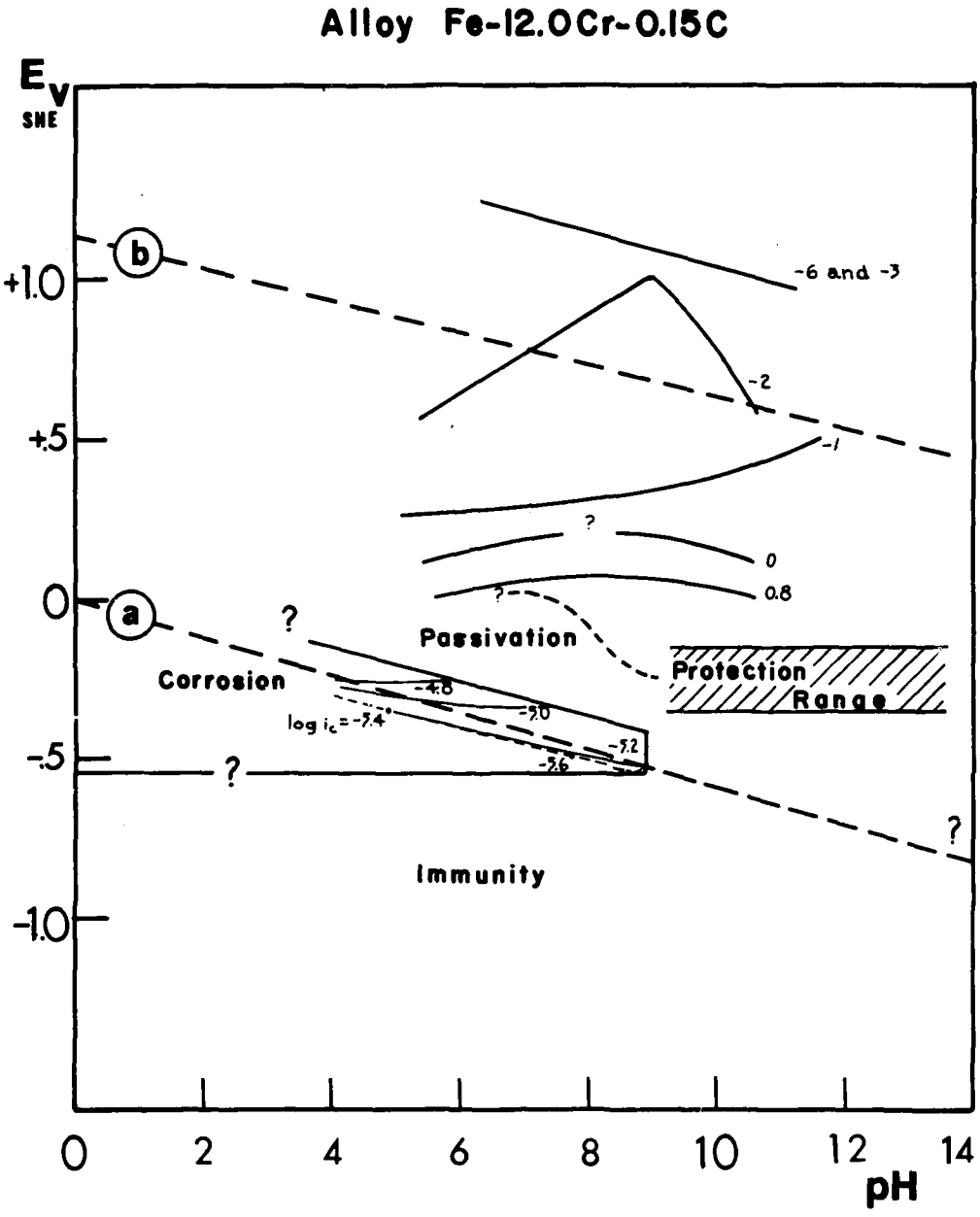

FIGURE 42: Experimental Pourbaix Diagram for Binary Fe-Cr Alloy Containing 12.0% Chromium. Rupture Potential and Protection Potential Range are Superimposed.

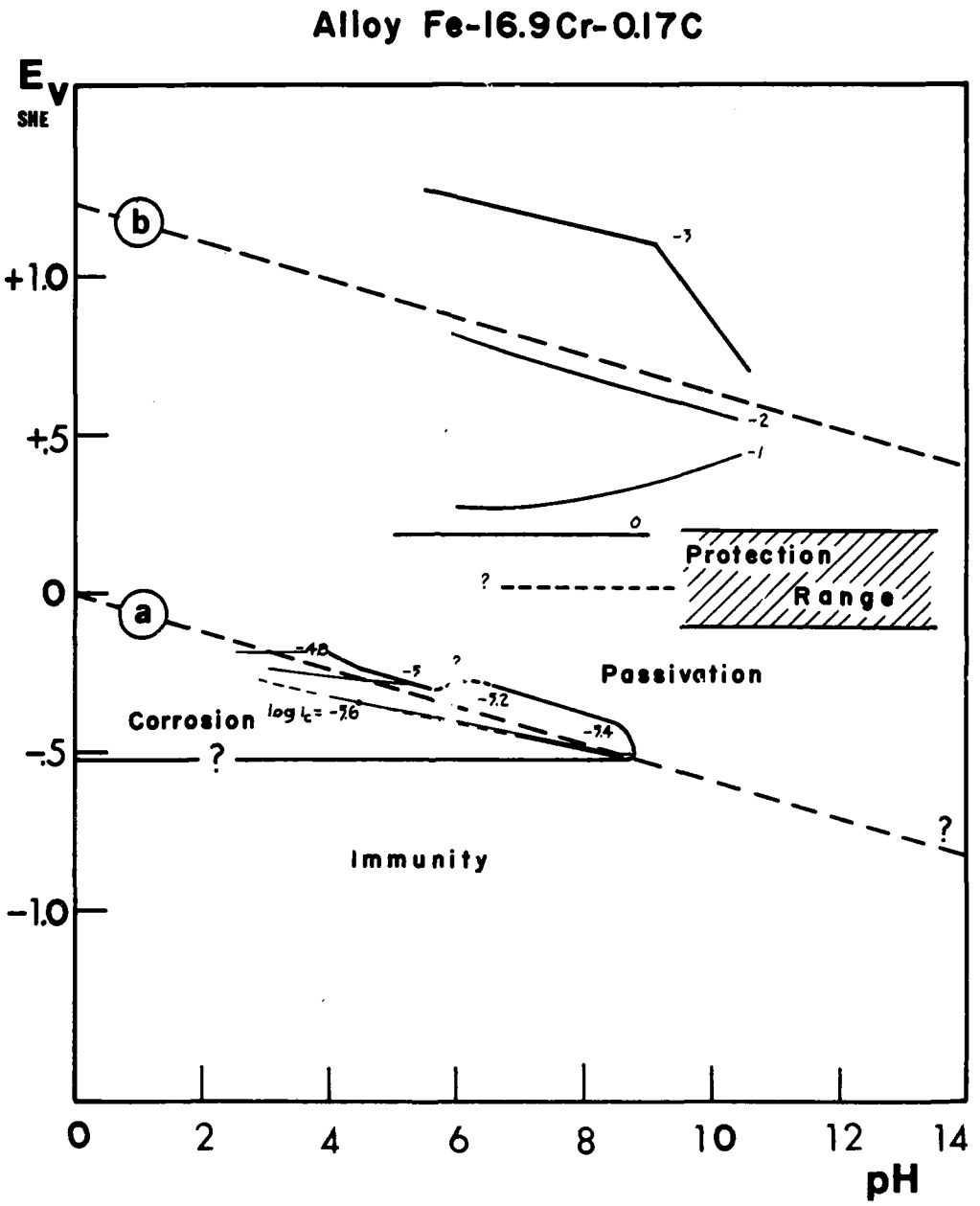

FIGURE 43: Experimental Pourbaix Diagram for Binary Fe-Cr Alloy Containing 16.9% Chromium. Rupture Potential and Protection Potential Range are Superimposed.

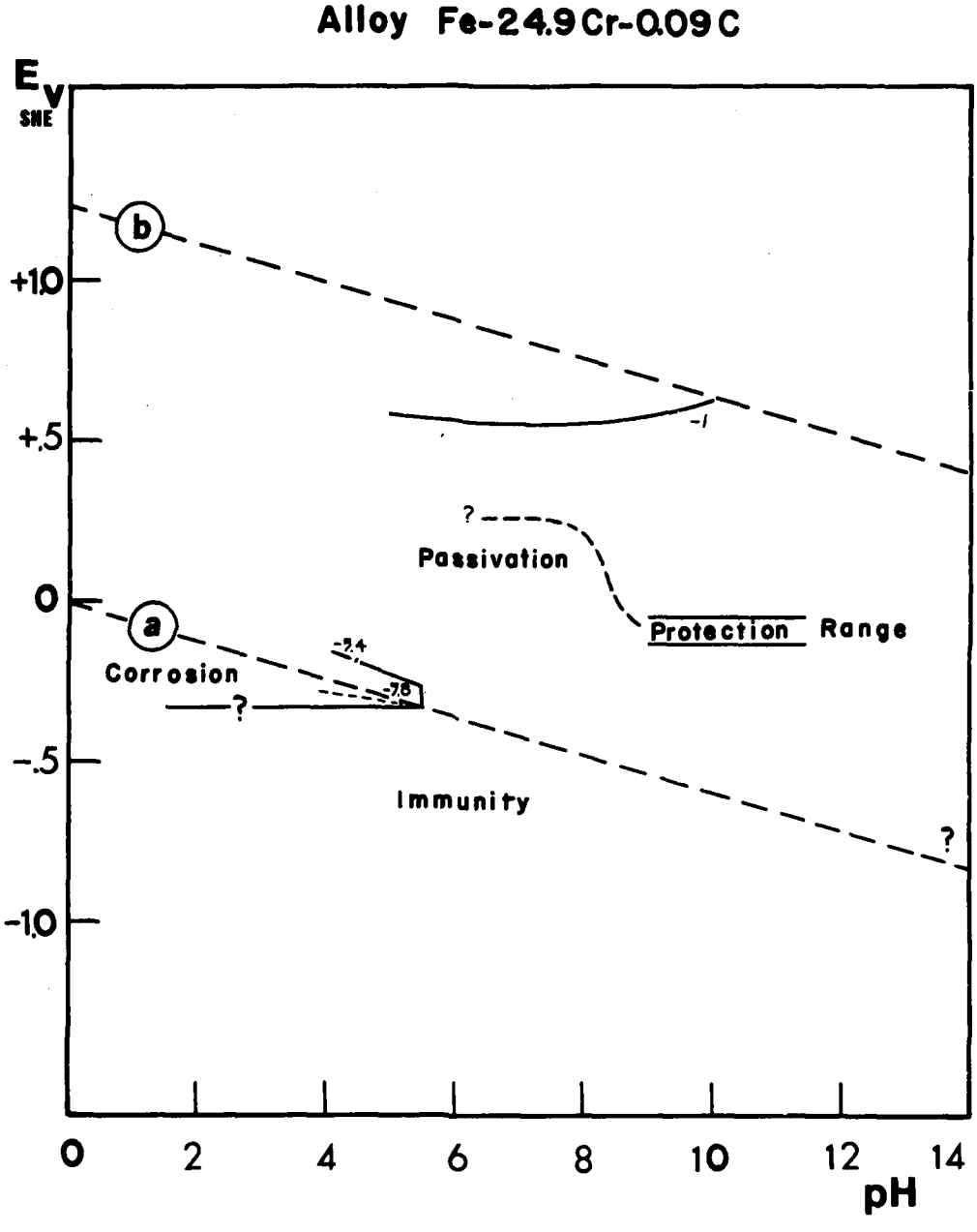

FIGURE 44: Experimental Pourbaix Diagram for Binary Fe-Cr Alloy Containing 24.9% Chromium. Rupture Potential and Protection Potential Range are Superimposed.

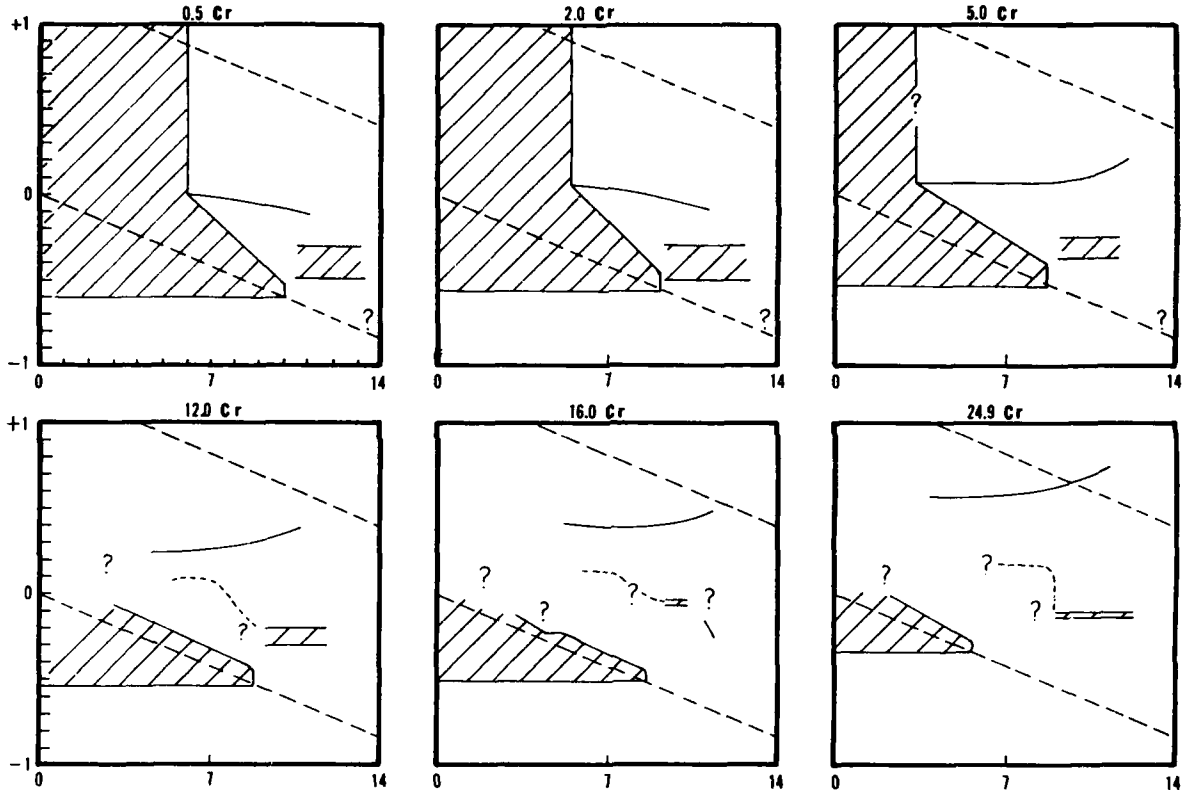

FIGURE 45: Schematic Experimental Pourbaix Diagrams for Six Binary Fe-Cr Alloys Presented for Comparison to Assess the Influence of Chromium Content on Corrosion Behavior in Solutions Containing 0.1M Chloride Ion.

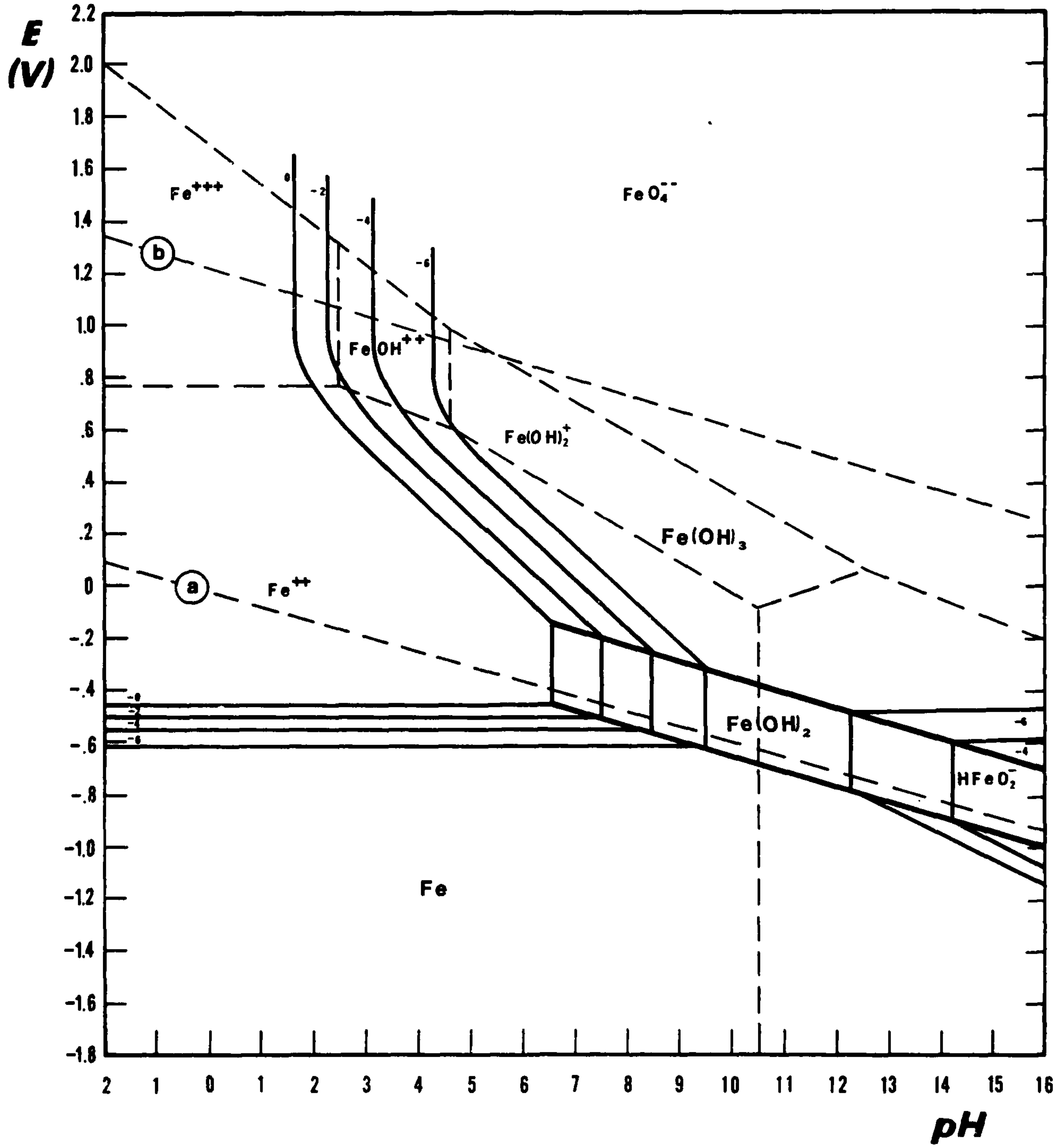

FIGURE 46. Equilibrium [illegible]

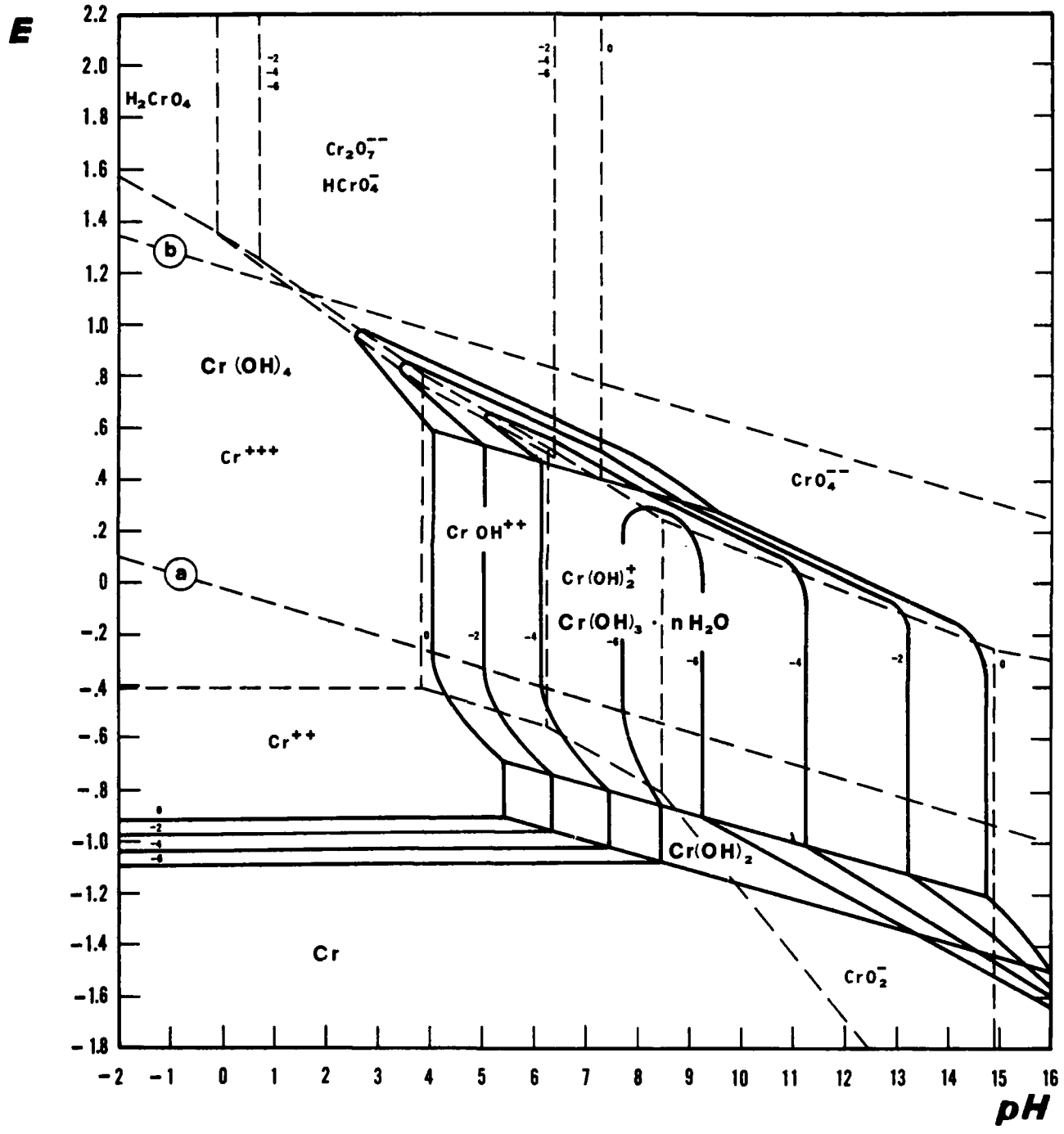
E
2.2
2.0
1.8
1.6
1.4
1.2
1.0
.8
.6
.4
.2
0
-.2
-.4
-.6
-.8
-1.0
-1.2
-1.4
-1.6
-1.8
H2CrO4
Cr2O7--
HCrO4-
b
Cr (OH)4
Cr+++
CrO4--
Cr OH++
Cr(OH)2+
Cr(OH)3 · n H2O
a
Cr++
Cr(OH)2
Cr
CrO2-
-2 -1 0 1 2 3 4 5 6 7 8 9 10 11 12 13 14 15 16
pH

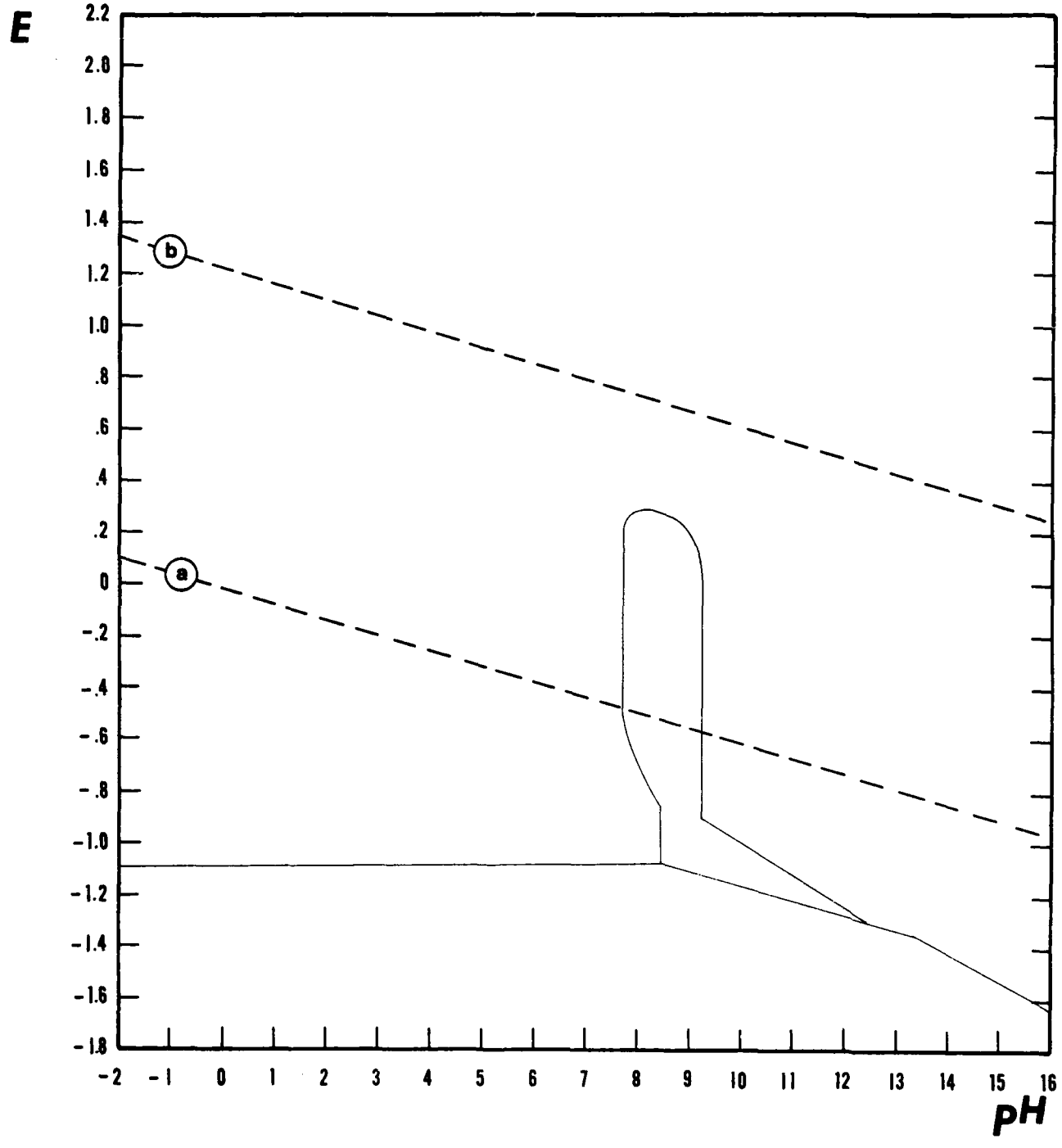

FIGURE 49. Theoretical Pourbaix Diagram. Adapted from Figure 45a for Chloride Solutions.

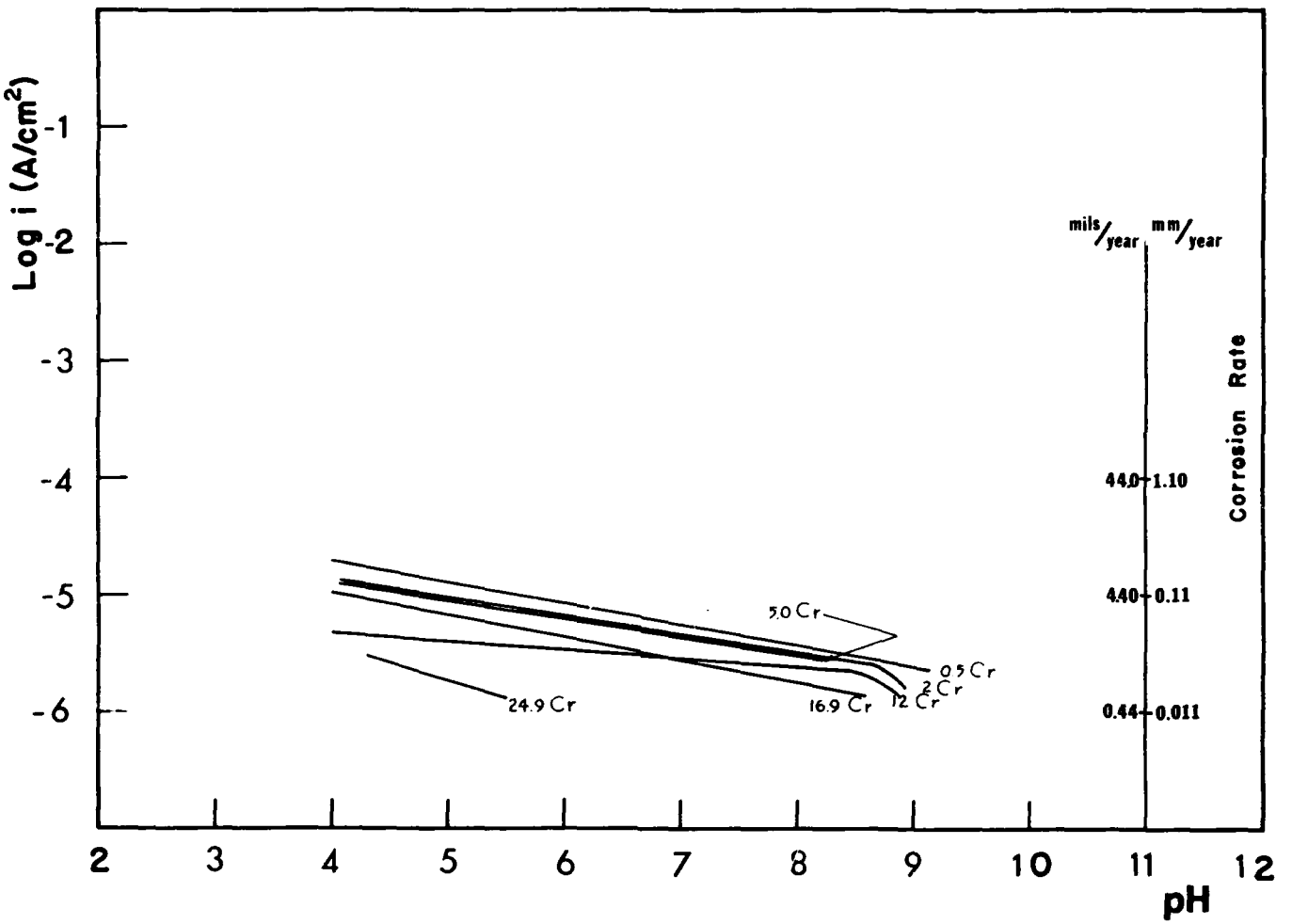

FIGURE 49: Corrosion Velocities for Six Binary Fe-Cr Alloys at the Zero Current Potential as a Function of pH.

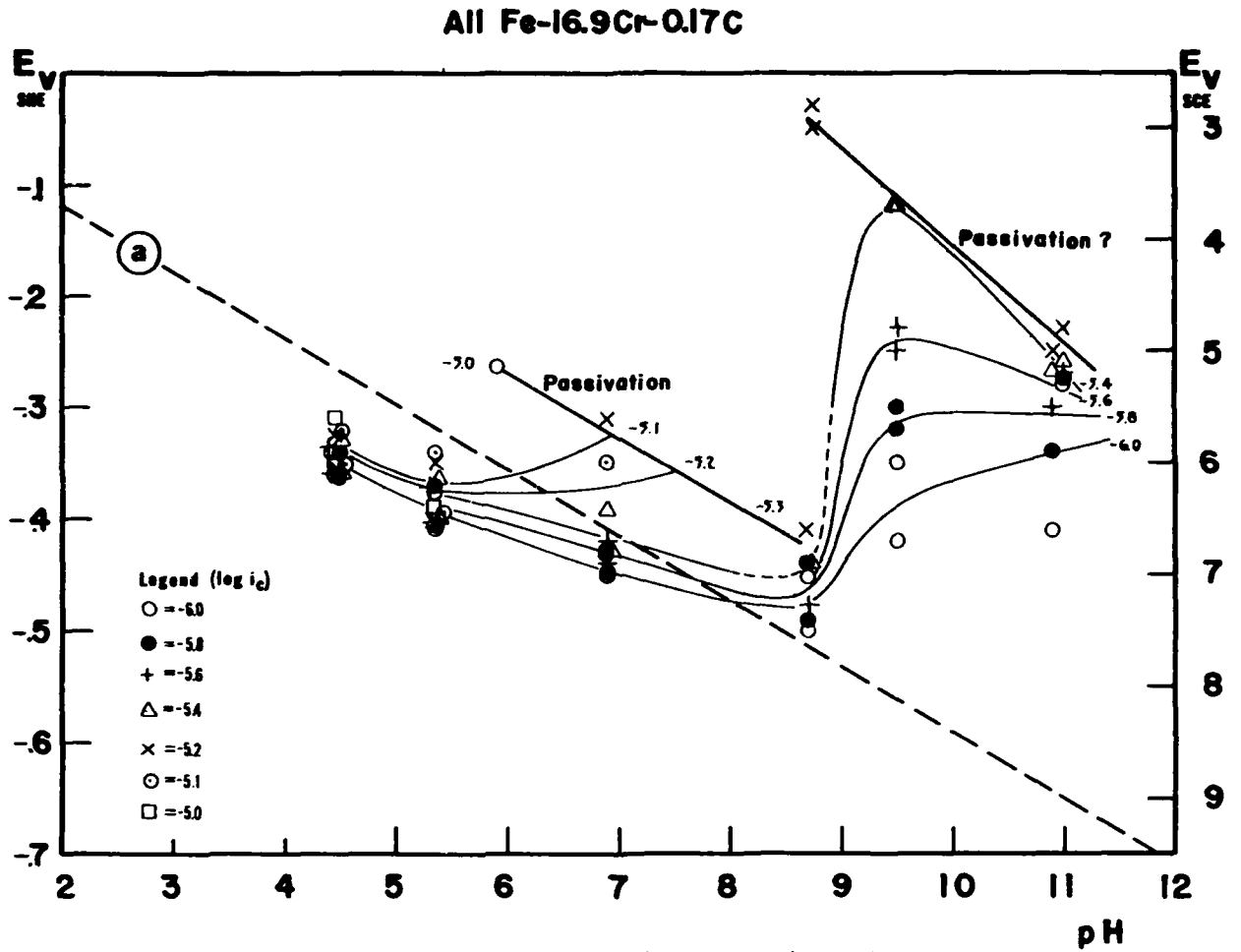

FIGURE 50: Use of Corrosion Velocity Trajectories to Indicate Corrosion Rates within the General Corrosion Region and also to Indicate the Boundary Between the General Corrosion Region and the Passivation Region for Binary Fe-Cr Alloys Containing 16.9% Chromium in 0.1M Chloride Solutions.